Huabin Zeng

CONTINUOUS ELECTROCHEMICAL ACTIVATION OF PEROXYDISULFATE MEDIATED BY SINGLE-ELECTRON SHUTTLE

ACTA UNIVERSITATIS LAPPEENRANTAENSIS 949

Huabin Zeng

CONTINUOUS ELECTROCHEMICAL ACTIVATION OF PEROXYDISULFATE MEDIATED BY SINGLE-ELECTRON SHUTTLE

Dissertation for the degree of Doctor of Science (Technology) to be presented with due permission for public examination and criticism at Lappeenranta-Lahti University of Technology LUT, Lappeenranta, Finland on the 7th of May, 2021, at noon.

Acta Universitatis
Lappeenrantaensis 949

Supervisor Associate Professor Eveliina Repo
LUT School of Engineering Science
Lappeenranta-Lahti University of Technology LUT
Finland

Reviewers Professor Anna Mikola
School of Engineering
Aalto University
Finland

Professor Tao Zhang
Research Center for Eco-Environmental Sciences,
Chinese Academy of Sciences
China

Opponent Associate Professor Florence Fourcade
University of Rennes 1
France

ISBN 978-952-335-625-2
ISBN 978-952-335-626-9 (PDF)
ISSN-L 1456-4491
ISSN 1456-4491

Lappeenranta-Lahti University of Technology LUT
LUT University Press 2021

Abstract

Huabin Zeng
Continuous Electrochemical Activation of Peroxydisulfate Mediated by Single-Electron Shuttle
Lappeenranta 2021
61 pages
Acta Universitatis Lappeenrantaensis 949
Diss. Lappeenranta-Lahti University of Technology LUT
ISBN 978-952-335-625-2, ISBN 978-952-335-626-9 (PDF), ISSN-L 1456-4491, ISSN 1456-4491

With the burgeoning development of various industries, an increasing number of organic compounds have been synthesized to satisfy societal demand. However, the unavoidable emissions of the used compounds into the natural environment have become a cause for considerable concern. Most importantly, traditional biological treatments have been proven ineffective for removing these emerging contaminants due to the non-biodegradable properties of the materials, which can be even toxic to microorganisms. For the purpose of solving the problem, advanced oxidation processes have been deemed promising technologies for the purposes; these involve the *in-situ* generation of reactive oxidative radicals, such as hydroxyl radicals (•OH) or sulfate radicals ($SO_4^{\bullet-}$). Although $SO_4^{\bullet-}$ can be readily formed from peroxydisulfate (PDS) activation by a single-electron reductive catalyst, the use of the catalyst has certain drawbacks, such as the amount of the catalyst required and its and subsequent disposal. By introducing an electron source (hydroxylamine, MoS_2, or boron) into the system, the catalyst can be theoretically regenerated, resulting in continuous PDS activation. Use of the electron sources as an electrochemical approach for PDS activation, in which electrons are employed as a reductive activator, can meet the demand for green chemistry.

In this thesis, the PDS activation process for the decontamination of organic compounds, is presented. The process was initiated by electrons donated by a Ti cathode. The concentration of $SO_4^{\bullet-}$ near the cathode was kept at a non-ignorable level, shifting the reductive atmosphere to an oxidative atmosphere for Cu-EDTA oxidation. In particular, incorporating the Cu(II)/Cu(I) redox pair with the electrochemically activated PDS system by substituting the Cu cathode for the Ti cathode accelerated the PDS activation considerably. The single-electron shuttle (Cu(II)/Cu(I) in this project) could bridge the cathode and PDS, continuously injecting a single electron into the PDS to yield $SO_4^{\bullet-}$. Meanwhile, another less toxic electron media, the Fe(III)/Fe(II) redox pair, was also proven to be efficient in catalyzing the cathodic activation of PDS. Employing the Pd/Al_2O_3 particle electrode in the three-dimensional reduction system allowed more active sites for Fe^{2+} regeneration, highly improving the performance of the system with regard to PDS activation and subsequent degradation of organic pollutants. We were also intrigued by atomic hydrogen (atomic H*) in the three-dimensional reduction system. As a strongly reductive radical with single-electron capacity, the atomic H* takes H^+/H_2O as

a precursor and forms H^+/H_2O after donating electrons, completely eliminating the conventional restriction on the operation pH for catalyzing PDS.

Herein, the present study was the first to propose a ternary system comprising an electron source, a single-electron shuttle, and a peroxide compound. This ternary system allowed researchers to minimize the catalyst dosage and rationally design the oxidation system by selecting a suitable constituent of the system for various purposes.

Keywords: Organic contamination, Peroxydisulfate, electrochemical activation, single electron transferring media, Fe^{2+}/Fe^{3+} pair, Cu^+/Cu^{2+} pair, H^*/H^+ pair

Acknowledgements

This research work for thesis was conducted in School of Engineering Sciences, Lappeenranta-Lahti University of Technology LUT in cooperation with the Chinese Academy of Sciences and Tsinghua University during September 2015 to August 2020. The expert research team and the enthusiasm for science made this research feasible.

I am very grateful for Associate Professor Eveliina Repo for acting as my supervisor during the thesis preparation and writing with great patience and carefulness. I am also grateful for her comments and suggestions for further study. I appreciate her support and assistance to finalize this thesis.

I would express my sincere appreciation to Professor Mika Sillanpää who offered the opportunity to conduct this work in Lappeenranta-Lahti University of Technology LUT in the beginning. I thank for his great support and guidance in this research work.

My sincere appreciation also expressed to Professor Xu Zhao, Chinese Academy of Sciences. I highly acknowledge his great support through the whole process. I am grateful for his profound comments in this research and patient guidance during the past several years.

I express my gratitude to Professor Jiuhui Qu, Professor Huijuan Liu, Professor Huachun Lan, professor Feiping Zhao, professor Yuri Park, Professor Yan Wang, Dr. Gong Zhang, Dr. Di Cao, Shanshan Liu, and Olga Pastushok for their contributions as co-authors and/or assistance in this research work.

I sincerely acknowledge the two reviewers of this thesis for their valuable comments. I also appreciate all the reviewers and editors of the papers included in this thesis for their constructive comments and suggestions.

I am thankful for members of the research group in Mikkeli, and Beijing for their assistance in my work. I appreciate all the friends during my stay in Finland for their help and concern which I will keep in mind always.

Finally, I would express gratitude for my families for their unconditional support and encouragement in my PhD study and my life.

Huabin Zeng
January 2021
Lappeenranta, Finland

Contents

Abstract

Acknowledgements

Contents

List of publications **9**

Nomenclature **11**

1 Introduction **13**
1.1 Organic contamination 13
1.2 Conventional processes for decontamination of organic pollutants 14
1.3 Peroxydisulfate & sulfate radicals 16
1.4 Electron-source/single-electron shuttle pairs 20
1.5 Aim & Research 23

2 Methodology **25**
2.1 Chemicals & Materials 25
2.1.1 Chemical reagents 25
2.1.2 Material preparation 26
2.2 Reactor configurations 26
2.2.1 Photoelectrocatalytic reactor 26
2.2.2 Electrocatalytic reactor 27
2.3 Analytical method 27
2.3.1 Organic detection 27
2.3.2 Analytical method 27

3 Result & Discussion **29**
3.1 PDS activation by cathodic reduction 29
3.1.1 Enhanced decomplexation of Cu-EDTA and simultaneous Cu recovery in the PEC system with addition of PDS 29
3.1.2 Cathodic activation of PDS via single-electron transfer 30
3.1.3 Acidification induced by PDS oxidation 32
3.2 Enhanced cathodic activation of PDS mediated by Cu^{+}/Cu^{2+} pair 34
3.2.1 Enhanced degradation of organic compounds 34
3.2.2 Cu^{+}/Cu^{2+} cycle for cathodic activation of PDS 36
3.3 Pd/electro-generated H_2 for accelerating Fe^{3+}/Fe^{2+} cycle 37
3.3.1 Acceleration of Fe^{3+}/Fe^{2+} cycle 37
3.3.2 Enhanced degradation of organic pollutants 40
3.4 PDS activation by atomic H* 42
3.4.1 Organic degradation in the Pd/ER system 42
3.4.2 Identification of reactive oxygen species 42

3.4.3 Two routes for PDS electroreduction on Pd(111) facet 44
3.4.4 Electron donor analysis 46

4 Conclusions & Prospective **49**

References **51**

Publications

List of publications

This dissertation is based on the following papers. The rights have been granted by publishers to include the papers in dissertation.

I. **Zeng H.B.,** Liu S.S., Chai B.Y., Cao D., Wang Y., and Zhao X., 2016. Enhanced Photoelectrocatalytic Decomplexation of Cu-EDTA and Cu Recovery by Persulfate Activated by UV and Cathodic Reduction. ***Environmental Science & Technology*** 50, 6459-6466.

II. Liu S.S., Zhao X., **Zeng H.B.,** Wang Y.B., Qiao M., and Guan W., 2017. Enhancement of Photoelectrocatalytic Degradation of Diclofenac with Persulfate Activated by Cu Cathode. ***Chemical Engineering Journal*** 320, 168-177.

III. **Zeng H.B.,** Zhao X., Zhao F.P., Park Y., and Sillanpää M., 2019. Accelerated Fe^{3+}/Fe^{2+} Cycle Using Atomic H* on Pd/Al_2O_3: A Novel Mechanism for an Electrochemical System with Particle Electrode for Iron Sludge Reduction in the Fe^{2+}/Peroxydisulfate Oxidation Process. ***Chemical Engineering Journal*** 382, 122972.

IV. **Zeng H.B.,** Lan H.C., An X.Q., Repo E., Park Y., Pastushok O., Liu H.J., and Qu J.H., 2020. Insight into Electroreductive Activation Process of Peroxydisulfate for Eliminating Organic Pollution: Essential Role of Atomic Hydrogen. ***Chemical Engineering journal*** 128355.

Author's contribution

Huabin Zeng conducted the experiments, analyzed the data with co-authors and had the main responsibility in writing paper I, III, and IV. Huabin Zeng conducted some parts of the experiments, analyzed the data and helped to prepare the first draft of paper II.

Other related publications

I. **Zeng H.B.,** Tian S.C., Liu H.F., Chai B.Y., and Zhao X., 2016. Photo-assisted Electrolytic Decomplexation of Cu-EDTA and Cu Recovery Enhanced by H_2O_2 and Electro-generated Active Chlorine. ***Chemical Engineering Journal*** 301, 371-379.

II. **Zeng H.B.,** Zhang G., Ji Q.H., Liu H.J., Hua X., Sillanpää, M., and Qu, J.H., 2020. pH-Independent Production of Hydroxyl Radical from Atomic H*-Mediated Electrocatalytic H_2O_2 Reduction: A Green Fenton Process without Byproducts. ***Environmental Science & Technology*** 54, 14725−14731.

III. **Zeng H.B.,** Zhao X., Zhao F.P., Park Y., Thangaraj S.K., Jänis J., and Sillanpää M., 2020. Oxidation of 2,4-Dichlorophenol in Saline Water by Unactivated Peroxymonosulfate: Mechanism, Kinetics and Implication for in-situ Chemical Oxidation. ***Science of the Total Environment***., 728, 138826.

IV. Shao H.X., Wang Y.B., **Zeng H.B.,** Zhang J.J., Wang Y., Sillanpää M., and Zhao X., 2019. Enhanced Photoelectrocatalytic Degradation of Bisphenol A by $BiVO_4$ Photoanode Coupling with Peroxymonosulfate. ***Journal of Hazardous Materials*** 394, 121105.

V. Cao D., **Zeng H.B.,** Yang B., and Zhao X., 2017. Mn Assisted Electrochemical Generation of Two-Dimensional Fe-Mn Layered Double Hydroxides for Efficient Sb(V) Removal. ***Journal of Hazardous Materials***, 336, 33-40.

Nomenclature

Abbreviations

2D	two dimensional
3D	three dimensional
CFD	computational fluid dynamics
LES	large eddy simulation
PDF	probability density function
PDS	Peroxydisulfate
PMS	Permonosulfate
AOPs	Advanced oxidation processes
HA	Hydroxylamine
BA	Benzoic acid
EDTA	Ethylenediaminetetraacetic acid
ICP-OES	Inductively coupled plasma-optical emission spectrometry
TOC	Total organic carbon
LSV	Linear Sweep Voltammetry
CV	Cyclic Voltammetry
SEM	Scanning electron microscopy
XRD	X-ray diffraction
XPS	X-ray photoelectron spectra
ESR	Electron spin resonance
PEC	Photoelectrocatalysis
PEC/PDS	Photoelectrocatalysis process with PDS addition
ER	Electroreduction
ER/PDS	Electroreduction process with PDS addition
PMSO	Methyl phenyl sulfoxide
$PMSO_2$	Methyl phenyl sulfone
$PhSO_2$	phenylsulfinic acid
2,4-DCP	2,4-Dichlorphenol
BPA	Bisphenol A

1 Introduction

1.1 Organic contamination

In the human environment, the number of chemical substances has surpassed 30 million, and this number is constantly increasing rapidly, with a high weekly rate. Among these substances, organic compounds account for the largest proportion (Kroes et al. 2000). With the booming development of various industries, especially the organic chemical, petrochemical, and pharmaceutical industries, it is inevitable that the organics from these industries are emitted into the environment, giving rise to various emerging pollutants recently detected in the environment (Gosset et al. 2016, Yang et al. 2017).

These organics can persist in the natural environment. Some organics, whose toxicity is sourced from the specific chemical structure of the organic compound itself and its physiological effects, may adversely affect the normal metabolic functions of organisms and even induce death (non-reactive toxicity) (Escher 2000). Others may disrupt the normal information transmission of cells or cause cell death or mutation, tissue necrosis or allergic reactions, or tumors in the tissues by modifying the pivotal proteins in the biological metabolism processes (reactive toxicity) (Kaim et al. 2013). These organics can accumulate in the food chain at toxic concentrations (Klopman and Tu 1997). Therefore, these organics not only pose a serious threat to human health and the ecosystems, but are also difficult to degrade via biological treatment methods.

In recent years, the environmental impacts of toxic and refractory organic matter have received increasing attention worldwide, and the associated pollution control and prevention has become a popular research topic (Hodges et al. 2018). The United States Environmental Protection Agency (USEPA) took the lead in systematically investigating the toxicity, biodegradability, and appearance of water bodies contaminated with various pollutants in the 1970s and passed the Clean Water Act in 1977 (Pichtel 2005). The case clearly specified 65 types of 129 priority pollutants, of which 114 were synthetic organic matter. The Japanese Environment Agency conducted a nationwide comprehensive environmental safety survey of chemicals in 1974, announced 600 priority toxic chemicals in 1986, and conducted extensive research on toxic organics in the country. In the "Discharge Standards for Water Quality Targets" promulgated by the European Community in 1975, blacklists and greylists were recorded, requiring member states to specify priority pollutants that were appropriate for their situation according to the requirements of the standard. The Information Center on Potentially Hazardous Chemicals was established at the United Nations Conference on Human and Environment in 1972, and the United Nations Environment Programme (UNEP) formally established the "Positive Toxic Chemicals Registry" in 1976. Its main responsibility is to control toxic chemical pollution and develop standards and strategies. The World Health Organization (WHO) has implemented the International Chemical Safety Program since 1980, focusing on evaluating the impact of existing chemicals on human health, establishing and improving chemical safety assessment methods, and training personnel. Based on the

pollution characteristics of domestic organic compounds, in combination with studies reported from other countries, the China National Environmental Monitoring Station has put forth the Chinese environmental priority reflecting China's environmental characteristics based on the toxicity of chemicals, possibility of their natural degradation, and probability of their appearance in water bodies. In the “blacklist”, 68 pollutants in 14 categories require priority control; of these, 58 types of toxic organic compounds are controlled in priority, accounting for 85.29% of the total.

The control of toxic and difficult-to-degrade organic matter is a global environmental governance problem. Therefore, comprehensive and effective management is essential for environmental workers today and in the future. In recent years, the pollution caused by refractory organics in the ecological environment and the damage to human health have increased substantially. Biological toxicity and stability of refractory organics entering the water body can cause a serious long-term deterioration of water quality, obstruct self-purification of the surface water, and endanger people's health. Therefore, research on the treatment technologies of these pollutants has considerable experimental and practical significance (Pitter and Chudoba 1990).

1.2 Conventional processes for decontamination of organic pollutants

In the past few decades, several applicable technologies for the decontamination of the organic pollutants have been developed; these technologies can be divided into biological (Kagle et al. 2009), physical (Bass et al. 2000), and chemical treatment technologies (Salimi et al. 2017). Biological treatment processes use aeration and a biological floc composed of protozoa and bacteria. In this way, municipal wastewater and industrial wastewater (food industry, dyeing and printing industry, or paper industry) can be readily decontaminated at an incredibly low cost via the enhancement of the metabolism of microorganisms and the degradation of organic matter (Zhao et al. 2014b). However, the metabolic functions of the microorganisms are adversely affected by the emerging organic pollutants (pharmaceutical and personal care products, PPCPs; emerging contaminants, ECs) or toxic constituents (heavy metals, such as Ni, Cu, or Zn) that coexist with the organic pollutants in wastewater (Zhao et al. 2014a, Zhao et al. 2013); these compounds induce the death of the microorganisms.

The non-biodegradability of these emerging organic pollutants in industrial wastewaters has necessitated other physicochemical processes for their efficient removal; these include coagulation (Liu et al. 2019a), adsorption (Alsbaiee et al. 2016), and oxidation/reduction processes (Zhao et al. 2014c). In contrast to other processes where water purification occurs only by pollutant transfer (coagulation or adsorption), advanced oxidation processes (AOPs) are known to be the most effective in converting bio-recalcitrant organic contaminants into inorganic matter through the mineralization of organics (Glaze et al. 1987, Nidheesh et al. 2013).

Typically, AOPs include the degradation of organic pollutants by generating reactive oxidative radicals with a high redox potential in situ. Such technologies include

electrochemical, photocatalytic, and Fenton or Fenton-like processes. Some commonly used radicals and their parent oxidants, including their redox potentials and involved oxidation processes, are listed in **Table 1.1**.

Table 1.1 Redox potential of commonly used oxidants and radicals.

Oxidation species	Redox potential	Generation approach	Ref.
$\cdot OH/H^+/H_2O$	+2.73 V	Electrocatalysis, photolysis, Fenton, Fenton-like	(Buxton et al. 1988)
$\cdot OH/OH^-$	+1.80 V	Electrocatalysis, photolysis, Fenton, Fenton-like	(Buxton et al. 1988)
$SO_4^{\cdot-}/SO_4^{2-}$	+2.60 V	Persulfate based AOPs	(Lee et al. 2020)
$H_2O_2/H^+/H_2O$	+1.78 V		(Wardman 1989)
$S_2O_8^{2-}/SO_4^{2-}$	+2.01 V		(Eberson 1982)
HSO_5^-/SO_4^{2-}	+1.75 V		(Spiro 1979)
$HO_2^{\cdot-}/H^+/H_2O_2$	+1.44 V	Fenton	(Wardman 1989)
$SO_5^{\cdot-}/SO_5^{2-}$	+1.10 V	Peroxymonosulfate (PMS) based AOPs, Fe^{3+}/SO_3^{2-}	(Das et al. 1999)
$O_2^{\cdot-}/H^+/H_2O_2$	+0.94 V	Fenton, photolysis	(Wardman 1989)
H_2O_2/OH^-	+0.88 V		(Wardman 1989)
$^1O_2/O_2^{\cdot-}$	+0.65 V	Persulfate based AOPs	(Buettner 1993)
$O_2^{\cdot-}/O_2$	+0.33 V	Fenton, photolysis	(Wardman 1989)

Among these oxidants, hydrogen peroxide (H_2O_2) has been widely applied in scientific and technological activities for environmental remediation because of its low price (approximately 200 USD per metric ton) and green properties. As an externally additive reagent, it only decomposes to H_2O or O_2 without leaving byproducts in the aqueous system (Noyori 2005). Moreover, its resultant hydroxyl radical (·OH), due to its high redox potential reaching 2.73 V in an acid solution and 1.8 V in a neutral solution (Buxton et al. 1988), can destroy almost any refractory structure or group present in the organic compounds, leading to their complete mineralization. However, owing to in situ chemical

oxidation, H_2O_2 is unstable and presents risks of explosion, making its storage, transportation, and application challenging. Therefore, other oxidants are being gradually taken into consideration by researchers.

1.3 Peroxydisulfate & sulfate radicals

Over the past decade, peroxydisulfate (PDS, $S_2O_8^{2-}$) has drawn significant attention as a promising alternative to H_2O_2 (Devi et al. 2016, Ghanbari and Moradi 2017, Oh et al. 2016). PDS contains the same peroxide bond as H_2O_2, substituting sulfur groups for the two hydrogen atoms in H_2O_2 (**Figure 1.1**). This structural change causes a slight decrease in the peroxide bond length from 1.469 Å (H_2O_2) to 1.347 Å (PDS); thus, PDS exhibits similar physicochemical properties, while maintaining its own unique nature. For instance, PDS has been shown to possess a higher chemical stability than H_2O_2 under ambient conditions, lowering the cost of storage and transportation (Zeng et al. 2019). When activated, PDS can produce highly oxidizing sulfate radicals ($SO_4^{\bullet-}$), which can readily oxidize organic contaminants by hydrogen abstraction or an electron abstraction mechanism (Deng and Ezyske 2011, Neppolian et al. 2008, Zhou et al. 2014) because of its high redox potential (E^0 = 2.6–3.1 V) (Lee et al. 2020). Compared with the well-known H_2O_2/·OH pairs, the technical advantages of the PDS/$SO_4^{\bullet-}$ pairs that have been identified include: 1) a higher amount of radicals can be produced from PDS than from H_2O_2 at the same concentration (Anipsitakis and Dionysiou 2004, He et al. 2013, Ling et al. 2010, Yu et al. 2013); 2) $SO_4^{\bullet-}$-based oxidation processes for organic degradation are relatively independent of the operating conditions, such as pH, initial peroxide loading, and background constituents (Luo et al. 2015, Lutze et al. 2015, Zhang et al. 2016b); and 3) as a non-selective radical, $SO_4^{\bullet-}$ exhibits higher reactivity toward electrophilic compounds compared with ·OH (Lee et al. 2020).

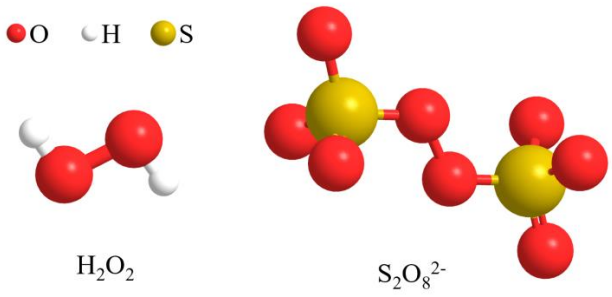

Figure 1.1 Ball-and-stick models of H_2O_2 and $S_2O_8^{2-}$.

Generally, PDS activation approaches can be classified into two categories (**Figure 1.2**). In the first approach, the homolytic cleavage of the peroxide bridge in the PDS molecule forms two sulfate radicals ($SO_4^{\bullet-}$) due to energy input in the form of photons (ultraviolet (UV) photolysis), microwaves, or heat (thermolysis) (**reaction 1.1, Table 1.2**). In these processes, secondary contamination is minimized due to the zero-addition of chemical

activators, which significantly lowers the cost of the downstream treatment for removing these activators. Despite this advantage, applying UV photolysis for PDS activation is limited due to the poor penetrability of UV rays in water, especially in wastewater with high chromaticity and turbidity (Zeng et al. 2016). Interestingly, in recently reported studies, thermal activation of PDS has exhibited excellent application potential in some research fields that cannot be subjected to traditional activation approaches, such as the in-situ remediation of polluted soil, surface water, or groundwater (Srivastava et al. 2016), flue gas denitrification/desulfurization (Liu et al. 2018), and sludge dewatering (Waclawek et al. 2016). Different from H_2O_2 decay to O_2 (and thus, a loss in its oxidation capacity), PDS can be thermally cleaved into two $SO_4^{\cdot-}$ at a low activation temperature of approximately 30 °C (Bruton and Sedlak 2017, Ji et al. 2017, Park et al. 2016, Peng et al. 2016, Srivastava et al. 2016).

$$S_2O_8^{2-} + \text{heat/UV/microwave} \rightarrow 2\ SO_4^{\cdot-} \qquad (1.1)$$

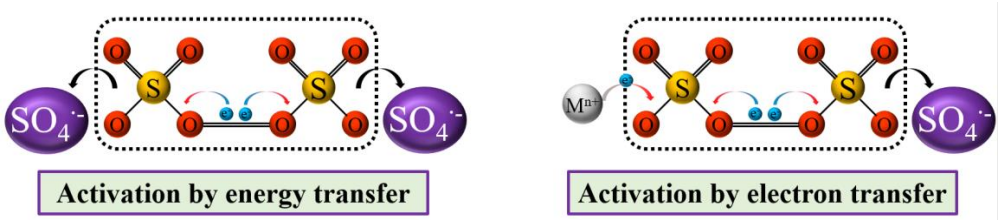

Figure 1.2 Activation of PDS through energy input and electron transfer process.

Table 1.2 PDS activation by energy input and its application on organic degradation.

Target pollutant	Energy form	Conditions	Ref.
phenol	Heat	C(pollutant),50 μM, C(PDS),2 mM, C(NO_2^-), 200 mM, Temperature,50 ℃, pH 7.0	(Ji et al. 2017)
Decabromodiph-enyl ether	heat	C(pollutant), 20 mg/kg; C(PDS), 0.5 M; pH, 3; T, 50 ℃	(Peng et al. 2016)
perfluorooctanoic acid	Heat	C(pollutant), 0.241 mM; C(PDS), 84 mM; T, 50 ℃	(Park et al. 2016)
tetrachloroethene	Joule heat		(Chowdhury et al. 2017)
concentrated leachate	Microwave	C(PDS), 20 mM; $pH_{initial}$, 3.0; P, 450 W	(Gu et al. 2018)
hospital wastewater	UV light	C(pollutant), 40 μM; C(PDS), 0.5 mM; UV intensity, 398 mW/cm^2; $pH_{initial}$, 6.5.	(Serna et al. 2017)
disinfection byproduct precursors	UV light	UV dose, 585 mJ/cm^2; C(PDS), 0.5 mM	(Chu et al. 2015)
2,4,6-trichloroanisole	UV light	C(TCA), 200 nM; C(PDS), 200 μM; pH, 8; I, 148 μW/cm^2	(Luo et al. 2016)

The other commonly used approach for PDS activation is the heterolytic cleavage of the peroxide bridge via single-electron injection into the PDS ions (Lee et al. 2020). As a two-electron acceptor, one molecule of PDS yields one molecule of $SO_4^{\cdot-}$ when accepting one electron, while the oxidation capacity of PDS is completely consumed by accepting two electrons. Therefore, the activator for PDS activation should meet two requirements: i) strong reductive ability and ii) one-electron capacity. As shown in **reaction 1.2**, the combination of transition metal ions (M=Fe, Co, Ag) with PDS can homogeneously oxidize carbamazepine, trichloroethylene, and triclosan (**Table. 1.3**) (Nfodzo and Choi 2011, Rao et al. 2014, Yuan et al. 2014). Nevertheless, the solution pH should be restricted under acidic conditions because of the inherent nature of metal ions, and the recovery of the catalyst in the form of hydroxide creates chemical sludges that require special disposal practices. It has been well documented that the immobilization of these ions, such as Fe^{2+}, on a solid catalyst makes catalyst recovery highly convenient while maintaining high catalytic activity over a wider pH range (Ma et al. 2019, Yue et al. 2016). Interestingly, the incorporation of CuO into Fe_2O_3 can provide more active sites for PDS adsorption and the subsequent electron transfer from the catalyst to PDS, further

oxidizing 2,4-dichlorophenol at a high rate (Sun et al. 2015). Even though the magnetic properties of some heterogeneous catalysts (e.g., $CuFe_2O_4$) facilitate their separation from the treated water (Li et al. 2019), the disposal of the used catalysts remains a problem. The single-electron transfer mechanism for PDS activation is further discussed in section 1.4.

$$S_2O_8^{2-} + M^{n+} \rightarrow M^{n+1} + SO_4^{2-} + SO_4^{\cdot-} \quad (1.2)$$

Table. 1.3 PDS activation by single electron injection and its application on organic degradation.

Target pollutant	Energy form	Conditions	Ref.
carbamazepine	Fe^{2+}	C(pollutant), 25 μM; [PDS], 1.0 mM; C(catalyst), 250 μM; pH, 3.0	(Rao et al. 2014)
trichloroethylene	Electrogenerated Fe^{2+}	C(pollutant), 0.40 mM; C(PDS), 5 mM; $pH_{initial}$, 5.6.	(Yuan et al. 2014)
triclosan	Ag^{+}	C(pollutant), 115 μM; [PDS], 775 μM; C(catalyst), 775 μM, pH, 7	(Nfodzo and Choi 2011)
triclosan	Co^{2+}	C(pollutant), 115 μM; [PDS], 775 μM; C(catalyst), 775 μM, pH, 7	(Nfodzo and Choi 2011)
polychlorinated biphenyls	ZVI-PDS	C(PDS)=10%;	(Fan et al. 2014)
acid orange 7	Fe_3O_4/MIL-101	C(pollutant), 25 ppm; [PDS], 25 mM; C(catalyst), 1.0 g/L; pH, 3.58	(Yue et al. 2016)
rhodamine B	γ-Fe_2O_3/Mn_3O_4	C(pollutant), 10 ppm; C(PDS), 50 mg/L; C(catalyst), 50 mg/L; pH, 5.1	(Ma et al. 2019)
2,4-dichlorophenol	CuO/Fe_3O_4	C(pollutant), 100 ppm; C(PDS), 10 mM; C(catalyst), 0.624 g/L; pH, 6.8	(Sun et al. 2015)
phenol	$CuFe_2O_4$	C(pollutant), 0.21 mM; C(PDS), 1 mM; C(catalyst), 0.75 g/L; pH, 9.5	(Li et al. 2019)
diethyl phthalate	$CuFe_2O_4$ /MWCNTs	C(pollutant), 285 μg/L; C(PDS), 250 mg/L; C(catalyst), 75 mg/L	(Zhang et al. 2016a)

1.4 Electron-source/single-electron shuttle pairs

The breakup of the peroxide bridge in PDS and the formation of corresponding radicals via an electron transfer mechanism from a single-electron reductant has been extensively investigated (Lee et al. 2020). Ferrous ions (Fe^{2+}) are of great interest for the effective activation of peroxide compounds due to their cost-effectiveness, low toxicity, and high catalytic activity in aqueous ecosystems (Zeng et al. 2019). The chain reactions initiated by Fe^{2+}/PDS pairs (**reactions 1.3–1.9**) are presented below, in which Fe^{2+} can rapidly activate the PDS via **reaction 1.3** (k = 30 M^{-1} s^{-1}) and result in Fe^{3+} accumulation in the aqueous system, while Fe^{2+} regeneration remains at a low rate as Fe^{2+} is involved in the continuous catalysis of the PDS oxidation process (**reactions 1.6** and **1.9**).

$Fe^{2+} + H_2O_2 \rightarrow Fe^{3+} + \cdot OH + OH^-$ (1.3) (Georgi et al. 2016)
$Fe^{2+} + S_2O_8^{2-} \rightarrow Fe^{3+} + SO_4^{\cdot-} + SO_4^{2-}$ (1.4) (Woods et al. 1963)
$S_2O_8^{2-} + SO_4^{\cdot-} \rightarrow S_2O_8^{\cdot-} + SO_4^{2-}$ (1.5) (Liu et al. 2014)
$Fe^{3+} + S_2O_8^{2-} \rightarrow Fe^{2+} + S_2O_8^{\cdot-}$ (1.6) (Liang and Su 2009b)
$2S_2O_8^{2-} + 2H_2O \rightarrow 3SO_4^{2-} + SO_4^{\cdot-} + O_2^{\cdot-} + 4\,H^+$ (1.7) (Furman et al. 2010)
$S_2O_8^{2-} + 2H_2O \rightarrow 2SO_4^{2-} + HO_2^- + 4\,H^+$ (1.8) (Furman et al. 2010)
$Fe^{3+} + O_2^{\cdot} \rightarrow Fe^{2+} + O_2$ (1.9) (Kwan and Voelker 2002)

Several approaches have been developed for accelerating the Fe^{3+}/Fe^{2+} cycle by introducing another electron donor (**Table 1.4**). For example, Liang and Guo (2010) reported that iron can serve as an electron source by reducing two moles of Fe^{3+} to produce three moles of Fe^{2+} (**reaction 1.10**). Therefore, the Fe^{3+}/PDS coupled with zero-valent iron (ZVI) ZVI induced a substantial oxidation of naphthalene particles (Liang and Guo 2010), cyclohexanoic acid (Drzewicz et al. 2012), and naphthenic acids, as well as the sterilization of the ballast water (Ahn et al. 2013). As the reaction proceeds, the Fe^{2+} gradually produced from the ZVI can accelerate radical production and abatement of organic pollutants (Zhou et al. 2008). Another promising electron donor is the cathode in an electro-reductive system, which is deemed a green electron source owing to its reagent-free property and zero-generation of byproducts (Wu et al. 2012). To enhance the Fe^{2+} regeneration, using a cathode with a high surface area, such as graphite, carbon fiber paper, or carbon felt, highly mitigated the mass transfer problem of iron ions on the cathode–solution interface (Chu et al. 2012). Recently, Xing et al. (2018) employed transition metal dichalcogenides (TMDCs, MoS_2, and WS_2) as a cocatalyst for Fenton or Fe^{2+}/PMS processes, where the exposure of reductive W^{4+}/Mo^{4+} active sites on the surface of WS_2/MoS_2 can greatly accelerate the rate-limiting step of the Fe^{3+}/Fe^{2+} conversion, which plays a vital role in the decomposition of H_2O_2/PMS and degradation of phenol/aromatic organics. A 3D-MoS_2 sponge loaded with MoS_2 nanospheres and graphene oxide (GO) was fabricated to maintain the Fe^{3+}/Fe^{2+} in a stable dynamic cycle, effectively promoting the oxidative degradation of various aromatic compounds (Zhu et al. 2020).

$Fe^0 + 2Fe^{3+} \rightarrow 3\,Fe^{2+}$ (1.10)
$Fe^{3+} + e^- \rightarrow Fe^{2+}$ (1.11)

It has been demonstrated that PDS can be continuously activated using the Fe^{2+}/Fe^{3+} pair as a single-electron transferring media and reductant as an electron source, where the iron concentration can be decreased to a low level and requires no further elevation regardless of the concentration of the organic compounds. More electron-source/M^{n+1} pair have been proposed for activating other peroxide compounds, such as H_2O_2 and PMS. As mentioned above, cathode/Fe^{3+} is a commonly used pair for initiating H_2O_2-based AOP at trace levels of dissolved iron, which is well-known as the electro-Fenton process (Chu et al. 2012). Applying the proper potential (e.g., −0.8 V on the graphite cathode) can steer the reactions on the cathode surface toward the desired Fe^{2+} regeneration and off the undesired hydrogen evolution. Another potential clean reductant is active H_2 on a Pd catalyst, which allows the production of $^{\bullet}OH$ via the Fe^{2+}/H_2O_2 catalyst/oxidant pair for rapid decontamination (Georgi et al. 2016). Researchers have explored other zero-valent metals as the electron source. Metallic Mo and Fe/Cu alloys not only induced the conversion of Fe^{3+} to Fe^{2+} but also promoted other processes for the synergetic oxidation of the targeted pollutants, such as singlet oxygenation ($^1O_2$) triggered by superoxide radicals on Mo and CuO-based Fenton oxidation on Fe/Cu alloys (Yamaguchi et al. 2018, Yi et al. 2019).

In 2011, Ma et al. (2011) first reported a homogeneous reductant (Hydroxylamine, NH_2OH, HA) to facilitate the Fe^{3+}/Fe^{2+} redox cycles, completely eliminating the limitations posed by mass transfer. The rapid degradation of benzoic acid (BA) was observed when HA was introduced into the Fenton process. The HA/Fe^{3+} electron-source/M^{n+1} pair was also employed to activate PMS and PDS (Li et al. 2020, Zou et al. 2013). This impeded the application of HA in these processes because the end products of HA degradation were confirmed to be NO_3^- and N_2O that are toxic and should be ideally be removed; however, the research determined a different but feasible route for minimizing iron sludge production. Other non-toxic reductants, such protocatechuic acid and ascorbic acid, have also been explored for application as electron sources (Lei et al. 2015, Shi et al. 2019); however, these compounds consumed reactive radicals instead of facilitating Fe^{3+} reduction (Li et al. 2020). The reactions of the reductant with both Fe^{3+} and radicals induced a requirement for a higher dosage of oxidants for degrading the targeted pollutants. Applying a ternary system to water purification necessitates another ideal reductant that is inherently non-toxic and forms non-toxic products.

In terms of the one-electron transferring media, the Cu^{2+}/Cu^{+} pair in the bulk solution has frequently been reported to be a viable substitute for Fe^{3+}/Fe^{2+} (Chi et al. 2019). Although some transitional metal ions exhibit the potential to play the role of M^{n+}/M^{n+1}, no further research has determined their performance on the single-electron transfer from the electron source to peroxide compounds, primarily because they belong to the metal type and have the inherent shortcomings of requiring a narrow pH range and post-treatment for catalyst removal. Tao et al. (2015) proposed using devolved oxygen for delivering the photoelectron from the g-C_3N_4 photocatalyst to PMS via a Haber-Weiss-like reaction (**reactions 1.12 and 1.13**). Unfortunately, more research is required regarding the use of this metal-free agent as single-electron transferring media. Therefore, the current research

Table. 1.4 Ternary systems reported in literatures.

Electron source	M^{n+}/M^{n+1}	Peroxide compound	Conditions	Ref.
cathode	Fe^{2+}/Fe^{3+}	H_2O_2	$\Delta C/C_0$(pollutant), 98%; j, 16.8mA/cm^2; C(Fe), 1 mM; C(oxidant), 12 mM; 60 min	(Chu et al. 2012)
ZVI	Fe^{2+}/Fe^{3+}	H_2O_2	$\Delta C/C_0$(pollutant), 100%; C(ZVI), 1g/L; C(oxidant), 15 mM; 10 min	(Zhou et al. 2008)
H_2/Pd	Fe^{2+}/Fe^{3+}	H_2O_2	$\Delta C/C_0$(pollutant), 100%; C(Pd), 5mg/L; C(Fe), 1 ppm; C(oxidant), 15 mM; 90 min	(Georgi et al. 2016)
Mo	Fe^{2+}/Fe^{3+}	H_2O_2	$\Delta C/C_0$(pollutant), 100%; C(Mo), 5mg/L; C(Fe), 4 ppm; C(oxidant), 0.4 mM; 5 min	(Yi et al. 2019)
Fe/Cu bimetal	Fe^{2+}/Fe^{3+}	H_2O_2	$\Delta C/C_0$(pollutant), 100%; C(Fe/Cu), 0.22g/L; 35 min	(Yamaguchi et al. 2018)
MoS_2	Fe^{2+}/Fe^{3+}	H_2O_2	$\Delta C/C_0$(pollutant), 100%; C(Fe), 0.4 ppm; C(oxidant), 4 µL; 5 min	(Zhu et al. 2020)
MoS_2	Fe^{2+}/Fe^{3+}	PMS	$\Delta C/C_0$(pollutant), 100%; C(Fe), 0.4 ppm; C(oxidant), 4 µL; 5 min	(Zhu et al. 2020)
WS_2	Fe^{2+}/Fe^{3+}	H_2O_2	$\Delta C/C_0$(pollutant), 40%; C(WS_2), 4 g/L; C(Fe), 8 ppm; C(oxidant), 4 µL; 5 min	(Dong et al. 2018)
HA	Fe^{2+}/Fe^{3+}	H_2O_2	$\Delta C/C_0$(pollutant), 84%; C(HA), 0.4mM; C(Fe), 0.6ppm; C(oxidant), 0.32mM; 15 min	(Chen et al. 2011)
HA	Fe^{2+}/Fe^{3+}	PMS	$\Delta C/C_0$(pollutant), 74%; C(HA), 0.4mM; C(Fe), 0.6ppm; C(oxidant), 0.4mM; 10 min	(Zou et al. 2013)
HA	Fe^{2+}/Fe^{3+}	PDS	$\Delta C/C_0$(pollutant), 62%; C(HA), 1.4mM; C(Fe), 0.6ppm; C(oxidant), 1mM; 10 min	(Li et al. 2020)
HA	Cu^{+}/Cu^{2+}	PMS	$\Delta C/C_0$(pollutant), 90%; C(HA), 1 mM; C(Fe), 0.64ppm; C(oxidant), 0.5mM; 10 min	(Chi et al. 2019)
Cu/graphene	Cu^{+}/Cu^{2+}	H_2O_2	$\Delta C/C_0$(pollutant), 88%; C(Cu/Graphene), 0.5g/L; 60 min	(Xu et al. 2019)
Photo-electron	$O_2/O_2^{\bullet-}$	PMS	$\Delta C/C_0$(pollutant), 95%; C(C_3N_4), 0.4 g/L; C(oxidant), 0.4g/L; 30 min	(Tao et al. 2015)

focuses on the exploration of other metal-free media for this model to develop a non-toxic oxidation system.

$$O_2 + e^- \rightarrow O_2^- \quad (1.12)$$

$$O_2^- + HSO_5^- \rightarrow {}^{\bullet}OH + SO_4^{2-} + O_2 \quad (1.13)$$

In the developed ternary system, the electron flow from the electron source to peroxide compounds using M^{n+1}/M^n as a single-electron shuttle is highly desired, whereas the direct redox reaction between the electron source and peroxide compounds is unwanted. The later decomposition route of peroxide compounds may waste their oxidation capacity without producing oxidative radicals, inducing a low C(pollutant)/C(peroxide) ratio in the AOPs. From this perspective, PDS has a higher application potential than PMS and H_2O_2 owing to its extremely high stability. For example, the ratio of C(BA)/C(peroxide) in the HA/Fe^{3+}/PDS system was determined to be 15% (Li et al. 2020), while the ratios in the HA/Fe^{3+}/PMS and HA/Fe^{3+}/H_2O_2 systems were only 10% and 7.5%, respectively (Chen et al. 2011, Zou et al. 2013). The higher ratio of C(pollutant)/C(peroxide) indicates the inert property of PDS towards HA. Similar results were also observed with another potential electron source (HSO_3^-), which could readily quench the PMS and H_2O_2 but reacted relatively slowly with PDS (Qi et al. 2017).

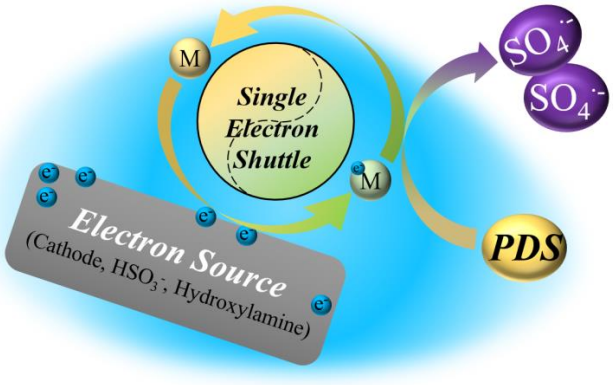

Figure 1.3 Schematics of ternary system for yielding $SO_4^{\bullet-}$ from PDS.

1.5 Aim & Research

In this study, the cathode was selected as the electron source in the electrochemical/ photoelectrochemical system, and the Cu^+/Cu^{2+}, Fe^{2+}/Fe^{3+}, and H^*/H^+ pairs were explored to ensure continuous injection of single-electron into the PDS. The results indicated that Cu^+, Fe^{2+}, and H* could readily activate the PDS and yield a large amount of $SO_4^{\bullet-}$. In the ternary system (**Figure 1.3**), the catalyst dosage could be reduced to a minimum value (using the Cu^+/Cu^{2+} and Fe^{2+}/Fe^{3+} pairs as single-electron transferring

media) and even a reagent-free process, using H* as an activator, could be achieved. In comparison with other activation approaches using transitional-metal-containing catalysts, PDS activation by the cathode prevents the costly transportation and storage of the activators as well as the downstream treatment required for the removal of the byproducts. The results presented in this thesis put forth a highly improved application potential of PDS oxidation.

2 Methodology

2.1 Chemicals & Materials

2.1.1 Chemical reagents

Table. 2.1 chemical reagents and their abbreviation.

No.	Chemical reagents	Abbreviation
1	Copper sulfate	$CuSO_4$
2	Sodium peroxydisulfate	$Na_2S_2O_8$, PDS
3	Sodium sulfite	Na_2SO_3
4	Sodium sulfate	Na_2SO_4
5	Ethylenediaminetetraacetic acid disodium salt	Na_2EDTA
6	Diclofenac sodium	$C_{14}H_{10}C_{l2}NNaO_2$
7	Bismuth(III) nitrate pentahydrate	$Bi\ (NO_3)_3 \bullet 5H_2O$
8	Molybdenum oxide	MoO_3
9	Diethylenetriaminepentaacetic acid	$C_{14}H_{23}N_3O_{10}$
10	Diethanolamine	$C_4H_{11}NO_2$
11	Sodium acetate anhydrous	CH_3COONa
12	Acetic acid	CH_3COOH
13	5, 5-dimethyl-1-pyrrolidine N-oxide	DMPO
14	Benzoic acid	BA
15	Ferric sulfate	$Fe_2(SO_4)_3$
16	Methanol	
17	Tert-butyl alcohol	TBA
18	Potassium iodide	KI
19	Potassium biphthalate	
20	phenol	
21	2,4-dichlorophenol	2,4-DCP
22	Carbamazepine	CBZ
23	Methylene blue	
24	Methyl phenyl sulfoxide	PMSO
25	Methyl phenyl sulfone	$PMSO_2$
26	Phenylsulfinic acid	$PhSO_2$
27	bisphenol	

2.1.2 Material preparation

The TiO_2 photoanode was prepared via the dip-coating method described by Shang et al. (Shang et al. 2003). A γ-Bi_2MoO_6/ITO photoanode was fabricated by depositing a Bi_2MoO_6 film onto an indium tin oxide (ITO) substrate from an amorphous heteronuclear complex solution using the dip-coating method. The Pd/Al_2O_3 catalyst was purchased from Sigma Aldrich (Finland) (10% Pd loading on Al_2O_3).

2.2 Reactor configurations

2.2.1 Photoelectrocatalytic reactor

In the first part, the photoelectrocatalytic (PEC) experiments in batch mode were performed in an undivided cell with a volume of 500 mL. A tubular TiO_2/Ti mesh electrode (50 mm diameter) was used as the anode, and the TiO_2 film was deposited onto the Ti plate via the dip-coating method described by Shang et al. (Shang et al. 2003). Tubular mesh stainless steel (66 mm) was used as the cathode. The gap between the anode and cathode was 8 mm. A UV lamp (main wavelength 254 nm; 9 W) in a quartz tube was placed in the center of the tubular TiO_2/Ti mesh electrode.

For the second experiment, the batch experiments were carried out using a divided quartz reactor of 54 mm × 50 mm × 60 mm. The reactor contained a 120 mL solution containing DCF (10 ppm) as the target contaminant. The PEC reaction was driven by an electrochemical workstation (CHI 660E, Shanghai Chenhua Instruments Co., Ltd) connected to a γ-Bi_2MoO_6 photoelectrode as the working electrode, a counter electrode, and a reference electrode (Ag/AgCl). The visible light source was a Xe lamp (PLS-SXE300; Beijing PerfectLight Co., Ltd, Beijing, China) with a UV cutoff filter (λ > 420 nm).

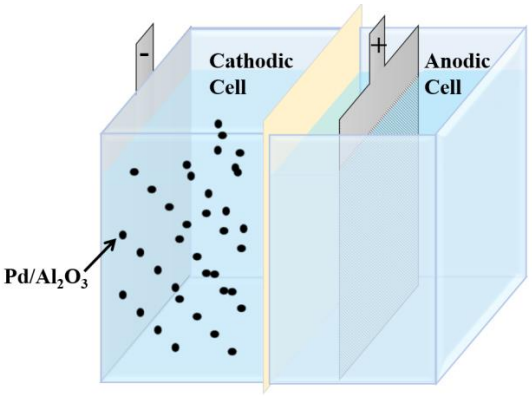

Figure 2.1 Schematic diagram of the two-cell electrochemical reactor for batch experiments.

2.2.2 Electrocatalytic reactor

The electrocatalytic reaction was conducted in a divided two-cell reactor, as shown in **Figure 2.1**. The model pollutant and Pd/Al_2O_3 catalyst were added to the cathodic cell simultaneously. The electrocatalytic experiments in this study were carried out under a deoxygenated atmosphere.

2.3 Analytical method

2.3.1 Organic detection

The concentration of the model contaminants was confirmed by high performance liquid chromatography (HPLC), equipped with a C18 column and UV detector. The specific details for the HPLC analysis of the organics are listed in **Table 2.1**.

Table 2.1 Analysis details of model contaminants by HPLC

Pollutant	Mobile phase (%)				λ
	Methanol	Acetonitrile	Acetic acid (0.1%)	Water	
Cu-complexes		8	92		254 nm
Diclofenac	50		50		228 nm
BA	50		50		228 nm
PMSO		20	80		230 nm
$PMSO_2$		20	80		230 nm
2,4-DCP	70			30	284 nm
phenol	80			20	272 nm
BPA	80			20	276 nm
Carbamazepine		60		40	285 nm

2.3.2 Analytical method

PDS concentration was determined using modified iodometry. For the method, Chromogenic agent A (potassium biphthalate, 0.1 M) and Chromogenic agent B (potassium iodide, 0.4 M; NaOH, 0.06 M; ammonium molybdate, 10^{-4} M) were prepared in deionized water, firstly, and then, aliquots (1.5 ml) of the samples were added in a 5-mL centrifuge tube with 0.75 ml of Chromogenic agent A and 0.75 ml of Chromogenic agent B. After waiting for 60 min (until the absorbance of the treated solution was stable), the absorbance of the treated solution was measured using a UV spectrophotometer (Hitachi U-3010) at λ = 352 nm. The Cu^{2+} concentration and the concentrations of other

metals were measured using a 700 series inductively coupled plasma-optical emission spectrometer (ICP-OES, Agilent Technology). Total organic carbon (TOC) content was determined using a Shimadzu TOC analyzer (TOC-VCPH, Shimadzu, Japan).

Electrochemical characterizations, including linear sweep voltammetry (LSV) and cyclic voltammetry (CV), were conducted in a single-compartment, three-electrode cell on a CHIN800D instrument (CH Instrument Co.). The morphologies of the materials were characterized using a JSM 6301 scanning electron microscope (SEM). X-ray photoelectron spectroscopy (XPS) was used to analyze the surface of the electrode using a PHI Quantera SXM (PHIEnvironmental 5300/ESCA, ULVAC-PHI, Inc.). The phase composition of the synthesized catalyst was studied using X-ray diffraction (XRD, PANalytical) with Co-Kα radiation ($\lambda = 0.1789$ nm, at 40 kV and 40 mA) over a 2θ range of 10–120°, with a step size of 0.02° and scan speed of 2°/min. Using DMPO as the trapping agent, active radicals were identified with electron spin resonance (ESR) on a Bruker ESR 300E with a microwave bridge (receiver gain, 1 × 105; modulation amplitude, 2 G; microwave power, 10 mW; modulation frequency, 100 kHz).

3 Result & Discussion

3.1 PDS activation by cathodic reduction

3.1.1 Enhanced decomplexation of Cu-EDTA and simultaneous Cu recovery in the PEC system with addition of PDS

The existence of Cu ions in the effluents from the electroplating, mining, and photographic industries makes the removal of organic contaminants via traditional biological processes challenging (Lopez-Munoz et al. 2009). In particular, the formation of stable Cu complexes (Cu-EDTA or $Cu(CN)_x$) results in the impossible pre-abatement of Cu ions and subsequent removal of organics (Pirkanniemi et al. 2007, Tunay and Kabdasli 1994). In the works of Zhao et al., PEC processes have exhibited the destruction of the chelating agents via oxidation by photogenerated holes or •OH generated from the semiconductor photoanode, with simultaneous Cu recovery via cathodic reduction (Zhao et al. 2014a, Zhao et al. 2013, Zhao et al. 2015). Unfortunately, the PEC oxidation of metal complexes only occurred around the photoanode with a low oxidation efficiency, necessitating a long retention time for a better performance in treating Cu complexes (**Figure 3.1a**). At a current density of 0.2 mA/cm^2 for 60 min, the removal efficiency of the Cu complexes was only 21.6% in the PEC system using a TiO_2-coated electrode as the photoanode for oxidizing Cu-EDTA and a stainless-steel cathode for Cu reduction. With the introduction of 5 mM PDS into the PEC system (PEC/PDS), the removal efficiency of Cu complexes was increased to 98.4%. Correspondingly, the recovery percentages of Cu^{2+} were elevated to 98.9% from 20.6% within 60 min. Meanwhile, the TOC variations in these processes were further compared, and the higher TOC removal in the PEC/PDS system (52.1%) compared with the PEC system (9.35%) indicated improved oxidation performance of the former.

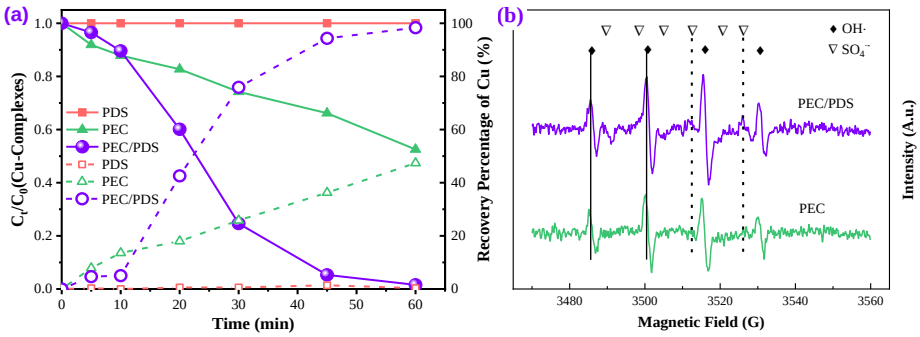

Figure 3.1 (a) System comparison for Cu-EDTA decomplexation and Cu recovery; ([Cu-EDTA], 0.2 mM; [PDS], 5 mM; initial solution pH, 3.0; current density, 0.2 mA/cm^2) (b) reactive oxygen radical analysis by ESR technology.

The enhancement of the oxidation and mineralization capacity of the PEC/PDS system might be ascribed to the increasing radical concentration, which could be verified by ESR analysis using DMPO as a radical trapping agent. As shown in **Figure 3.1b**, the hyperfine splitting constants of DMPO-$^{\bullet}$OH can be observed in the PEC system, indicating the generation of $^{\bullet}$OH on the TiO_2 photoanode under UV radiation (Danilczuk et al. 2009, Laine et al. 2008). With the addition of PDS, the signal of DMPO-$^{\bullet}$OH increased, and another signal of DMPO-$SO_4^{\bullet-}$ appeared. According to previous studies, the improvement in the $SO_4^{\bullet-}$ concentration could contribute to the photolytic formation of $SO_4^{\bullet-}$ using PDS as the parent oxidant (**Reaction 1.1**). Meanwhile, the unstable DMPO-$SO_4^{\bullet-}$ could be readily transformed into DMPO-$^{\bullet}$OH in the water [3], inducing the signal enhancement of DMPO-$^{\bullet}$OH.

3.1.2 Cathodic activation of PDS via single-electron transfer

The impact of the $S_2O_8^{2-}$ concentration and current density on the degradation of Cu-EDTA and Cu recovery was studied to optimize the conditions for the PEC/PDS process. The performance of the PEC/PDS system as a function of time was studied with varying PDS concentrations (**Figure 3.2a**). The decomplexation ratios of the Cu complexes with the initial PDS concentrations of 0, 5, 20, and 50 mM were 27.4%, 98.4%, 88.1%, and 57.7%, respectively. According to the results, the optimal dosage of PDS for Cu-complex abatement was 5 mM. A similar trend was observed for Cu recovery. Meanwhile, the effect of current density on the performance of the PEC/PDS process (**Figure 3.2b**) suggested that a higher current density induced better performance in the removal of Cu complexes and simultaneous recovery of Cu. By applying 1.0 mA/cm^2 in the PEC/PDS system, the complexation of Cu-EDTA and Cu recovery on the cathode could be completed within 45 min.

Additionally, as evident from **Figure 3.2a** and **3.2b**, the decomposition of Cu complexes and Cu recovery could be noticeably divided into two phases based on the kinetics. In the lag phase, Cu-complex removal and Cu recovery proceeded at a low rate, then subsequently increased significantly. As shown in **Figure 3.2a**, the transition points between the two phases appeared at 10 min, 20 min, and 45 min, when the initial concentrations of PDS were 5 mM, 20 mM, and 50 mM, respectively. The lag phase continued for a longer time with higher concentrations of PDS. Notably, the reaction rate remained relatively stable in the PEC process without PDS. In **Figure 3.2b**, the rate increased at 60 min, 30 min, 10 min, and 10 min with the current densities of 0.1 mA/cm^2, 0.2 mA/cm^2, 0.5 mA/cm^2, and 1.0 mA/cm^2, respectively. Thus, we can conclude that the reaction time of the initial stage had a positive correlation with the initial concentration of PDS, while it was negatively correlated with the current density.

Based on the lag time analysis, PDS reduction on the cathode may have occurred, which was further confirmed by LSV analysis of the Cu^{2+}, Cu-EDTA, and $S_2O_8^{2-}$ solutions in 0.1 M Na_2SO_4. It can be seen from Figure **3.2c** that the current increased at a potential lower than 0.05 V, suggesting that the Cu^{2+} reduction began at a potential of 0.05 V vs. Ag/AgCl. Similar analysis for the Cu-EDTA solution demonstrated that the cathodic

reduction of Cu-EDTA began at the potential of -0.25 V. The lower potential of the chelated Cu^{2+} than the free Cu^{2+} indicated an increasing difficulty in the Cu^{2+} reduction induced by complexation. Surprisingly, the PDS reduction started at a potential of 0.20 V. The positive shift in the potential for the PDS reduction implied that PDS could be reduced before the Cu^{2+}/Cu-EDTA reduction.

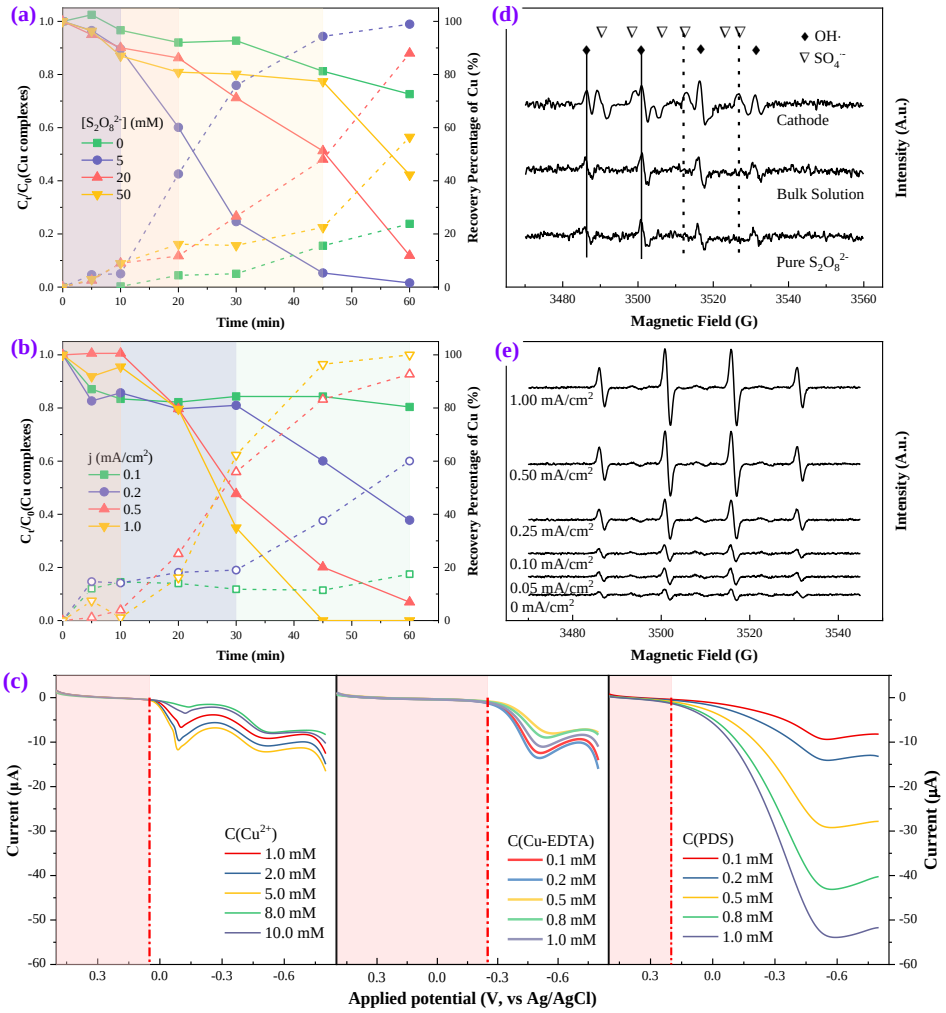

Figure 3.2 Effect of PDS concentration (a) and current density (b) on the PEC/PDS process ([Cu-EDTA], 0.5 mM; [$Na_2S_2O_8$], 10 mM; current density, 0.2 mA/cm^2; initial solution pH, 3.0; current density, 0.2 mA/cm^2); (c) LSV analysis of (a) $S_2O_8^{2-}$, (b) Cu^{2+} and (c) Cu-EDTA in 0.1 M Na_2SO_4 (Solution pH, 3.0); (d) ESR spectra in the bulk solution and around the cathode of the EC/$S_2O_8^{2-}$ process; (e) Effect of the current density on the ESR signals of DMPO-OH at the solution pH of 10.0.

To elucidate the product of the PDS reduction, an ESR analysis was applied at different positions of the electrochemical system with the addition of PDS (EC/PDS). With respect to the EC/PDS process, nearly no enhanced signals of DMPO-$SO_4^{\bullet-}$ and DMPO-$^{\bullet}OH$ in the bulk solution were observed (**Figure 3.2d**). Interestingly, obvious DMPO-SO_4 signals appeared around the cathode, and the intensity of the radicals increased with the current density (**Figure 3.2e**). The results suggest that the PDS could be activated to form $SO_4^{\bullet-}$ via cathodic reduction (**reaction 3.1**).

$$S_2O_8^{2-} + e^- \rightarrow SO_4^{2-} + SO_4^{\cdot-} \quad (3.1)$$

Therefore, in the PEC/PDS process, cathodic activation and UV photolytic activation accelerated the production of active radicals, enhancing the Cu-complex oxidation and Cu recovery performance.

3.1.3 Acidification induced by PDS oxidation

In our previous studies on Cu recovery from the complexed Cu^{2+} by the PEC system, the alkaline or neutral solution pH significantly impeded its cathodic recovery owing to the in situ precipitation of the decomplexed Cu^{2+} onto the Bi_2MoO_6 photoanode in the form of CuO, Cu_2O, or $Cu(OH)_2$ (Zhao et al. 2015). Therefore, in the PEC process employed in the current study, the performance of the decomplexation of Cu-EDTA and Cu recovery deteriorated under alkaline and neutral conditions (**Figure 3.3a**), which can be attributed to the Cu-involved deposition blocking the active sites on the photoanode and thereby decreasing the decomplexation capacity (Zhao et al. 2014b). In contrast, varying the solution pH had a negligible impact on the PEC/PDS process (**Figure 3.3b**), revealing that the addition of $S_2O_8^{2-}$ allows highly efficient Cu-complex decomplexation and Cu recovery over a wide pH range.

Furthermore, the influence of the initial solution pH on the distribution of Cu species was evaluated. In the PEC system, almost no deposition of Cu appeared on the anode, while it increased with an increase in the solution pH (**Figure 3.3c**). The results were identical to those of a previous study by Zhao et al. (2015). With the addition of PDS, the Cu precipitation exhibited considerably different behaviors with varying initial solution pH. Only 1.71%, 1.18%, and 0.511% Cu was precipitated on the anode with the solution pHs of 3.0, 7.0, and 11.0, respectively. The recovery ratios of Cu were determined to be 61.9%, 59.8%, and 53.2%, respectively. Furthermore, in contrast to the Cu(II) precipitation on the anode of the PEC system, the Cu species on the cathode were determined to be the desired Cu(0) in the PEC/PDS system (XPS analysis in **Figure 3.3e**).

The variations in the solution pH throughout the PEC/PDS processes were also monitored. As shown in **Figure 3.3d**, the solution pH values in the PEC processes were stable at their initial values, with a slight decrease. In contrast, the solution pH rapidly decreased to approximately 2.1 in the PEC/PDS processes with various initial pHs. Due to the narrow gap in the redox potential between $SO_4^{\bullet-}$ (2.5–3.1 V) and $^{\bullet}OH$ (1.8–2.7 V), we attributed the acidification to the inter-conversion of $SO_4^{\bullet-}$ to $^{\bullet}OH$ as shown in **reaction 3.2** (Liang

and Su 2009a). The reaction revealed that the produced $SO_4^{\bullet-}$ was transformed into $^{\bullet}OH$ by reacting with OH^-. Consequently, the solution pH decreased during the initial phase. The acidic conditions facilitate the decomplexation and Cu recovery process better than the alkaline conditions (Zhao et al. 2013).

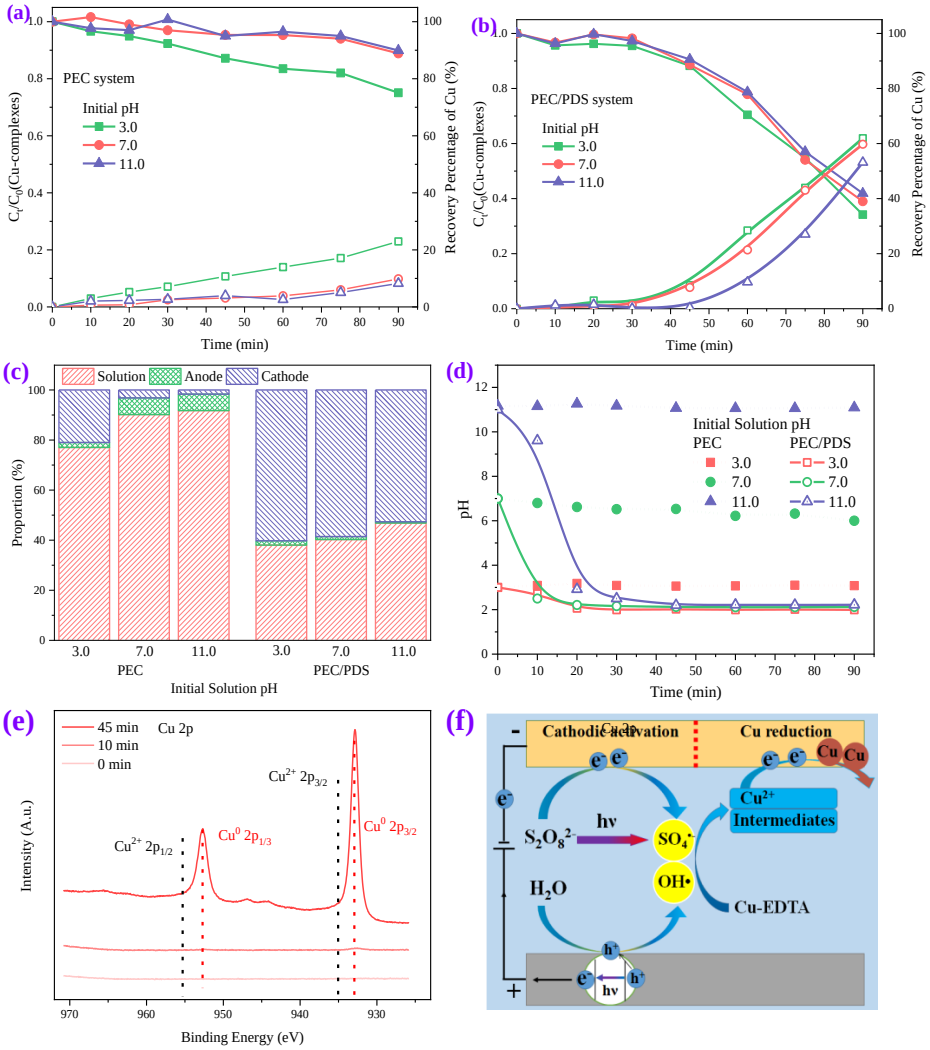

Figure 3.3 Effect of initial solution pH on the Cu-EDTA decomplexation and Cu recovery in PEC system (a) and PEC/PDS system (b); (c) The copper mass balance and (d) variation in the solution pH in the PEC process and the PEC/$S_2O_8^{2-}$ process under various initial solution pHs. ([Cu-EDTA], 1.0 mM; [$Na_2S_2O_8$], 50 mM; current density, 0.2 mA/cm^2); (e) XPS analysis of the titanium cathode at different reaction times in the PEC/$S_2O_8^{2-}$ process; (f) Schematic of the PEC/$S_2O_8^{2-}$ process.

$$SO_4^{\bullet-} + OH^- \rightarrow {}^{\bullet}OH + SO_4^{2-} \quad (3.2)$$

In conclusion, Cu-EDTA was oxidized and decomposed by $SO_4^{\bullet-}$ through UV photolysis and cathodic reduction of PDS. With the destruction of the EDTA structure, Cu^{2+} was liberated. Meanwhile, the conversion of $SO_4^{\bullet-}$ to $^{\bullet}OH$ rapidly created an acidic condition against the precipitation of the liberated Cu^{2+}. Once the $S_2O_8^{2-}$ ions were consumed, the cathodic reduction of the Cu^{2+} ions dominated the cathodic reaction. The Cu^{2+} ions were efficiently deposited onto the cathode, followed by Cu^0 electroreduction.

3.2 Enhanced cathodic activation of PDS mediated by Cu^+/Cu^{2+} pair

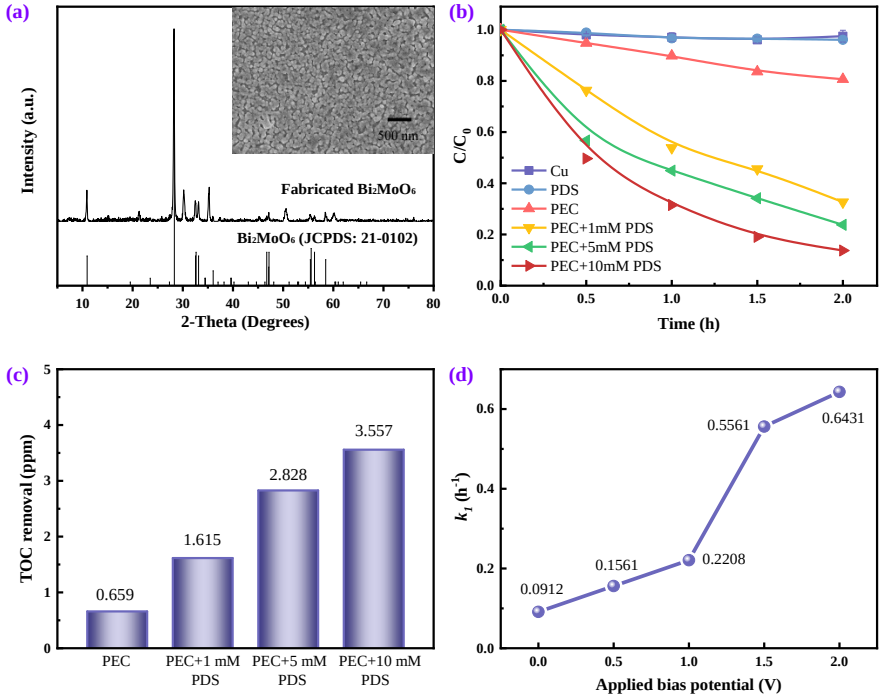

Figure 3.4 (a) Characterizations of Bi_2MoO_6 photoanode; (b) Variations in diclofenac sodium degradation efficiency in various systems; (c) TOC removal in various systems; (d) First-order kinetic rate constants of diclofenac degradation in the PEC/PDS system with different applied potentials. ([Diclofenac], 10 mg/L; initial solution pH, 5.62; applied potential, 1.5 V)

3.2.1 Enhanced degradation of organic compounds

In this work, a visible-light-sensitive photoanode (γ-Bi_2MoO_6) was fabricated (Zhang et al. 2011). As shown in **Figure 3.4a** (insert), a chapped surface, which was identical to the assembled particles in other studies (Dong et al. 2014), of the Bi_2MoO_6 membrane on the electrode was observed through SEM analysis. Furthermore, the XRD analysis revealed

that the peaks of the prepared electrode were in line with the Bi_2MoO_6 standard (JCPDS: 21-0102). Both the sharpness of the XRD reflections and the small half peak width demonstrated the high crystallinity of the desired photocatalyst on the synthesized photoanode. Corresponding to the cell parameters (a = 5.50, b = 16.24, c = 5.49), the resulting crystalline phase could be confirmed as an orthorhombic structure.

Using the prepared photoanode and Cu cathode, the performance of the PEC/PDS system on diclofenac degradation was investigated. The degradation efficiency of diclofenac after 2 h was significantly improved to 67.35% with the addition of 1 mM PDS into the PEC system, compared with 3.04% removal in the individual PDS oxidation and 19.35% in the PEC process (**Figure 3.4b**). With an increase in the PDS dosage to 10 mM, the treatment efficiency also improved to 86.28%. Accordingly, the TOC removal was also improved from 0.659 ppm to 3.557 ppm with the addition of 10 mM PDS. Furthermore, the applied potential displayed a positive relationship with the first-order kinetic constant of diclofenac degradation.

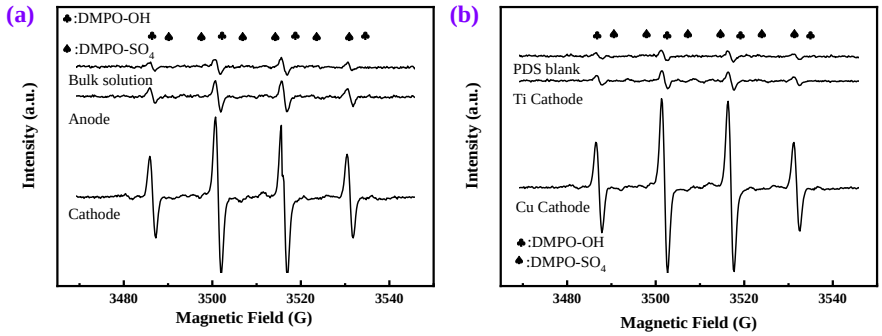

Figure 3.5 (a) ESR analysis in bulk solution, near the anode and cathode in the Bi_2MoO_6/Cu/PEC/PDS system; (b) ESR analysis of the PDS aqueous solution, near the cathodes of the Bi_2MoO_6/Ti/PEC/PS system and the Bi_2MoO_6/Cu/PEC/PDS system.

Positive effects of the applied potential and PDS dosage on the diclofenac degradation suggested that the enhanced performance may be ascribed to the PDS activation by the Cu cathode. This could be confirmed by ESR analysis using DMPO as a trapping agent for the radicals (Zeng et al. 2016). As shown in **Figure 3.5a**, DMPO-$^{\bullet}$OH and DMPO-SO_4 were observed in the bulk solution and near the anode/cathode, indicating the generation of $^{\bullet}OH$ and $SO_4^{\bullet-}$ with the PDS addition into the PEC system. Interestingly, the concentrations of $^{\bullet}OH$ and $SO_4^{\bullet-}$ were higher than those in the bulk solution and near the anode. The ESR signals around the Cu cathode were even higher than those around the Ti cathode, indicating the presence of a new single-electron medium when Cu was employed in the PEC/PDS system.

3.2.2 Cu^{+}/Cu^{2+} cycle for cathodic activation of PDS

To explore the essential medium for the signle-electron transfer from the cathode to the PDS, we further investigated the changes to the Cu cathode. Interestingly, the fresh Cu foil cathode gradually became dark red during the PEC/PDS process. The surface change of the Cu foil was first determined by SEM analysis. As shown in **Figure 3.6a**, the surface of the unused foil was relatively smooth, except for some scratches caused by the Cu foil pretreatment by sandpaper polishing. In contrast, a porous structure was observed on the Cu cathode after the reaction (**Figure 3.6b, c**), implying the generation of a new layer.

Comparing the XRD results of the fresh and used Cu foils revealed that a new peak at 335.1 eV was observed on the Cu foil used in the PEC/PDS process, which was assigned to the newly created Cu(II) on the Cu(0) substrate (952.5 eV and 932.6 eV) (**Figure 3.6d**) (McIntyre et al. 1981, Miller and Simmons 1993, Wagner 1975). Moreover, the XRD analysis (**Figure 3.6e**) revealed that Cu_2O may be simultaneously produced on the Cu foil, owing to the uniformity of the detected XRD signals with the Cu_2O standard (JCPDS: 78-2076). These results demonstrate that the porous structure of the Cu cathode may be induced by the generated Cu(II)/Cu(I) in the PEC/PDS process, and the Cu(I)/C(II) on the Cu substrate may act as a single-electron medium. To further confirm the results, in situ Raman spectroscopy was employed to determine the copper species variations durng the PEC/PDS process. As shown in **Figure 3.6f**, no signals were detected on the fresh Cu foil. After a 5 min reaction, some Raman peaks appeared at 145, 216, 414, and 624 cm^{-1}, indicating the emergence of Cu_2O (Ren et al. 2015), and the signals became stronger as the reaction progressed.

These results demonstrate that metallic Cu can be oxidized by PDS to form Cu(II)/Cu(I) (**reaction 3.3**), and Cu(I) has been reported to be an efficient activator for peroxide compounds (**reaction 3.5**) (Chi et al. 2019), which may play a role in the single-electron shuttle in this system. The produced Cu(II) was then reduced by photoelectrons, and Cu(I) was continuously regenerated (**reaction 3.4**). Using photoelectrons as the electron donor, the accelerated Cu(II)/Cu(I) cycle as a single-electron transfer channel, and PDS as an oxidant, the PEC/PDS system could continuously output $SO_4^{\bullet-}$ radicals and subsequently degrade diclofenac.

$$Cu + S_2O_8^{2-} \rightarrow Cu(II) + 2\ SO_4^{2-} \quad (3.3)$$

$$Cu(II) + e^- \rightarrow Cu(I) \quad (3.4)$$

$$Cu(I) + S_2O_8^{2-} \rightarrow Cu(II) + SO_4^{\bullet-} + SO_4^{2-} \quad (3.5)$$

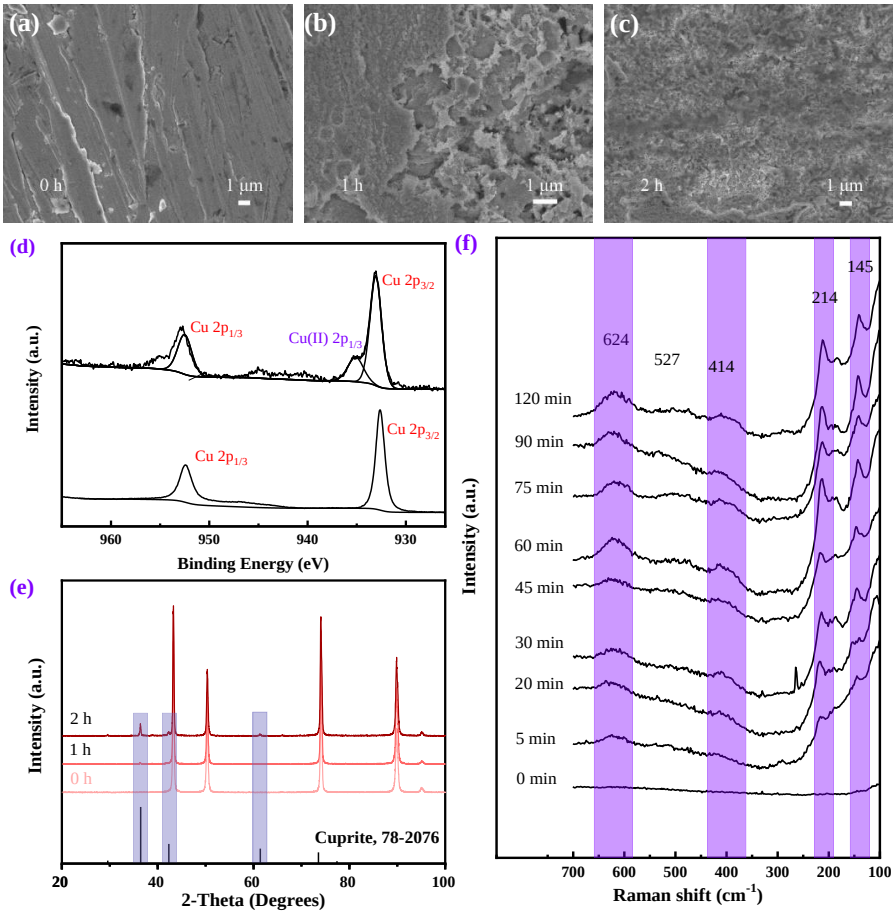

Figure 3.6. (a–c) FE-SEM images of Cu foil at various times in PEC/PDS system; (d) XRD patterns of copper foil at different reaciton times in PEC/PDS system; (f) XPS Cu 2p spectra of the Cu foil before and after the reaction; (g) In situ Raman spectroscopic analysis of the copper cathode during the reaction process. (Applied bias potential, 1.5 V; [PDS], 5 mM; initial solution pH, 5.62)

3.3 Pd/electro-generated H_2 for accelerating Fe^{3+}/Fe^{2+} cycle

3.3.1 Acceleration of Fe^{3+}/Fe^{2+} cycle

Given the hypotoxicity of copper ions (Cu^{2+}/Cu^{+} pairs) that necessitates a strict downstream step for removing the leached Cu, the Fe^{3+}/Fe^{2+} pair was further explored as a more suitable single-electron shuttle. In the electro-Fenton process, where Fe^{3+} can be readily reduced by two-dimensional cathodes in dual/single-cell electrochemical systems, such as graphite, or carbon felt (Barhoumi et al. 2017, Chu et al. 2012, Fleszar and Sobkowiak 1983, Özcan et al. 2008, Panizza and Cerisola 2001, Ridruejo et al. 2018,

Sirés et al. 2007, Sirés et al. 2006, Sudoh et al. 1986), the dissolved iron should meet a concentration requirement (millimolar level) due to the mass transfer limitation. Herein, a three-dimensional electroreduction (3D-ER) system was constructed using commercial Pd/Al_2O_3 as the particle electrode (50 mg/120 mL) that provided a large area and abundant active sites for the Fe^{3+} reactions.

The properties of the Pd/Al_2O_3 particle and the corresponding substrate (α-Al_2O_3) were characterized by SEM, XRD, and XPS analyses. The SEM results (**Figure 3.7a**) demonstrated that, on the smooth surface of the α-Al_2O_3 substrate presented in **Figure 3.7b**, many flower-like particles were successfully attached. These particles were mostly identified as Pd^0 species (340.5 eV, Pd^0 $3d_{2/3}$; 335.2 eV, Pd^0 $3d_{5/3}$) by XPS results (**Figure 3.7c**) (Militello and Simko 1994). Meanwhile, the coverage of the Pd crystals on the surface slightly weakened the Al_2O_3-involving signals (74.7 eV, Al^{3+} 2p; 351.6 eV, O^{2-} 1s; **Figure 3.7c inset**) (Tan et al. 1991). Furthermore, comparing the XRD analysis of the Pd/Al_2O_3 particle with the α-Al_2O_3 substrate, a face-centered cubic structure of the coated Pd catalyst was revealed (**Figure 3.7d**). The peak of Pd/Al_2O_3 (39.4°) could be ascribed to the Pd(111) of the metallic Pd crystal; the exposure of the Pd(111) facet allowed the active sites on the catalyst to trap electrons and produce atomic H* (Quaino and Santos 2015).

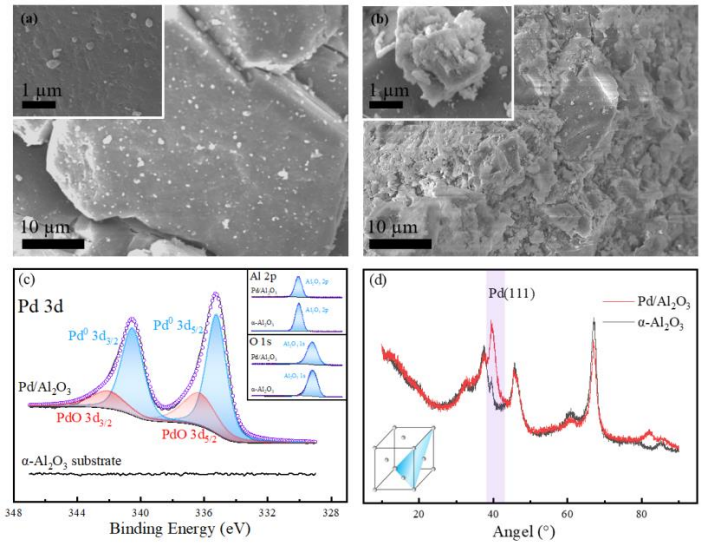

Figure 3.7. SEM images of the α-Al_2O_3 substrate (a) and the Pd/Al_2O_3 catalyst (b); XPS spectra (c) and XRD spectra (d) of α-Al_2O_3 substrate and Pd/Al_2O_3 catalyst.

As expected, an extremely fast reduction of 20 ppm Fe^{3+} (360 μM) in the 3D-ER system occurred with a half-time of approximately 30 s (**Figure 3.8a**), while no variation in the iron species was observed in the absence of the Pd/Al_2O_3 catalyst. To better elucidate the reduction mechanism, we reduced the reaction rate of Fe^{3+} by decreasing the dosage of Pd/Al_2O_3 ten-fold (5 mg/120 mL). It has been well documented that electroreduction can

be achieved via direct electron transfer or an indirect mechanism via atomic H* (Lan et al. 2016, She et al. 2019, Zhao et al. 2014c, Zhou et al. 2019a). In the Pd-involved 3D-ER system, atomic H* can be generated via proton conversion by the electro-induction or dissociative adsorption of electro-generated H_2 (**reactions 3.5 and 3.6**). Ter-butyl alcohol (TBA) was employed to quench atomic H*, subsequently clarifying the importance of two reductive approaches in Fe^{3+} reduction (Lan et al. 2016). As shown in **Figure 3.8b**, strong inhibition of the Fe^{2+} generation occurred with the addition of TBA (36 mM and 360 mM). We further visualized the significance of the two mechanisms by fitting the processes with pseudo-first-order kinetics (**Figure 3.8c**). With the addition of 36 mM and 360 mM of TBA, the reduction kinetics demonstrated a constant decrease by 77.81% and 83.97%, respectively. The decrease in the Fe^{3+} reduction rate confirmed the critical role of atomic H*, as well as the assisted role of the direct electron transfer mechanism.

$$\equiv Pd + H^+ + e^- \rightarrow \equiv Pd\text{-}H^* \quad (3.5)$$

$$\equiv Pd\text{-}H_2 \rightarrow 2 \equiv Pd\text{-}H^* \quad (3.6)$$

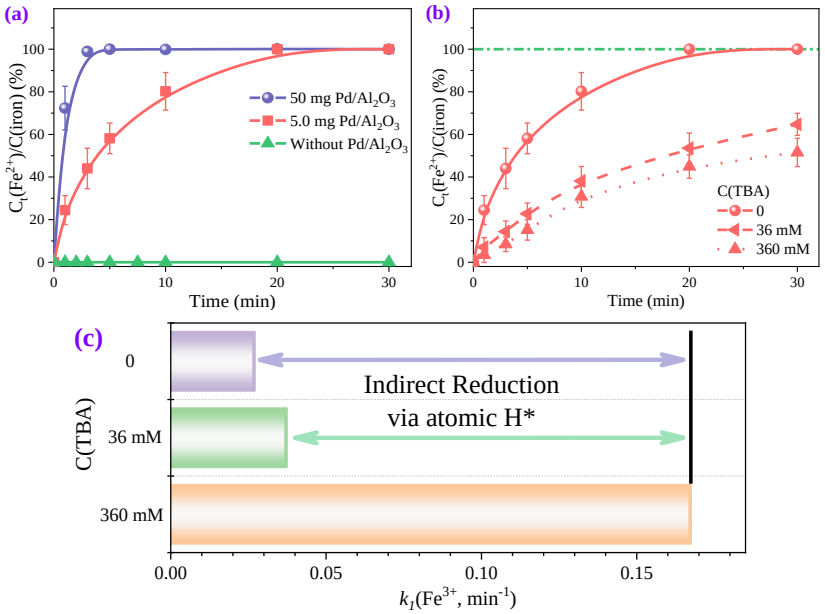

Figure 3.8 (a) Reduction ratio of Fe^{3+} ions in the Pd-EC system (initial solution pH, 3.0; C(iron ions), 360 μM); (b) Quenching experiment on Fe^{3+} reduction by TBA ([Fe^{3+}], 360 μM; [Pd/Al_2O_3], 50 mg/120 ml; current, 0.1 A; initial solution pH, 3.0); (c) First-order kinetic constants for Fe^{3+} reduction.

3.3.2 Enhanced degradation of organic pollutants

As elucidated in **Section 3.3.1**, a stable Fe^{2+} concentration in the solution can be achieved using a cathode as an electron source and Pd/Al_2O_3 as a catalyst for trapping electrons in the form of atomic H*. An experiment for PDS activation (10 mM) under the Pd/Al_2O_3 enhanced electroreduction condition (pH 3.0, deoxygenated atmosphere) was conducted. Removal of organics reached a high level of 80.12% in 120 min (**Figure 3.7a**) when BA was chosen as a radical probe because of its high kinetic constants with $^{\bullet}OH$ and $SO_4^{\bullet-}$ (Lindsey and Tarr 2000, Nate et al. 1977). The acceleration of Fe(III)/Fe(II) by electro-generated H_2 induced the continuous activation of PDS to enhance the degradation of BA. Both $^{\bullet}OH$ and $SO_4^{\bullet-}$ in the enhanced system were determined by ESR analysis (**Figure 3.7b**). Meanwhile, with the addition of ethanol as a radical quenching agent (Zeng et al. 2019), the BA degradation was highly inhibited, indicating the vital role of these radicals in the BA oxidation process (**Figure 3.7c**).

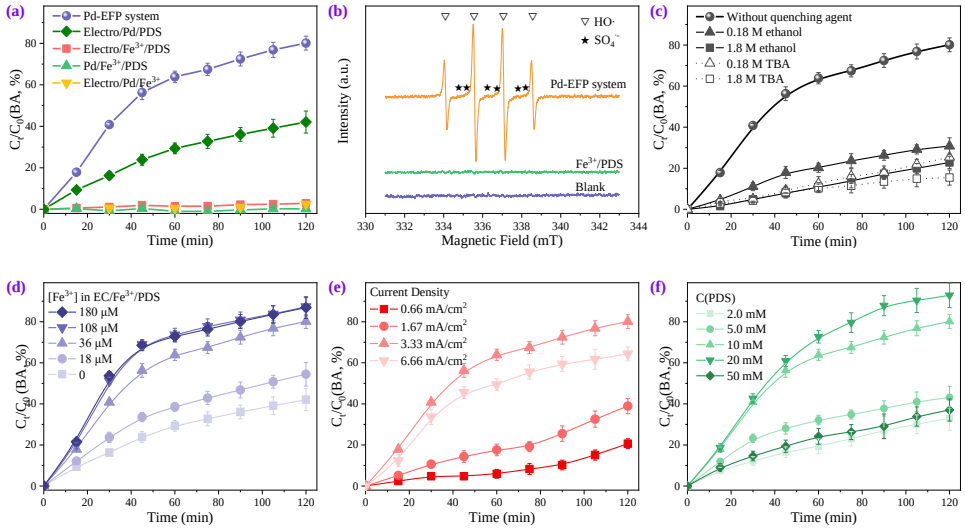

Figure 3.7. (a) Enhanced performance of Pd/Al_2O_3-ER process on the Fe^{3+}/PDS oxidation of BA; radical identification by (b) ESR analysis and (c) quenching experiments analysis; Effect of (d) iron dosage, (e) current density and (f) PDS dosage on the BA degradation by Pd-ER/PDS system.

We further optimized the operating parameters of the process. As shown in Figure **3.7d**, the system exhibited a stronger oxidation capacity with the addition of a higher Fe^{3+} dosage. Even with the addition of 2 ppm (36 μM) Fe^{3+} (EU emission standard), BA degradation with an efficiency up to 80.12% was attained in 120 min. In the wastewater treatment process, the dissolved iron ions produced iron sludge, and sludge production was assessed by the ratio of C_0(iron)/ΔC(pollutant). According to previous studies, the ratio varied from 3.6 to 125 in the Fe^{2+}/PDS process (**Table 3.1**) (Bu et al. 2016, Jiang et al. 2013, Long et al. 2014, Rao et al. 2014, Shang et al. 2019, Wang and Wang 2017,

Zhou et al. 2013); this ratio in our system decreased to 0.2 (lower than 1.0), implying the recycling of iron ions in the system as well as the trace production of iron sludge in the post-treatment process. Furthermore, for the traditional Fe^{2+}/PDS process, excess Fe^{2+} had a detrimental effect on the decontamination of organics because of the quenching effect toward $^{\bullet}OH$ and $SO_4^{\bullet-}$ radicals (**reactions 3.7. and 3.8**). In our system, the Fe^{2+}/PDS ratio was no more than 0.0036 (compared with 0.16–1.0 in other literature, **Table 3.1**) (Bu et al. 2016, Jiang et al. 2013, Long et al. 2014, Rao et al. 2014, Shang et al. 2019, Wang and Wang 2017, Zhou et al. 2013), indicating that Fe^{2+} ions were predominantly used for PDS activation (**reaction 1.4**) rather than radical quenching (**reactions 3.7 and 3.8**). The addition of trace iron not only benefits the post-treatment of dissolved iron, but also improves the contaminant oxidation efficiency of the Fenton-like process.

Table 3.1 Comparison of pollutant concentration, iron dosage, and PDS dosage in the Fe^{2+}/PDS system.

ΔC(pollutant)	C(Fe)	C(PDS)	C(Fe) /ΔC(pollutant)	C(Fe) /C(PDS)	Ref.
40 μM	1.6 mM	2 mM	40	0.16	(Jiang et al. 2013)
10 μM	0.4 mM	0.4 mM	40	1	(Bu et al. 2016)
4.2 μM	1 mM	5 mM	238	0.2	(Shang et al. 2019)
0.7 mM	3.6 mM	5 mM	5.1	0.72	(Long et al. 2014)
0.84 mM	5.8 mM	20 mM	6.9	0.29	(Rao et al. 2014)
0.8 mM	8.1 mM	35 mM	10.13	0.23	(Rao et al. 2014)
25 μM	0.25 mM	1 mM	10	0.25	(Rao et al. 2014)
50 μM	4 mM	4 mM	80	1	(Wang et al. 2017)
32 μM	2 mM	2 mM	62.5	1	(Zhou et al. 2013)
172 μM	15 mM	10 mM	87.2	1.5	Fe^{2+}/PDS
144 μM	36 μM	10 mM	0.25	0.0036	This study

$$^{\bullet}OH + Fe^{2+} \rightarrow OH^{-} + Fe^{3+} \quad (3.7)$$

$$SO_4^{\bullet-} + Fe^{2+} \rightarrow SO_4^{2-} + Fe^{3+} \quad (3.8)$$

Meanwhile, a higher current density could substantially enhance Fe^{3+}/Fe^{2+} by yielding more H_2 as a reductant. A proper dosage of PDS (20 mM) can maximize the oxidation process.

In conclusion, the new system exhibited continuous oxidation capacity using a cathode (electro-induced atomic H* and electro-generated H_2) as an electron source, Fe^{2+}/Fe^{3+}

pair as an electron shuttle, Pd/Al_2O_3 particles for the catalytic reduction of Fe^{3+} ions, and PDS as an oxidant.

3.4 PDS activation by atomic H*

3.4.1 Organic degradation in the Pd/ER system

As described in **Section 3.3**, PDS can oxidize BA even in the absence of iron ions. One reasonable hypothesis is that single-electron injection into PDS can be mediated by H^*/H^+ pairs. As shown in **Figure 3.8a**, 45.08% of BA in the Pd/ER system was rapidly degraded at a first-order kinetic constant of 0.0097 min^{-1} (k_1, R^2 = 0.9965), whereas the ER system and Pd/Al_2O_3 individually showed negligible degradation of BA (C_0(BA)=50 μM; C_0(PDS)=20 mM; C(Pd/Al_2O_3)=0.5 g/L; current=100 mA; initial solution pH=3.0; anaerobic atmosphere). These results demonstrate that a synergetic activation of PDS occurred in the Pd/ER system. Meanwhile, by monitoring the variations in the PDS concentration as a function of time, simultaneous degradation can be observed with a zero-order kinetic constant of 0.3002 $mM \cdot min^{-1}$ (k_0, R^2 = 0.9971).

We further evaluated the oxidation capacity of the system by degrading several model contaminants (10 μM). As shown in **Figure 3.8b**, these organic compounds can be easily degraded with efficiencies of more than 80% in 60 min, demonstrating that the system involves a strong and non-selective oxidation process.

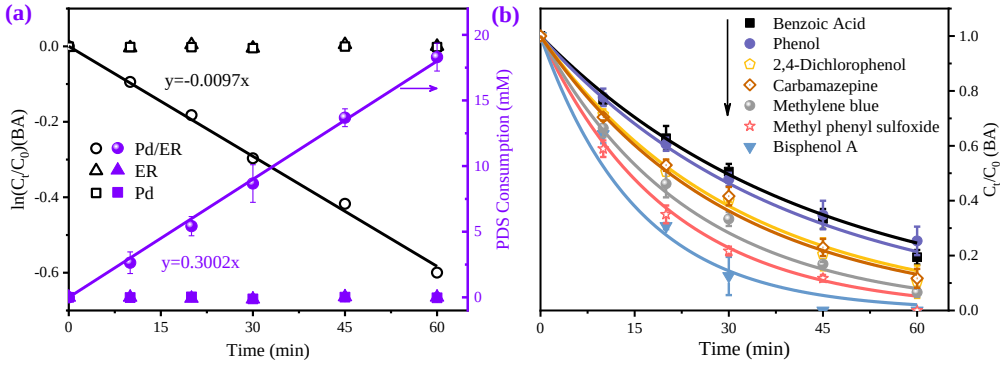

Figure 3.8 (a) BA degradation and PDS consumption in Pd/Al_2O_3 adsorption, ER process, and Pd/ER process; (b) Degradation of various organics in the H*/PDS system. ([Organic compounds], 10 μM; [Pd/Al_2O_3], 0.5 g/L; [PDS], 20 mM; current, 0.1 A; solution pH 3.0)

3.4.2 Identification of reactive oxygen species

ESR analysis was then used for the direct identification of radicals in the system using DMPO as a spin-trapping reagent. As displayed in **Figure 3.9a**, nine characteristic peaks of DMPO−H are observed in the Pd/ER system, suggesting the formation of atomic H*. With the addition of PDS into the Pd/ER system, $SO_4^{\bullet-}$ and its symbiotic radical ($^{\bullet}OH$)

(**reaction 3.9**) can be clearly observed, accompanied by the disappearance of atomic H*. The data revealed that the oxidizing radical may originate as a result of PDS reduction by atomic H*. The quenching experiment using ethanol as a scavenger for both ˙OH and $SO_4^{\bullet-}$ further confirmed the essential roles of •OH and $SO_4^{\bullet-}$ in the BA degradation process (**Figure 3.9b**) (Zeng et al. 2019).

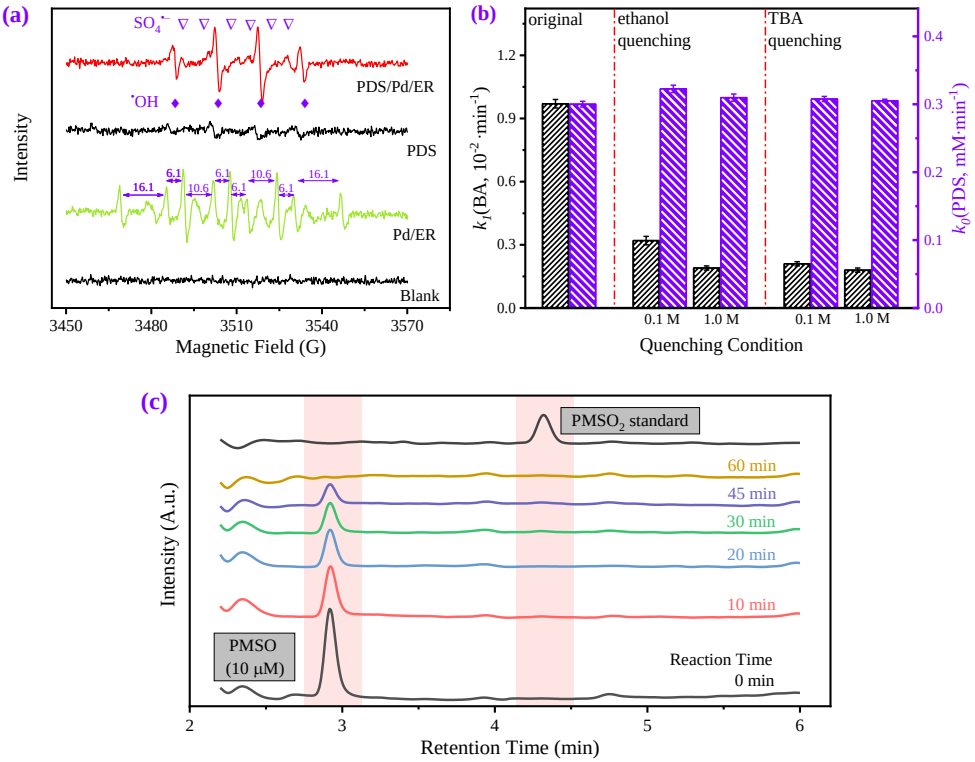

Figure 3.9 (a) Identification of reactive species by ESR analysis; (b) *k*-value comparison of BA degradation (k_1) and PDS consumption (k_0) under different quenching conditions; (c) HPLC spectra of samples in the H*/PDS system (BA, 50 μM; PDS, 20 mM; Pd/Al_2O_3, 0.5 g/L; Applied current, 0.10 A; initial solution pH, 3.0; deoxygenated atmosphere)

It has been widely reported that atomic H* can be formed in the 3D electroreduction system with a Pd-particle electrode (Lan et al. 2016, Zhao et al. 2014c). Like Fe^{2+} ion (most representative single-electron activator for the activation of peroxide compounds), atomic H* (a single-electron reductive radical) can theoretically cleave the peroxide bridge in the PDS molecule and forms $SO_4^{\bullet-}$ radical for subsequent oxidation of BA (**reaction 6**) (Pan et al. 2018). Comparing the inhibitory results of ethanol and TBA on BA removal demonstrated the significance of atomic H* on the activation of PDS (**Figure 3.9b**). As a scavenger of both atomic H* and ˙OH, TBA showed lower activity with $SO_4^{\bullet-}$ radical (Liang and Su 2009b). Hence, this should have implied a stronger inhibition of organic degradation by ethanol than that by TBA in $SO_4^{\bullet-}$-based oxidation systems, as

documented in previous literature (Rastogi et al. 2009). However, our batches for BA degradation with the ethanol addition revealed a higher k_1-value than that with the addition of TBA in this system, which may be ascribed to the simultaneous inhibition of both the reactive radical formation from atomic H* and BA degradation by $^{\bullet}OH$. The abnormal phenomena unravel the necessity of atomic H* on unleashing the oxidative power of PDS.

$$SO_4^{\bullet-} + OH^- \rightarrow SO_4^{2-} + {}^{\bullet}OH \quad (3.9)$$

$$\equiv Pd\text{-}H^* + S_2O_8^{2-} \rightarrow \equiv Pd + H^+ + SO_4^{2-} + SO_4^{\bullet-} \quad (3.10)$$

$$\equiv Pd\text{-}H^* + SO_4^{\bullet-} \rightarrow \equiv Pd + H^+ + SO_4^{2-} \quad (3.11)$$

In addition, different from AOPs using metal activators, where radicals ($^{\bullet}OH$, $SO_4^{\bullet-}$) and high valent cationic species [Fe(IV), Mn(III), Cu(III), or Cr(V)], were all involved in the decomposition of organics (Dong et al. 2020a, Dong et al. 2020b, Liu et al. 2019b, Wang et al. 2020, Wang et al. 2018), the H*/PDS system can theoretically avoid the involvement of high valent cationic species owing to the employment of metal-free activator. Degradation experiment using methyl phenyl sulfoxide (PMSO) as a probe of reactive oxygen species can verify the hypothesis. Phenylsulfinic acid ($PhSO_2$) was formed from the radical oxidation while PMSO was converted into methyl phenyl sulfone ($PMSO_2$) by high valent cationic species (Wang et al. 2018). As presented in Figure **3.9c**. The HPLC results in the H*/PDS system showed that only negligible signal of $PMSO_2$ appeared through the whole process of PMSO degradation. The above analysis revealed that atomic H* can reduce PDS, followed by $SO_4^{\bullet-}$ generation for organic decontamination.

3.4.3 Two routes for PDS electroreduction on Pd(111) facet

Problem comes from that the value of $\Delta c(PDS)/\Delta c(BA)$ was calculated as 700, which was identical to values in other electrochemical activation processes of PDS (Chen and Huang 2015, Chen et al. 2014, Liu et al. 2020, Matzek et al. 2018). According to the property of PDS, the meaningless consumption of PDS can be due to the inhibition of excess atomic H* on the $SO_4^{\bullet-}$ (**reaction 7**), or that two-electron reduction of PDS occurs via non-radical route. We monitored the PDS decomposition for investigating the quenching mechanism. As shown in the **Figure 3.9b**, the TBA showed negligible influence on the PDS decay while it obviously inhibited PDS activation by atomic H* and following BA degradation. The results excluded the possibility of PDS consumption via a two-step reduction of two atomic H*, and suggested an unknown mechanism on the non-radical decomposition of PDS.

For better elaborating the PDS decomposition with the assistance of Pd/Al_2O_3 catalyst, DFT technology was employed in elucidating the PDS decomposition by two electroreduction mechanism (indirect reduction via atomic H* and direct electron transfer). In the DFT analysis, a hyphen indicates the states where two units are bonded with each other, whereas the plus sign represents a separate state. According to XRD results of Pd/Al_2O_3 catalyst, we constructed a Pd(111) facet as the catalytical platform for PDS decomposition. In the indirect reduction approach of PDS, the H^+ ion firstly

adsorbed on the Pd atom with a Gibbs free energy change (ΔG) of −1.324 eV, the negative value indicated that the physical adsorption can spontaneously occur (**Figure 3.10**). Then, the atomic H* was generated through the formation of a Pd–H* bond (ΔG = 0.232 eV) with the Pd-H^+ accepting one-electron. Subsequently, the PDS molecule in the bulk solution coupled Pd-H* to form a ≡Pd-H*-$S_2O_8^{2-}$ adduct (ΔG = −3.321 eV), followed by structure conversion into a transition state (TS1) with ΔG value of 0.916 eV. The charge density analysis demonstrated that the electron was successfully injected into the PDS molecule from Pd-H* adduct with the formation of ≡Pd-H*-$S_2O_8^{2-}$ adduct. In the meantime, the electron-injection into the $S_2O_8^{2-}$ induced a longer length of the peroxide bond from 1.347 Å ($S_2O_8^{2-}$) to 1.498 Å (≡Pd-H*-$S_2O_8^{2-}$), suggesting the following cleavage of the peroxide bond with the generation of the desired $SO_4^{\bullet-}$. It can be easily concluded that the phase where TS1 was formed was the determining step through the whole process (ΔG_{ds}), with the highest ΔG among these elementary reactions (Zhou et al. 2019b). Only when the system was driven across the uphill energy barrier, can the reaction smoothly proceed (Wei et al. 2012).

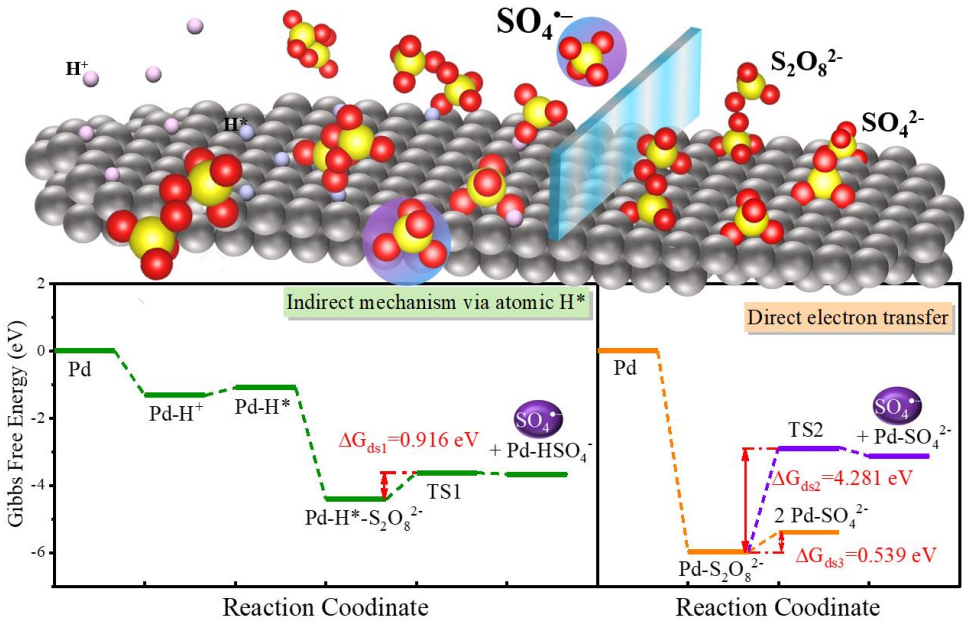

Figure 3.10 Gibbs free energy variations for PDS decomposition on the Pd(111) facet via different reduction approaches: indirect reduction via atomic H* and direct electron transfer.

PDS decomposition via direct electron transfer was then studied by DFT analysis, with assuming $SO_4^{\bullet-}$ as reduction product. Different from the indirect reduction mechanism, $S_2O_8^{2-}$ directly adsorbed on the Pd atoms instead of atomic H* (ΔG = –5.977 eV). The

≡Pd-$S_2O_8^{2-}$ was then evolved into two less oxidative ≡Pd-$SO_4^{\bullet-}$, accompanied with the cleavage of peroxide bond in the PDS molecule (Feng et al. 2017). The single-electron transfer could steer the PDS decomposition towards free $SO_4^{\bullet-}$ radical. The system exhibited a high oxidation ability when $SO_4^{\bullet-}$ fell off the Pd atom. Nevertheless, the ΔG of determining step for this reaction route (4.281 eV) was obviously higher than that in the indirect reduction approach. The comparison excluded the generation mechanism of $SO_4^{\bullet-}$ via the direct electron transfer and demonstrated that the atomic H* could readily initiate the PDS oxidation with yielding the desired $SO_4^{\bullet-}$. By contrast, if we supposed the product of PDS reduction as inert SO_4^{2-}, the ΔG_{ds} was determined to be only 0.539 eV. Much lower ΔG_{ds} (0.539 eV to 4.281 eV) indicated that the PDS reaction on the Pd catalyst via direct electron transfer was oriented to the production of SO_4^{2-}.

Hence, it can be concluded that these two mechanisms steered the PDS electroreduction toward different products: PDS formed $SO_4^{\bullet-}$ via the atomic H* reduction, whereas PDS inclined to accepted two-electron in one-step (direct electron transfer).

3.4.4 Electron donor analysis

The optimized conditions for PDS decomposition and $SO_4^{\bullet-}$ generation were further explored in the Pd/ER system. The kinetic constants (k_0 for PDS decay and k_1 for BA degradation) are listed in **Table 3.2**. According to **Batch 1–3**, higher current on the system can positively stimulate the PDS decomposition, which is directly related to the H_2 generation rate. This can be contributed to the role of two-electron donor played by H_2 in the direct electron transfer process. Interestingly, varying the PDS and catalyst dosages presented negligible influence on the k_0-value for PDS decomposition (**Batch 1, 4~8**). The insensitivity to these two factors suggested that PDS can react with H_2 at an ultrafast rate, and the PDS diffusion didn't become the rate-limiting step during the process. By contrast, these factors imposed different influence on the $SO_4^{\bullet-}$ production, which was characterized using BA as radical probe. The k_1-value for BA oxidation was improved by applying higher current/potential or adding more Pd/Al_2O_3 catalyst, while k_1 showed unaffected by different concentration of PDS.

As mentioned in **section 3.3**, atomic H* can be generated from proton conversion by the electro-induction or dissociative adsorption of H_2 (**reaction 3.5** and **3.6**) (Georgi et al. 2016, Lan et al. 2016, Xu et al. 2017, Zeng et al. 2019). For elaborating their roles in the PDS decomposition process, we developed two systems to differentiate these active hydrogen species. We ruled out the electro-induced atomic H* by monitoring the BA degradation in the H_2/Pd system, where contained PDS as radical precursor. To our surprise, there is no any BA degradation observed through the whole PDS decomposition process (**Figure 3.11**). The results were controversy to the generally believed approach of atomic H* formation from the dissociation of dihydrogen. By contrast, the adsorbed H_2 molecules on the Pd catalyst may directly act as a two-electron donor (≡Pd-H_2^*, **reaction 3.12**) without necessary formation of atomic H* (Jiang et al. 2017). In addition, a three-cell electrochemical reactor was designed, in which electrochemically generated H_2 was blocked in the cathodic cell and only electro-induced atomic H* in the middle cell.

In this case, BA degradation with decomposition of trace PDS revealed the efficient yield of $SO_4^{\bullet-}$ via the activation of PDS induced by the electro-induced atomic H*.

$$\equiv Pd + H_2 \rightarrow \equiv Pd\text{-}H_2^* \quad (3.12)$$

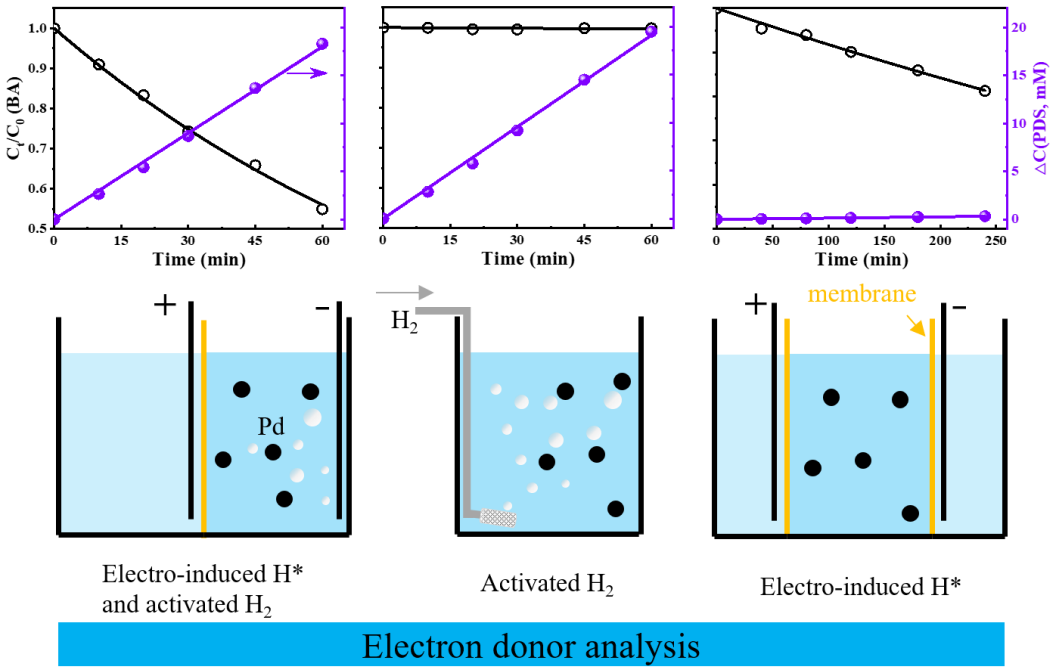

Figure 3.11 Effects of different approaches for atomic H* generation on BA degradation and PDS decomposition. (BA, 50 μM; PDS, 20 mM; Pd/Al_2O_3, 0.5 g/L; applied current, 0.10 A; initial solution pH, 3.0; deoxygenated atmosphere)

The aforementioned researches demonstrated two electron donors for PDS decay in the Pd/ER system: the activation of PDS into $SO_4^{\bullet-}$ was initiated by electro-induced atomic H*, while Pd-activated H_2 played a role as a two-electron donor for the direct electron transfer process. Maximizing the valid activation of PDS necessitated mothed to enhance the production of electro-induced atomic H* and simultaneous inhibition of the H_2 yield. In the electrochemical system, the H_2 generation quantitatively depended on the applied current, while the atomic H* production via the electro-induction depended on the catalyst concentration and electric field. Unfortunately, both electro-induced atomic H* and electro-generated H_2 simultaneously increased with an elevation of applied current. In contrast, higher dosage of Pd/Al_2O_3 catalyst to 1.0 g/L can provide more active sites for proton adsorption and conversion into atomic H*, thus inducing higher $SO_4^{\bullet-}$ levels and simultaneously accelerating the organic degradation process.

Table. 3.2 Effects of the applied current, PDS concentration, and Pd/Al_2O_3 dosage on the kinetics constants (*k*-value) of PDS consumption and BA degradation. (BA, 50 µM; initial solution pH, 3.0; deoxygenated atmosphere)

No.	Current (A)	C(PDS) (mM)	C(Pd/Al_2O_3) (g/L)	k_1 (BA) (min^{-1})	k_0 (PDS) (mM/min)
1.	0.1	20	0.5	0.0097	0.2982
2.	0.05	20	0.5	0.0051	0.1595
3.	0.02	20	0.5	0	0.0657
4.	0.1	20	1.0	0.0169	0.3026
5.	0.1	20	0.2	0.0031	0.3163
6.	0.1	20	0.1	0.0019	0.3121
7.	0.1	50	0.5	0.0087	0.3002
8.	0.1	10	0.5	0.0074	0.2802

In conclusion, the reactive oxygen species ($SO_4^{\bullet-}$/$^{\bullet}OH$) could be readily formed by the single-electron reduction of PDS by electro-induced atomic hydrogen (atomic H*, indirect reduction mechanism), while the direct two-electron transfer from H_2 to PDS consumed its oxidation capacity without yielding radicals due to the higher energy barrier. By increasing the concentration of the Pd/Al_2O_3 catalyst in the ER system, more atomic H* could be generated for PDS activation and the subsequent degradation of organics. The H^*/H^+ pair was proven to be an efficient single-electron transferring medium for PDS activation.

4 Conclusions & Prospective

To improve the quality of human life, a plethora of organic compounds have been synthesized by various industries. However, the emissions resulting from their production have caused serious environmental concerns. In addition, traditional biological treatment methods have been proven to be ineffective in removing these emerging contaminants due to their non-biodegradable properties and toxicity to microorganisms. AOPs have been deemed a promising technology that generate reactive oxidative radicals in situ, for the treatment of these pollutants. Although $SO_4^{\bullet-}$ can be readily formed via PDS activation by a single-electron donor, the catalyst is deactivated after donating the electrons. By introducing an electron source into the system, the catalyst can be regenerated, resulting in continuous PDS activation. Among the electron injection approaches, the electrochemical approach of PDS activation, in which electrons are employed as a reductive activator, can meet the demand for green chemistry.

First, the PEC system as an electron source using Ti foil as the cathode was explored. With the addition of 5 mM PDS into the PEC system, the decomplexation ratio of Cu-EDTA increased from 47.5% to 98.4% in the PEC process within 60 min. Correspondingly, the recovery percentage of Cu increased from 47.4% to 98.3%. In addition to the photolytic activation of PDS, $S_2O_8^{2-}$ was activated to generate $SO_4^{\bullet-}$ radicals through cathodic reduction. The produced $SO_4^{\bullet-}$ enhanced the Cu-EDTA oxidation, subsequently liberating the Cu^{2+} ions. Meanwhile, acidification induced by the conversion of $SO_4^{\bullet-}$ to $^{\bullet}OH$ favored the recovery of Cu on the cathode. When PDS was consumed, Cu recovery proceeded quickly via cathodic reduction.

Although PDS activation via electrons on the cathode was demonstrated, the key media for single-electron transfer between the cathode and PDS was not identified; hence, a more efficient activation process was explored. We further substituted the Ti foil with Cu foil as the cathode in the PEC/PDS system. Interestingly, the ESR analysis demonstrated that the radical signals in the new system were 10-fold stronger than those in the PEC/PDS/Ti system. Accordingly, the PEC/PDS system exhibited a stronger oxidation capacity toward diclofenac. SEM analysis and XPS of the fresh and used Cu foils revealed that Cu(II) appeared on the surface of the Cu cathode, and in situ Raman spectroscopy indicated that Cu(I) existed throughout the PEC/PDS process. The above results on the valence variation of the Cu species allowed us to propose that the Cu(II)/Cu(I) pair acted as the single-electron transfer media. The involvement of Cu(II)/Cu(I) could effortlessly transfer a single photoelectron from the cathode to PDS for $SO_4^{\bullet-}$ production, preventing the PDS from the consecutive two-electron reduction and the complete loss of its oxidation capacity.

Then, we employed a more readily available Fe^{2+}/Fe^{3+} redox pair (single-electron shuttle) in the more commonly used electroreduction system (electron source). We constructed a trace-iron based ER/PDS system using Pd/Al_2O_3 particles as the particle electrodes and externally added PDS as an oxidant. In the system, the electro-generated H_2 exhibited a strong reductive ability to accelerate the Fe^{3+}/Fe^{2+} cycle in the Fe^{2+}/PDS system with the

assistance of a Pd/Al_2O_3 catalyst. Both the indirect reduction mechanisms via atomic H* and direct electron transfer were involved in the electroreduction process. The quenching experiments indicated that Fe^{3+} reduction predominantly occurred via an indirect reduction mechanism, while the direct electron transfer played an insignificant role in the process. Benefiting from the accelerated Fe^{3+}/Fe^{2+} cycle, the ER/Fe^{3+}/PDS system could continuously output $SO_4^{\bullet-}$ for BA degradation with a removal efficiency of 80.12% in 120 min. The process involved the electro-generated H_2 as an electron source, leaving only H_2O in the Fe^{3+} reduction process. The non-toxic property provided a green solution for reducing iron sludge production, while the oxidation performance remained unchanged.

Except for the Fe^{3+}/Fe^{2+} pair as a single-electron shuttle, we were also intrigued by the atomic H* in the ER/PDS system, which is also a strong single-electron reductant. Our results indicated that using a Pd/Al_2O_3 catalyst as the particle electrode for initiating PDS oxidation in the cathodic cell could degrade various organic pollutants by varying the kinetic constants from 0.0256 min^{-1} to 0.0645 min^{-1}. The reactive oxygen species were determined to be $SO_4^{\bullet-}$/$^{\bullet}OH$ by ESR analysis, quenching experiments, and PMSO degradation analysis. Furthermore, these radicals were readily formed from the single-electron reduction of PDS by electro-induced atomic hydrogen (atomic H*, indirect reduction mechanism), while direct two-electron transfer from H_2 to PDS consumed its oxidation capacity without yielding radicals due to the higher energy barrier.

This study was the first to design a ternary system comprising an electron source, a single-electron shuttle, and a peroxide compound. The ternary system facilitates a rational design for the construction of an oxidation system for continuously producing radicals according to the water matrix. In our following work, the ternary system will be further employed for the treatment of different types of actual wastewaters, such as contaminated ground water or ballast water, and then choose suitable elements for the system.

References

Ahn, S., Peterson, T.D., Righter, J., Miles, D.M. and Tratnyek, P.G., 2013. *Disinfection of Ballast Water with Iron Activated Persulfate*. Environmental Science & Technology 47(20), 11717-11725.

Alsbaiee, A., Smith, B.J., Xiao, L.L., Ling, Y.H., Helbling, D.E. and Dichtel, W.R., 2016. *Rapid removal of organic micropollutants from water by a porous beta-cyclodextrin polymer*. Nature 529(7585), 190-U146.

Anipsitakis, G.P. and Dionysiou, D.D., 2004. *Radical generation by the interaction of transition metals with common oxidants*. Environmental Science & Technology 38(13), 3705-3712.

Barhoumi, N., Oturan, N., Ammar, S., Gadri, A., Oturan, M.A. and Brillas, E., 2017. *Enhanced degradation of the antibiotic tetracycline by heterogeneous electro-Fenton with pyrite catalysis*. Environmental Chemistry Letters 15(4), 689-693.

Bass, D.H., Hastings, N.A. and Brown, R.A., 2000. *Performance of air sparging systems: a review of case studies*. Journal of Hazardous Materials 72(2-3), 101-119.

Bruton, T.K. and Sedlak, D.L., 2017. *Treatment of Aqueous Film-Forming Foam by Heat-Activated Persulfate Under Conditions Representative of In Situ Chemical Oxidation*. Environmental Science & Technology 51(23), 13878-13885.

Bu, L., Shi, Z. and Zhou, S., 2016. *Modeling of Fe(II)-activated persulfate oxidation using atrazine as a target contaminant*. Separation and Purification Technology 169, 59-65.

Buettner, G.R., 1993. *The Pecking Order of Free Radicals and Antioxidants: Lipid Peroxidation, -Tocopherol, and Ascorbate*. Archives of Biochemistry 300(2), 535-543.

Buxton, G.V., Greenstock, C.L., Helman, W.P. and Ross, A.B., 1988. *Critical Review of rate constants for reactions of hydrated electrons, hydrogen atoms and hydroxyl radicals(·OH/·O-) in Aqueous Solution*. Journal of Physical and Chemical Reference Data 17(2), 513-886.

Chen, L.W., Ma, J., Li, X.C., Zhang, J., Fang, J.Y., Guan, Y.H. and Xie, P.C., 2011. *Strong Enhancement on Fenton Oxidation by Addition of Hydroxylamine to Accelerate the Ferric and Ferrous Iron Cycles*. Environmental Science & Technology 45(9), 3925-3930.

Chen, W.S. and Huang, C.P., 2015. *Mineralization of aniline in aqueous solution by electrochemical activation of persulfate*. Chemosphere 125, 175-181.

Chen, W.S., Jhou, Y.C. and Huang, C.P., 2014. *Mineralization of dinitrotoluenes in industrial wastewater by electro-activated persulfate oxidation*. Chemical Engineering Journal 252, 166-172.

Chi, H.Z., He, X., Zhang, J.Q., Wang, D., Zhai, X.D. and Ma, J., 2019. *Hydroxylamine enhanced degradation of naproxen in Cu^{2+} activated peroxymonosulfate system at acidic condition: Efficiency, mechanisms and pathway*. Chemical Engineering Journal 361, 764-772.

Chowdhury, A.I.A., Gerhard, J.I., Reynolds, D. and O'Carroll, D.M., 2017. *Low Permeability Zone Remediation via Oxidant Delivered by Electrokinetics and*

Activated by Electrical Resistance Heating: Proof of Concept. Environmental Science & Technology 51(22), 13295-13303.

Chu, W.H., Li, D.M., Gao, N.Y., Templeton, M.R., Tan, C.Q. and Gao, Y.Q., 2015. *The control of emerging haloacetamide DBP precursors with UV/persulfate treatment*. Water Research 72, 340-348.

Chu, Y.Y., Qian, Y., Wang, W.J. and Deng, X.L., 2012. *A dual-cathode electro-Fenton oxidation coupled with anodic oxidation system used for 4-nitrophenol degradation*. Journal of Hazardous Materials 199, 179-185.

Danilczuk, M., Schlick, S. and Coms, F.D., 2009. *Cerium(III) as a Stabilizer of Perfluorinated Membranes Used in Fuel Cells: In Situ Detection of Early Events in the ESR Resonator*. Macromolecules 42(22), 8943-8949.

Das, T.N., Huie, R.E. and Neta, P., 1999. *Reduction Potentials of SO_3^-, SO_5^-, and $S_4O_6^{3-}$ Radicals in Aqueous Solution*. The Journal of Physical Chemistry A 103(18), 3581-3588.

Deng, Y. and Ezyske, C.M., 2011. *Sulfate radical-advanced oxidation process (SR-AOP) for simultaneous removal of refractory organic contaminants and ammonia in landfill leachate*. Water Research 45(18), 6189-6194.

Devi, P., Das, U. and Dalai, A.K., 2016. *In-situ chemical oxidation: Principle and applications of peroxide and persulfate treatments in wastewater systems*. Science of the Total Environment 571, 643-657.

Dong, C.C., Ji, J.H., Shen, B., Xing, M.Y. and Zhang, J.L., 2018. *Enhancement of H_2O_2 Decomposition by the Co-catalytic Effect of WS_2 on the Fenton Reaction for the Synchronous Reduction of Cr(VI) and Remediation of Phenol*. Environmental Science & Technology 52(19), 11297-11308.

Dong, F., Li, Q.Y., Sun, Y.J. and Ho, W.K., 2014. *Noble Metal-Like Behavior of Plasmonic Bi Particles as a Cocatalyst Deposited on $(BiO)_2CO_3$ Microspheres for Efficient Visible Light Photocatalysis*. ACS Catalysis 4(12), 4341-4350.

Dong, H.Y., Li, Y., Wang, S.C., Liu, W.F., Zhou, G.M., Xie, Y.F. and Guan, X.H., 2020a. *Both Fe(IV) and Radicals Are Active Oxidants in the Fe(II)/Peroxydisulfate Process*. Environmental Science & Technology Letters 7(3), 219-224.

Dong, H.Y., Wei, G.F., Cao, T.C., Shao, B.B., Guan, X.H. and Strathmann, T.J., 2020b. *Insights into the Oxidation of Organic Cocontaminants during Cr(VI) Reduction by Sulfite: The Overlooked Significance of Cr(V)*. Environmental Science & Technology 54(2), 1157-1166.

Drzewicz, P., Perez-Estrada, L., Alpatova, A., Martin, J.W. and El-Din, M.G., 2012. *Impact of Peroxydisulfate in the Presence of Zero Valent Iron on the Oxidation of Cyclohexanoic Acid and Naphthenic Acids from Oil Sands Process-Affected Water*. Environmental Science & Technology 46(16), 8984-8991.

Eberson, L., 1982. *Advances in physical organic chemistry*, pp. 79-185, Elsevier.

Escher, B.I., 2000. *Molecular mechanisms in aquatic ecotoxicology: specif and non-specific membrane toxicity*.

Fan, G.P., Cang, L., Fang, G.D. and Zhou, D.M., 2014. *Surfactant and oxidant enhanced electrokinetic remediation of a PCBs polluted soil*. Separation and Purification Technology 123, 106-113.

Feng, Y., Lee, P.H., Wu, D.L. and Shih, K.M., 2017. *Surface-bound sulfate radical-dominated degradation of 1,4-dioxane by alumina-supported palladium (Pd/Al_2O_3) catalyzed peroxymonosulfate*. Water Research 120, 12-21.

Fleszar, B. and Sobkowiak, A.J.E.A., 1983. *Hydroxylation of benzene and phenol during electroreduction of oxygen*. 28(10), 1315-1318.

Furman, O.S., Teel, A.L. and Watts, R.J., 2010. *Mechanism of Base Activation of Persulfate*. Environmental Science & Technology 44(16), 6423-6428.

Georgi, A., Polo, M.V., Crincoli, K., Mackenzie, K. and Kopinke, F.D., 2016. *Accelerated Catalytic Fenton Reaction with Traces of Iron: An Fe-Pd-Multicatalysis Approach*. Environmental Science & Technology 50(11), 5882-5891.

Ghanbari, F. and Moradi, M., 2017. *Application of peroxymonosulfate and its activation methods for degradation of environmental organic pollutants: Review*. Chemical Engineering Journal 310, 41-62.

Glaze, W.H., Kang, J.W. and Chapin, D.H., 1987. *The Chemistry of Water Treatment Processes Involving Ozone, Hydrogen Peroxide and Ultraviolet Radiation*. Ozone-Science & Engineering 9(4), 335-352.

Gosset, A., Ferro, Y. and Durrieu, C., 2016. *Methods for evaluating the pollution impact of urban wet weather discharges on biocenosis: A review*. Water Research 89, 330-354.

Gu, Z.P., Chen, W.M., Li, Q.B., Wang, Y., Wu, C.W. and Zhang, A.P., 2018. *Degradation of recalcitrant organics in landfill concentrated leachate by a microwave-activated peroxydisulfate process*. RSC Advances 8(57), 32461-32469.

He, X.X., de la Cruz, A.A. and Dionysiou, D.D., 2013. *Destruction of cyanobacterial toxin cylindrospermopsin by hydroxyl radicals and sulfate radicals using UV-254 nm activation of hydrogen peroxide, persulfate and peroxymonosulfate*. Journal of Photochemistry and Photobiology a-Chemistry 251, 160-166.

Hodges, B.C., Cates, E.L. and Kim, J.H., 2018. *Challenges and prospects of advanced oxidation water treatment processes using catalytic nanomaterials*. Nature Nanotechnology 13(8), 642-650.

Ji, Y.F., Wang, L., Jiang, M.D., Lu, J.H., Ferronato, C. and Chovelon, J.M., 2017. *The role of nitrite in sulfate radical-based degradation of phenolic compounds: An unexpected nitration process relevant to groundwater remediation by in-situ chemical oxidation (ISCO)*. Water Research 123, 249-257.

Jiang, G.M., Lan, M.N., Zhang, Z.Y., Lv, X.S., Lou, Z.M., Xu, X.H., Dong, F. and Zhang, S., 2017. *Identification of Active Hydrogen Species on Palladium Nanoparticles for an Enhanced Electrocatalytic Hydrodechlorination of 2,4-Dichlorophenol in Water*. Environmental Science & Technology 51(13), 7599-7605.

Jiang, X.X., Wu, Y.L., Wang, P., Li, H.J. and Dong, W.B., 2013. *Degradation of bisphenol A in aqueous solution by persulfate activated with ferrous ion*. Environmental Science and Pollution Research 20(7), 4947-4953.

Kagle, J., Porter, A.W., Murdoch, R.W., Rivera-Cancel, G. and Hay, A.G., 2009. *Advances in Applied Mircobiology*, Vol 67. Laskin, A.I. (ed), pp. 65-108, Elsevier Academic Press Inc, San Diego.

Kaim, W., Schwederski, B. and Klein, A., 2013. *Bioinorganic Chemistry--Inorganic Elements in the Chemistry of Life: An Introduction and Guide*, John Wiley & Sons.

Klopman, G. and Tu, M.H., 1997. *Structure-biodegradability study and computer-automated prediction of aerobic biodegradation of chemicals*. Environmental Toxicology and Chemistry 16(9), 1829-1835.

Kroes, R., Galli, C., Munro, I., Schilter, B., Tran, L.-A., Walker, R., Würtzen, G., 2000. *Threshold of toxicological concern for chemical substances present in the diet: a practical tool for assessing the need for toxicity testing*. Food & Chemical Toxicology 38(2-3), 255-312.

Kwan, W.P. and Voelker, B.M., 2002. *Decomposition of hydrogen peroxide and organic compounds in the presence of dissolved iron and ferrihydrite*. Environmental Science & Technology 36(7), 1467-1476.

Laine, D.F., Blumenfeld, A. and Cheng, I.F., 2008. *Mechanistic study of the ZEA organic pollutant degradation system: Evidence for H_2O_2, $HO^{\cdot}$, and the homogeneous activation of O_2 by Fe(II)EDTA*. Industrial & Engineering Chemistry Research 47(17), 6502-6508.

Lan, H.C., Mao, R., Tong, Y.T., Liu, Y.Z., Liu, H.J., An, X.Q. and Liu, R.P., 2016. *Enhanced Electroreductive Removal of Bromate by a Supported Pd-In Bimetallic Catalyst: Kinetics and Mechanism Investigation*. Environmental Science & Technology 50(21), 11872-11878.

Lee, J., von Gunten, U. and Kim, J.-H., 2020. *Persulfate-Based Advanced Oxidation: Critical Assessment of Opportunities and Roadblocks*. Environmental Science & Technology 54(6), 3064-3081.

Lei, Y., Zhang, H., Wang, J.W. and Ai, J., 2015. *Rapid and continuous oxidation of organic contaminants with ascorbic acid and a modified ferric/persulfate system*. Chemical Engineering Journal 270, 73-79.

Li, Y., Baghi, R., Filip, J., Islam, S., Hope-weeks, L. and Yan, W.L., 2019. *Activation of Peroxydisulfate by Ferrite Materials for Phenol Degradation*. ACS Sustainable Chemistry & Engineering 7(9), 8099-8108.

Li, Z.Y., Wang, L., Liu, Y.L., Zhao, Q. and Ma, J., 2020. *Unraveling the interaction of hydroxylamine and Fe(III) in Fe(II)/Persulfate system: A kinetic and simulating study*. Water Research 168.

Liang, C. and Su, H.-W., 2009a. *Identification of Sulfate and Hydroxyl Radicals in Thermally Activated Persulfate*. Industrial & Engineering Chemistry Research 48(11), 5558-5562.

Liang, C.J. and Guo, Y.Y.. 2010. *Mass Transfer and Chemical Oxidation of Naphthalene Particles with Zerovalent Iron Activated Persulfate*. Environmental Science & Technology 44(21), 8203-8208.

Liang, C.J. and Su, H.W., 2009b. *Identification of Sulfate and Hydroxyl Radicals in Thermally Activated Persulfate*. Industrial & Engineering Chemistry Research 48(11), 5558-5562.

Lindsey, M.E. and Tarr, M.A., 2000. *Quantitation of hydroxyl radical during Fenton oxidation following a single addition of iron and peroxide*. Chemosphere 41(3), 409-417.

Ling, S.K., Wang, S.B. and Peng, Y.L., 2010. *Oxidative degradation of dyes in water using Co^{2+}/H_2O_2 and Co^{2+}/peroxymonosulfate*. Journal of Hazardous Materials 178(1-3), 385-389.

Liu, H.Z., Bruton, T.A., Doyle, F.M. and Sedlak, D.L., 2014. *In Situ Chemical Oxidation of Contaminated Groundwater by Persulfate: Decomposition by Fe(III)- and Mn(IV)-Containing Oxides and Aquifer Materials*. Environmental Science & Technology 48(17), 10330-10336.

Liu, J.W., Cheng, S.H., Cao, N., Geng, C.X., He, C., Shi, Q., Xu, C.M., Ni, J.R., DuChanois, R.M., Elimelech, M. and Zhao, H.Z., 2019a. *Actinia-like multifunctional nanocoagulant for single-step removal of water contaminants*. Nature Nanotechnology 14(1), 64.

Liu, W.F., Sun, B., Qiao, J.L. and Guan, X.H., 2019b. *Influence of Pyrophosphate on the Generation of Soluble Mn(III) from Reactions Involving Mn Oxides and Mn(VII)*. Environmental Science & Technology 53(17), 10227-10235.

Liu, Y.X., Liu, Z.Y., Wang, Y., Yin, Y.S., Pan, J.F., Zhang, J. and Wang, Q., 2018. *Simultaneous absorption of SO_2 and NO from flue gas using ultrasound/Fe^{2+}/heat coactivated persulfate system*. Journal of Hazardous Materials 342, 326-334.

Liu, Z., Ren, B.X., Ding, H.J., He, H., Deng, H.P., Zhao, C., Wang, P. and Dionysiou, D.D., 2020. *Simultaneous regeneration of cathodic activated carbon fiber and mineralization of desorbed contaminations by electro-peroxydisulfate process: Advantages and limitations*. Water Research 171.

Long, A., Lei, Y. and Zhang, H., 2014. *Degradation of Toluene by a Selective Ferrous Ion Activated Persulfate Oxidation Process*. Industrial & Engineering Chemistry Research 53(3), 1033-1039.

Lopez-Munoz, M.J., Aguado, J., van Grieken, R. and Marugan, J., 2009. *Simultaneous photocatalytic reduction of silver and oxidation of cyanide from dicyanoargentate solutions*. Applied Catalysis B-Environmental 86(1-2), 53-62.

Luo, C.W., Jiang, J., Ma, J., Pang, S.Y., Liu, Y.Z., Song, Y., Guan, C.T., Li, J., Jin, Y.X. and Wu, D.J., 2016. *Oxidation of the odorous compound 2,4,6-trichloroanisole by UV activated persulfate: Kinetics, products, and pathways*. Water Research 96, 12-21.

Luo, C.W., Ma, J., Jiang, J., Liu, Y.Z., Song, Y., Yang, Y., Guan, Y.H. and Wu, D.J., 2015. *Simulation and comparative study on the oxidation kinetics of atrazine by UV/H_2O_2, UV/HSO_5^- and $UV/S_2O_8^{2-}$*. Water Research 80, 99-108.

Lutze, H.V., Bircher, S., Rapp, I., Kerlin, N., Bakkour, R., Geisler, M., von Sonntag, C. and Schmidt, T.C., 2015. *Degradation of Chlorotriazine Pesticides by Sulfate Radicals and the Influence of Organic Matter*. Environmental Science & Technology 49(3), 1673-1680.

Ma, Q.L., Zhang, X.Y., Guo, R.N., Zhang, H.X., Cheng, Q.F., Xie, M.Z. and Cheng, X.W., 2019. *Persulfate activation by magnetic gamma-Fe_2O_3/Mn_3O_4 nanocomposites for degradation of organic pollutants*. Separation and Purification Technology 210, 335-342.

Matzek, L.W., Tipton, M.J., Farmer, A.T., Steen, A.D. and Carter, K.E., 2018. *Understanding Electrochemically Activated Persulfate and Its Application to Ciprofloxacin Abatement*. Environmental Science & Technology 52(10), 5875-5883.

McIntyre, N.S., Sunder, S., Shoesmith, D.W. and Stanchell, F.W., 1981. *Chemical information from XPS—applications to the analysis of electrode surfaces*. Journal of Vacuum Science & Technology 18(3), 714-721.

Militello, M.C. and Simko, S., 1994. *Elemental palladium by XPS*. Surface Science Spectra 3(4), 387-394.

Miller, A. and Simmons, G., 1993. *Copper by XPS*. Surface ence Spectra 2(1), 55-60.

Nate, P., Madhavan, V., Zemel, H. and Fessenden, R., 1977. *Rate constants and mechanism of reaction of $SO_4^{\cdot-}$ with aromatic compounds*. Journal of the American Chemical Society 99, 163-164.

Neppolian, B., Celik, E. and Choi, H., 2008. *Photochemical oxidation of arsenic(III) to arsenic(V) using peroxydisulfate ions as an oxidizing agent*. Environmental Science & Technology 42(16), 6179-6184.

Nfodzo, P. and Choi, H., 2011. *Triclosan decomposition by sulfate radicals: Effects of oxidant and metal doses*. Chemical Engineering Journal 174(2-3), 629-634.

Nidheesh, P.V., Gandhimathi, R. and Ramesh, S.T., 2013. *Degradation of dyes from aqueous solution by Fenton processes: a review*. Environmental Science and Pollution Research 20(4), 2099-2132.

Noyori, R., 2005. *Pursuing practical elegance in chemical synthesis*. Chemical Communications (14), 1807-1811.

Oh, W.D., Dong, Z.L. and Lim, T.T., 2016. *Generation of sulfate radical through heterogeneous catalysis for organic contaminants removal: Current development, challenges and prospects*. Applied Catalysis B-Environmental 194, 169-201.

Özcan, A., Şahin, Y. and Oturan, M.A., 2008. *Removal of propham from water by using electro-Fenton technology: kinetics and mechanism*. Chemosphere 73(5), 737-744.

Pan, Y., Su, H.R., Zhu, Y.T., Molamahmood, F.V. and Long, M.,2018. *CaO_2 based Fenton-like reaction at neutral pH: Accelerated reduction of ferric species and production of superoxide radicals*. Water Research 145, 731-740.

Panizza, M. and Cerisola, G., 2001. *Removal of organic pollutants from industrial wastewater by electrogenerated Fenton's reagent*. Water Research 35(16), 3987-3992.

Park, S., Lee, L.S., Medina, V.F., Zull, A. and Waisner, S., 2016. *Heat-activated persulfate oxidation of PFOA, 6:2 fluorotelomer sulfonate, and PFOS under conditions suitable for in-situ groundwater remediation*. Chemosphere 145, 376-383.

Peng, H.J., Zhang, W., Xu, L.Y., Fu, R.B. and Lin, K.F., 2016. *Oxidation and mechanism of decabromodiphenyl ether (BDE209) by thermally activated persulfate (TAP) in a soil system*. Chemical Engineering Journal 306, 226-232.

Pichtel, J. ,2005. *Waste management practices: municipal, hazardous, and industrial*, CRC press.

Pirkanniemi, K., Metsdrinne, S. and Sillanpaa, M., 2007. *Degradation of EDTA and novel complexing agents in pulp and paper mill process and waste waters by Fenton's reagent*. Journal of Hazardous Materials 147(1-2), 556-561.

Pitter, P. and Chudoba, J., 1990. *Biodegradability of organic substances in the aquatic environment*, CRC press Boca Raton.

Qi, C., Liu, X., Li, Y., Lin, C., Ma, J., Li, X. and Zhang, H., 2017. *Enhanced degradation of organic contaminants in water by peroxydisulfate coupled with bisulfite*. Journal of Hazardous Materials 328, 98-107.

Quaino, P. and Santos, E., 2015. *Hydrogen Evolution Reaction on Palladium Multilayers Deposited on Au(111): A Theoretical Approach*. Langmuir 31(2), 858-867.

Rao, Y.F., Qu, L., Yang, H. and Chu, W., 2014. *Degradation of carbamazepine by Fe(II)-activated persulfate process*. Journal of Hazardous Materials 268, 23-32.

Rastogi, A., Ai-Abed, S.R. and Dionysiou, D.D., 2009. *Sulfate radical-based ferrous-peroxymonosulfate oxidative system for PCBs degradation in aqueous and sediment systems*. Applied Catalysis B-Environmental 85(3-4), 171-179.

Ren, D., Deng, Y.L., Handoko, A.D., Chen, C.S., Malkhandi, S. and Yeo, B.S., 2015. *Selective Electrochemical Reduction of Carbon Dioxide to Ethylene and Ethanol on Copper(I) Oxide Catalysts*. Acs Catalysis 5(5), 2814-2821.

Ridruejo, C., Centellas, F., Cabot, P.L., Sires, I. and Brillas, E., 2018. *Electrochemical Fenton-based treatment of tetracaine in synthetic and urban wastewater using active and non-active anodes*. Water Research 128, 71-81.

Salimi, M., Esrafili, A., Gholami, M., Jafari, A.J., Kalantary, R.R., Farzadkia, M., Kermani, M. and Sobhi, H.R., 2017. *Contaminants of emerging concern: a review of new approach in AOP technologies*. Environmental Monitoring and Assessment 189(8), 22.

Serna-Galvis, E.A., Ferraro, F., Silva-Agredo, J. and Torres-Palma, R.A., 2017. *Degradation of highly consumed fluoroquinolones, penicillins and cephalosporins in distilled water and simulated hospital wastewater by UV-254 and UV-254/persulfate processes*. Water Research 122, 128-138.

Shang, J., Li, W. and Zhu, Y.F., 2003. *Structure and photocatalytic characteristics of TiO_2 film photocatalyst coated on stainless steel webnet*. Journal of Molecular Catalysis A-Chemical 202(1-2), 187-195.

Shang, W., Dong, Z., Li, M., Song, X., Zhang, M., Jiang, C. and Sun, F., 2019. *Degradation of diatrizoate in water by Fe(II)-activated persulfate oxidation*. Chemical Engineering Journal 361, 1333-1344.

She, X.Y., Yang, Q., Yao, F.B., Zhong, Y., Ren, W.C., Chen, F., Sue, J., Ma, Y.H., Fe, Z.Y., Wang, D.B. and Li, X.M., 2019. *Electrocatalytic hydrodechlorination of 4-chlorophenol on Pd supported multi-walled carbon nanotubes particle electrodes*. Chemical Engineering Journal 358, 903-911.

Shi, X.D., Li, Y.T., Zhang, Z., Sun, L. and Peng, Y.Z., 2019. *Enhancement of ciprofloxacin degradation in the Fe(II)/peroxymonosulfate system by protocatechuic acid over a wide initial pH range*. Chemical Engineering Journal 372, 1113-1121.

Sires, I., Garrido, J.A., Rodriguez, R.M., Brillas, E., Oturan, N. and Oturan, M.A., 2007. *Catalytic behavior of the Fe^{3+}/Fe^{2+} system in the electro-Fenton degradation of the antimicrobial chlorophene*. Applied Catalysis-B: Environmental 72(3-4), 382-394.

Sirés, I., Garrido, J.A., Rodríguez, R.M., Centellas, F., Arias, C. and Brillas, E., 2006. *Electrochemical degradation of paracetamol from water by catalytic action of Fe^{2+}, Cu^{2+}, and UVA light on electrogenerated hydrogen peroxide*. Journal of the Electrochemical Society 153(1), D1-D9.

Spiro, M., 1979. *The standard potential of the peroxosulphate/sulphate couple*. Electrochimica Acta 24(3), 313-314.

Srivastava, V.J., Hudson, J.M. and Cassidy, D.P., 2016. *Achieving synergy between chemical oxidation and stabilization in a contaminated soil*. Chemosphere 154, 590-598.

Sudoh, M., Kodera, T., Sakai, K., Zhang, J.Q. and Koide, K., 1986. *Oxidative degradation of aqueous phenol effluent with electrogenerated Fenton's reagent*. Journal of Chemical Engineering of Japan 19(6), 513-518.

Sun, C., Zhou, R., Jianan, E., Sun, J.Q. and Ren, H.J., 2015. *Magnetic CuO@Fe3O4 nanocomposite as a highly active heterogeneous catalyst of persulfate for 2,4-dichlorophenol degradation in aqueous solution*. Rsc Advances 5(70), 57058-57066.

Tan, B.J., Klabunde, K.J. and Sherwood, P.M.A., 1991. *XPS studies of solvated metal atom dispersed (SMAD) catalysts. Evidence for layered cobalt-manganese particles on alumina and silica*. Journal of the American Chemical Society 113(3), 855-861.

Tao, Y.F., Ni, Q., Wei, M.Y., Xia, D.S., Li, X.X. and Xu, A.H., 2015. *Metal-free activation of peroxymonosulfate by g-C_3N_4 under visible light irradiation for the degradation of organic dyes*. RSC Advances 5(55), 44128-44136.

Tunay, O. and Kabdasli, N.I., 1994. *Hydroxide precipitation of complexed metals*. Water Research 28(10), 2117-2124.

Waclawek, S., Grubel, K., Dennis, P., Vinod, V.T.P. and Cernik, M., 2016. *A novel approach for simultaneous improvement of dewaterability, post-digestion liquor properties and toluene removal from anaerobically digested sludge*. Chemical Engineering Journal 291, 192-198.

Wagner, C., 1975. *Chemical shifts of Auger lines, and the Auger parameter*. Faraday Discussions of the Chemical Society 60, 291-300.

Wang, L.H., Xu, H.D., Jiang, N., Wang, Z.M., Jiang, J. and Zhang, T., 2020. *Trace Cupric Species Triggered Decomposition of Peroxymonosulfate and Degradation of Organic Pollutants: Cu(III) Being the Primary and Selective Intermediate Oxidant*. Environmental Science & Technology 54(7), 4686-4694.

Wang, S. and Wang, J., 2017. *Comparative study on sulfamethoxazole degradation by Fenton and Fe(II)-activated persulfate process*. Rsc Advances 7(77), 48670-48677.

Wang, Z., Jiang, J., Pang, S.Y., Zhou, Y., Guan, C.T., Gao, Y., Li, J., Yang, Y., Qu, W. and Jiang, C.C., 2018. *Is Sulfate Radical Really Generated from Peroxydisulfate Activated by Iron(II) for Environmental Decontamination?* Environmental Science & Technology 52(19), 11276-11284.

Wardman, P., 1989. *Reduction potentials of one-electron couples involving free radicals in aqueous solution*. Journal of Physical Chemical Reference Data 18(4), 1637-1755.

Wei, G.F., Fang, Y.H. and Liu, Z.P., 2012. *First Principles Tafel Kinetics for Resolving Key Parameters in Optimizing Oxygen Electrocatalytic Reduction Catalyst*. Journal of Physical Chemistry C 116(23), 12696-12705.

Woods, R., Kolthoff, I. and Meehan, E., 1963. *Arsenic (IV) as an intermediate in the induced oxidation of arsenic (III) by the iron (II)-persulfate reaction and the photoreduction of iron (III). I. Absence of oxygen*. Journal of the American Chemical Society 85(16), 2385-2390.

Wu, J., Zhang, H. and Qiu, J.J., 2012. *Degradation of Acid Orange 7 in aqueous solution by a novel electro/Fe^{2+}/peroxydisulfate process*. Journal of Hazardous Materials 215, 138-145.

Xu, L.J., Yang, Y.J., Li, W.Y., Tao, Y.J., Sui, Z.G., Song, S. and Yang, J., 2019. *Three-dimensional macroporous graphene-wrapped zero-valent copper nanoparticles as efficient micro-electrolysis-promoted Fenton-like catalysts for metronidazole removal*. Science of the Total Environment 658, 219-233.

Xu, Y., Lin, H., Li, Y.K. and Zhang, H., 2017. *The mechanism and efficiency of MnO_2 activated persulfate process coupled with electrolysis*. Science of the Total Environment 609, 644-654.

Yamaguchi, R., Kurosu, S., Suzuki, M. and Kawase, Y., 2018. *Hydroxyl radical generation by zero-valent iron/Cu (ZVI/Cu) bimetallic catalyst in wastewater treatment: Heterogeneous Fenton/Fenton-like reactions by Fenton reagents formed in-situ under oxic conditions*. Chemical Engineering Journal 334, 1537-1549.

Yang, Y., Ok, Y.S., Kim, K.H., Kwon, E.E. and Tsang, Y.F., 2017. *Occurrences and removal of pharmaceuticals and personal care products (PPCPs) in drinking water and water/sewage treatment plants: A review*. Science of the Total Environment 596, 303-320.

Yi, Q.Y., Ji, J.H., Shen, B., Dong, C.C., Liu, J., Zhang, J.L. and Xing, M.Y., 2019. *Singlet Oxygen Triggered by Superoxide Radicals in a Molybdenum Cocatalytic Fenton Reaction with Enhanced Redox Activity in the Environment*. Environmental Science & Technology 53(16), 9725-9733.

Yu, Z.Y., Wang, W.H., Song, L., Lu, L.Q., Wang, Z.Y., Jiang, X.F., Dong, C.N. and Qiu, R.Y., 2013. *Acceleration comparison between Fe^{2+}/H_2O_2 and Co^{2+}/oxone for decolouration of azo dyes in homogeneous systems*. Chemical Engineering Journal 234, 475-483.

Yuan, S.H., Liao, P. and Alshawabkeh, A.N., 2014. *Electrolytic Manipulation of Persulfate Reactivity by Iron Electrodes for Trichloroethylene Degradation in Groundwater*. Environmental Science & Technology 48(1), 656-663.

Yue, X.X., Guo, W.L., Li, X.H., Zhou, H.H. and Wang, R.Q., 2016. *Core-shell Fe_3O_4@MIL-101(Fe) composites as heterogeneous catalysts of persulfate activation for the removal of Acid Orange 7*. Environmental Science and Pollution Research 23(15), 15218-15226.

Zeng, H., Zhao, X., Zhao, F., Park, Y. and Sillanpää, M., 2019. *Accelerated Fe^{3+}/Fe^{2+} Cycle using Atomic H* on Pd/Al_2O_3: A Novel Mechanism for an Electrochemical System with Particle Electrode for Iron Sludge Reduction in the Fe^{2+}/Peroxydisulfate Oxidation Process*. Chemical Engineering Journal 122972.

Zeng, H.B., Liu, S.S., Chai, B.Y., Cao, D., Wang, Y. and Zhao, X., 2016. *Enhanced Photoelectrocatalytic Decomplexation of Cu-EDTA and Cu Recovery by Persulfate Activated by UV and Cathodic Reduction*. Environmental Science & Technology 50(12), 6459-6466.

Zhang, L.W., Man, Y. and Zhu, Y.F., 2011. *Effects of Mo Replacement on the Structure and Visible-Light-Induced Photocatalytic Performances of Bi_2WO_6 Photocatalyst*. ACS Catalysis 1(8), 841-848.

Zhang, X.L., Feng, M.B., Qu, R.J., Liu, H., Wang, L.S. and Wang, Z.Y., 2016a. *Catalytic degradation of diethyl phthalate in aqueous solution by persulfate activated with nano-scaled magnetic $CuFe_2O_4$/MWCNTs*. Chemical Engineering Journal 301, 1-11.

Zhang, Y.Q., Zhang, J.F., Xiao, Y.J., Chang, V.W.C. and Lim, T.T., 2016b. *Kinetic and mechanistic investigation of azathioprine degradation in water by UV, UV/H_2O_2 and UV/persulfate*. Chemical Engineering Journal 302, 526-534.

Zhao, X., Guo, L.B., Hu, C.Z., Liu, H.J. and Qu, J.H., 2014a. *Simultaneous destruction of Nickel(II)-EDTA with TiO_2/Ti film anode and electrodeposition of nickel ions on the cathode*. Applied Catalysis B-Environmental 144, 478-485.

Zhao, X., Guo, L.B. and Qu, J.H., 2014b. *Photoelectrocatalytic oxidation of Cu-EDTA complex and electrodeposition recovery of Cu in a continuous tubular photoelectrochemical reactor*. Chemical Engineering Journal 239, 53-59.

Zhao, X., Guo, L.B., Zhang, B.F., Liu, H.J. and Qu, J.H., 2013. *Photoelectrocatalytic Oxidation of Cu(II)-EDTA at the TiO_2 Electrode and Simultaneous Recovery of Cu(II) by Electrodeposition*. Environmental Science & Technology 47(9), 4480-4488.

Zhao, X., Li, A., Mao, R., Liu, H. and Qu, J., 2014c. *Electrochemical removal of haloacetic acids in a three-dimensional electrochemical reactor with Pd-GAC particles as fixed filler and Pd-modified carbon paper as cathode*. Water Research 51, 134-143.

Zhao, X., Zhang, J.J., Qiao, M., Liu, H.J. and Qu, J.H., 2015. *Enhanced Photoelectrocatalytic Decomposition of Copper Cyanide Complexes and Simultaneous Recovery of Copper with a Bi_2MoO_6 Electrode under Visible Light by EDTA/$K_4P_2O_7$*. Environmental Science & Technology 49(7), 4567-4574.

Zhou, D.N., Chen, L., Zhang, C.B., Yu, Y.T., Zhang, L. and Wu, F., 2014. *A novel photochemical system of ferrous sulfite complex: Kinetics and mechanisms of rapid decolorization of Acid Orange 7 in aqueous solutions*. Water Research 57, 87-95.

Zhou, J., Lou, Z., Xu, J., Zhou, X., Yang, K., Gao, X., Zhang, Y. and Xu, X., 2019a. *Enhanced electrocatalytic dechlorination by dispersed and moveable activated carbon supported palladium catalyst*. Chemical Engineering Journal 358, 1176-1185.

Zhou, L., Zheng, W., Ji, Y., Zhang, J., Zeng, C., Zhang, Y., Wang, Q. and Yang, X., 2013. *Ferrous-activated persulfate oxidation of arsenic(III) and diuron in aquatic system*. Journal of Hazardous Materials 263, 422-430.

Zhou, T., Li, Y.Z., Ji, J., Wong, F.S. and Lu, X.H., 2008. *Oxidation of 4-chlorophenol in a heterogeneous zero valent iron/H_2O_2 Fenton-like system: Kinetic, pathway and effect factors*. Separation and Purification Technology 62(3), 551-558.

Zhou, Y.J., Zhang, G., Ji, Q.H., Zhang, W., Zhang, J.Y., Liu, H.J. and Qu, J.H., 2019b. *Enhanced Stabilization and Effective Utilization of Atomic Hydrogen on Pd-In Nanoparticles in a Flow-through Electrode*. Environmental Science & Technology 53(19), 11383-11390.

Zhu, L., Ji, J., Liu, J., Mine, S., Matsuoka, M., Zhang, J. and Xing, M., 2020. *Designing 3D-MoS_2 Sponge as Excellent Cocatalysts in Advanced Oxidation Processes for Pollutant Control*. Angewandte Chemie International Edition

Zou, J., Ma, J., Chen, L.W., Li, X.C., Guan, Y.H., Xie, P.C. and Pan, C., 2013. *Rapid Acceleration of Ferrous Iron/Peroxymonosulfate Oxidation of Organic Pollutants by*

Promoting Fe(III)/Fe(II) Cycle with Hydroxylamine. Environmental Science & Technology 47(20), 11685-11691.

Publication I

Zeng, H.B., Liu, S.S., Chai, B.Y., Cao, D., Wang, Y., and Zhao, X.

Enhanced Photoelectrocatalytic Decomplexation of Cu-EDTA and Cu Recovery by Persulfate Activated by UV and Cathodic Reduction

Reprinted with permission from
Environmental Science & Technology
Vol. 50, pp. 6459-6466, 2016

Environmental Science & Technology

Article

pubs.acs.org/est

Enhanced Photoelectrocatalytic Decomplexation of Cu–EDTA and Cu Recovery by Persulfate Activated by UV and Cathodic Reduction

Huabin Zeng,[†,‡] Shanshan Liu,[†,‡] Buyu Chai,[†] Di Cao,[†,‡] Yan Wang,[†] and Xu Zhao*[,†,‡]

[†]Key Laboratory of Drinking Water Science and Technology, Research Center for Eco-Environmental Sciences, Chinese Academy of Sciences, Beijing 100085, China

[‡]University of Chinese Academy of Sciences, Beijing 100085, China

Supporting Information

ABSTRACT: In order to enhance Cu–EDTA decomplexation and copper cathodic recovery via the photoelectrocatalytic (PEC) process, $S_2O_8^{2-}$ was introduced into the PEC system with a TiO_2/Ti photoanode. At a current density of 0.2 mA/cm^2 and initial solution pH of 3.0, the decomplexation ratio of Cu complexes was increased from 47.5% in the PEC process to 98.4% with 5 mM $S_2O_8^{2-}$ addition into the PEC process (PEC/$S_2O_8^{2-}$). Correspondingly, recovery percentage of Cu was increased to 98.3% from 47.4% within 60 min. It was observed that nearly no copper recovery occurred within the initial reaction period of 10 min. Combined with the analysis of ESR and electrochemical LSV curves, it was concluded that activation of $S_2O_8^{2-}$ into $SO_4^{\cdot-}$ radicals by cathodic reduction occurred, which was prior to the reduction of liberated Cu^{2+} ions. UV irradiation of $S_2O_8^{2-}$ also led to the production of $SO_4^{\cdot-}$. The generated $SO_4^{\cdot-}$ radicals enhanced the oxidation of Cu–EDTA. After the consumption of $S_2O_8^{2-}$, the Cu recovery via cathodic reduction proceeded quickly. Acidification induced by the transformation of $SO_4^{\cdot-}$ to OH· favored the copper cathodic recovery. The combined PEC/$S_2O_8^{2-}$ process was also efficient for the TOC removal from a real electroplating wastewater with the Cu recovery efficiency higher than 80%.

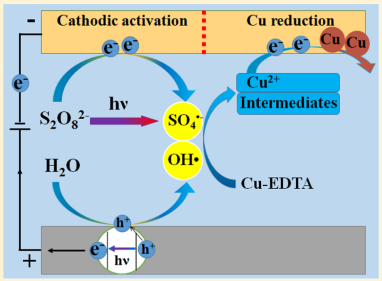

INTRODUCTION

The Cu ions and chelating agents, such as EDTA and CN^-, widely coexisted in the effluents from the electroplating, mining and photographic industries.[1] The stable Cu complexes formed from chelating agents and copper ions were difficult to be removed by conventional processes, such as coagulation, adsorption, precipitation and biological process.[2,3] To achieve an effective treatment of Cu complexes, not only the destruction of the chelating agents but also the copper recovery was desirable.

Photoelectrocatalytic (PEC) process can destroy the Cu–EDTA, Ni–EDTA, and $Cu(CN)_3^{2-}$ with the simultaneous recovery of the liberated Cu/Ni ions reported in our previous work.[4−6] Under the light irradiation, photogenerated holes and induced hydroxyl radicals (OH·) from the semiconductor photoanode can destroy metal-complexes, and the liberated metal ions were deposited onto the cathode by electrochemical reduction, which was convenient for the recovery.[6] Unfortunately, the PEC oxidation of metal-complexes mainly occurred around the photoanode with a low oxidation efficiency and long reaction time, which limited its application.

In recent years, persulfate ($S_2O_8^{2-}$) has received an increasing interest in both scientific research and application for the groundwater remediation and wastewater treatment.[7−9] When being activated, they can produce strong sulfate radicals ($SO_4^{\cdot-}$), which can react with a wide range of organic and inorganic contaminants,[10−12] due to its high redox potential, even compared with that of OH·.[13,14] Generally, $S_2O_8^{2-}$ activation to $SO_4^{\cdot-}$ can be initiated under the thermal, photochemical and metal ions catalysis conditions.[15−18] In the application of $S_2O_8^{2-}$ for in situ chemical oxidation, the low reactivity of $S_2O_8^{2-}$ under low temperature or the natural minerals conditions ensured the $S_2O_8^{2-}$ reaching the contaminated zone.[9,19] However, in order to employ the $S_2O_8^{2-}$ in the wastewater treatment, acceleration of the $S_2O_8^{2-}$ activation was desired. It has been exhibited that 4-chloro-3-methylphenol was abated within 3–59 s in pressurized hot water and in supercritical water with the $S_2O_8^{2-}$ addition activated by high temperature.[20] To some extent, the limitation in such homogeneous processes was the energy consumption, as well as the thermal pollution to the environment.[18] The coupling of $S_2O_8^{2-}$ with metals such as Fe^{2+} and Co^{2+} led to the formation of $SO_4^{\cdot-}$ radicals (reaction 1 ∼ 2), which were responsible for the rapid removal of microcystin-LR and bisphenol A.[15,21]

$$S_2O_8^{2-} + Fe^{2+} \rightarrow SO_4^{\cdot-} + SO_4^{2-} + Fe^{3+} \quad (1)$$

$$S_2O_8^{2-} + Co^{2+} \rightarrow SO_4^{\cdot-} + SO_4^{2-} + Co^{3+} \quad (2)$$

Received: February 5, 2016
Revised: May 15, 2016
Accepted: May 23, 2016

DOI: 10.1021/acs.est.6b00632
Environ. Sci. Technol. XXXX, XXX, XXX−XXX

In these processes, the subsequent recovery of metal ions had to be performed for the purpose of catalysts reuse and prevention from secondary contamination.[15] The copper and iron oxides were employed as heterogeneous catalysts for $S_2O_8^{2-}$ activation and convenient to reuse, the metal leaching at acid condition cannot be completely avoided and the rate of heterogeneous activation remained low.[22−24] With respect to the UV activation, large amount of $SO_4^{\cdot-}$ were produced in the bulk solution, which led to the efficient degradation of 2,4-dichlorophenol.[25] And secondary pollution was greatly minimized with sulfate ions as the only end-product.[12] Furthermore, the photolysis activation can work over a broad pH range.[12,17,24]

In light of the UV photolysis activation, $S_2O_8^{2-}$ ions were added into the PEC system consisting of TiO_2 photoanode and stainless steel cathode with the UV light irradiation. The results indicated that, in comparison with the individual PEC process, the Cu−EDTA destruction and the recovery of the liberated Cu^{2+} ions by a cathodic deposition were largely improved with the addition of $S_2O_8^{2-}$. $SO_4^{\cdot-}$ generated by the UV activation of $S_2O_8^{2-}$ was confirmed. Based on the ESR and XPS analysis, it was found that, at the initial reaction phase, a cathodic activation of $S_2O_8^{2-}$ ions occurred, leading to the production of $SO_4^{\cdot-}$ radicals, which can also enhance the destruction of Cu−EDTA. After the consumption of $S_2O_8^{2-}$ ions, the electrodeposition of the liberated Cu^{2+} ions occurred quickly. Furthermore, the enhanced mechanism induced by $S_2O_8^{2-}$ was proposed.

EXPERIMENTAL SECTION

Chemicals. Copper sulfate ($CuSO_4$), sodium persulfate ($Na_2S_2O_8$) and sodium sulfite (Na_2SO_3) were purchased from Acros. Sodium sulfate (Na_2SO_4) and ethylenediaminetetraacetic acid disodium salt (Na_2EDTA) were purchased from Sinopharm chemical reagent Co., Ltd. China.

The simulated wastewater containing Cu−EDTA was prepared by mixing a solution of $CuSO_4$ and Na_2EDTA to obtain a 1:1 molar ratio of Cu^{2+}/EDTA. Solution pH regulation was performed using either 100 mM NaOH or 50 mM H_2SO_4. Deionized water was used for the preparation and dilution of the solutions. A sample of a real electroplating wastewater was taken from Quanzhou City, China. The wastewater contained Cu^{2+} ions and organic chelating agent including EDTA. The concentration of Cu was determined to be 65 mg/L; Total organic carbon (TOC) was measured to be 244 mg/L; Solution pH was measured to be 2.6; the qualities of the real wastewater were shown in the Supporting Information Table SI-1.

Setup and Experiment. The PEC experiments with a batch mode were performed in an undivided cell with a volume of 500 mL. The tubular TiO_2/Ti mesh electrode (50 mm diameter) was used as anode, and the TiO_2 film was deposited onto the Ti plate via a dip-coating method as described by Shang et al.[26] A tubular mesh stainless steel (66 mm) was used as cathode. The gap between the anode and cathode was 8 mm. A UV lamp (main wavelength 254 nm; 9 W) in a quartz tube was put in the center of the tubular TiO_2/Ti mesh electrode.

Analytical Method. The concentration of total Cu complexes was measured by a high-performance liquid chromatography (HPLC, 1260, Agilent Technology) with a C18 column and ultraviolet detector. The elution was comprised of 92% oxalic acid (concentration, 15 mM; pH, 3.0)/8% acetonitrile (V/V) at a temperature of 25 °C. The flow rate was set as 1 mL/min and the detection wavelength was set as 254 nm. The detection method of total Cu complexes was attached in the Supporting Information (Text SI-1).

Concentration of total Cu^{2+} ions was measured using 700 series inductively coupled plasma-optical emission spectrometry (ICP-OES, Agilent Technology). Total organic carbon (TOC) was measured using a Shimadzu TOC analyzer (TOC-VCPH, Shimadzu, Japan). The procedure of the copper mass balance was illustrated in the Text SI-2 (Supporting Information) in details. The pH was measured using a 9165 BN pH electrode connected to an Orion-828 pH analyzer (Orion Research, Inc., Beverly, MA). The linear sweep voltammetry (LSV) was conducted in a single-compartment, three electrode cell on a CHIN800D instrument (CH Instrument Co.). $S_2O_8^{2-}$ concentration was determined colorimetrically by a similar method to H_2O_2 on a spectrophotometer, which was illustrated in the Supporting Information (Text SI-3).[27]

The morphology of the cathode was characterized using JSM 6301 scanning electron microscopy (SEM). X-ray photoelectron spectra (XPS) were used to analyze the surface variation of the electrode using a PHI Quantera SXM (PHIEnvironmental 5300/ESCA, ULVAC-PHI, Inc.). Prior to the measurement, the electrode was washed with water to remove electrolyte. Formation of active radicals was identified with electron spin resonance (ESR) on a Bruker ESR 300E with a microwave bridge (receiver gain, 1 × 105; modulation amplitude, 2 G; microwave power, 10 mW; modulation frequency, 100 kHz). Since the $HO_2^{\cdot-}/O_2^{\cdot-}$ in water are very unstable and underwent facile disproportionation rather than slow reaction with DMPO,[28] OH· and $SO_4^{\cdot-}$ were identified with ESR in the experiment. The samples (100 μL) were collected from the reaction solution at different times. For OH· and $SO_4^{\cdot-}$ measurement, the sample mixed immediately with 20 μL DMPO (0.2 M) to form DMPO−OH adduct and DMPO−SO_4 adduct.

RESULTS AND DISCUSSION

Enhanced Performance of $S_2O_8^{2-}$ Addition on the PEC Process. The performance of the PEC process for the Cu−EDTA destruction and Cu recovery with the addition of the given amount of $S_2O_8^{2-}$ into the PEC process was examined first. The recovery percentage of Cu^{2+} ions was defined as following:

$$R_{Cu} = 100\% \times (\text{initial amount of } Cu^{2+}\text{ions} - \text{remained amount of } Cu^{2+}\text{ions})\text{in the reaction cell} / \text{initial amount of } Cu^{2+}\text{ions in the reaction cell}$$

As shown in Figure 1(a), decomplexation ratio of Cu complexes are 47.5% in the PEC process with the current density of 0.2 mA/cm^2 at 60 min. By contrast, in the PEC process with the $S_2O_8^{2-}$ addition (PEC/$S_2O_8^{2-}$), the decomplexation ratio is increased to 98.4%. Meantime, with the addition of the same amount of $S_2O_8^{2-}$ ions, Cu complexes decomplexation and copper recovery by the UV irradiation (UV/$S_2O_8^{2-}$) process and the electro-oxidation (EC/$S_2O_8^{2-}$) process were also tested as a reference. In the UV/$S_2O_8^{2-}$ process, nearly no decomplexation of Cu complexes occur (Figure 1(a)). With the Cu−EDTA destruction, complexation occurred between the Cu^{2+} ions with the generated intermediates including ethylendiamine diacetate (EDDA), nitrilotriacetic acid (NTA) and iminodiacetic acid (IDA), which was illustrated in the Supporting Information Text SI-4. As a result, nearly no concentration decrease of total Cu complexes is observed. In the EC/$S_2O_8^{2-}$ process, decomplexation ratio of Cu complexes are 21.6%. Similar results can be obtained for the Cu recovery (Figure 1(a)). The above results indicated that not only efficient decomplexation of Cu complexes

DOI: 10.1021/acs.est.6b00632
Environ. Sci. Technol. XXXX, XXX, XXX−XXX

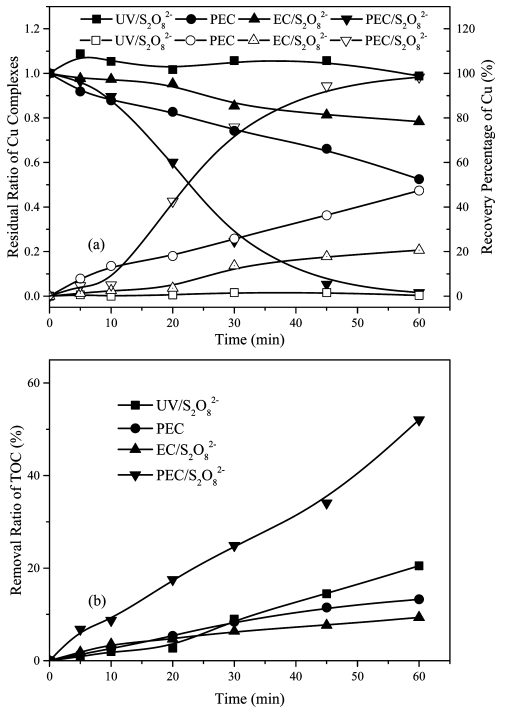

Figure 1. (a) Variation of residual Cu complexes ratio and recovery percentage of Cu and (b) TOC removal ratio in the UV/$S_2O_8^{2-}$ process, PEC process, EC/$S_2O_8^{2-}$ process and PEC/$S_2O_8^{2-}$ process. ((Cu-EDTA), 0.2 mM; ($Na_2S_2O_8$), 5 mM; initial solution pH, 3.0; current density, 0.2 mA/cm^2).

was obtained but also Cu recovery was largely improved when a given amount of 5 mM $S_2O_8^{2-}$ was added into the PEC process.

In the individual PEC process, the oxidation destruction of Cu complexes was mainly induced by the active radicals, particularly OH·, generated from the TiO_2 photoanode under UV light irradiation.[4] Due to the limitation of the diffusion mass transfer and low concentration of generated OH·, the destruction efficiency of Cu complexes was low. It has been reported that the UV photolysis of one molar of $S_2O_8^{2-}$ produced two molar of $SO_4^{\cdot-}$ according to the reaction 3.[29]

$$S_2O_8^{2-} + h\nu \rightarrow 2SO_4^{\cdot-} \quad (3)$$

The addition of $S_2O_8^{2-}$ into the PEC system may lead to an efficient production of $SO_4^{\cdot-}$ in the bulk solution. Therefore, it can be concluded that the efficient decomplexation of Cu complexes was induced by the oxidation of $SO_4^{\cdot-}$ radicals in the bulk solution and active OH· generated via the PEC process. With the improved destruction of Cu-complexes, liberated copper ions were efficiently recovered by the cathodic reduction deposition. TOC variation under the various processes was furthermore compared. As shown in Figure 1(b), TOC removal efficiencies increase with the reaction time for all of the processes. At 60 min, TOC removal efficiencies are 20.5%, 13.3%, 9.35%, and 52.1% for the UV/$S_2O_8^{2-}$ process, PEC process, EC/$S_2O_8^{2-}$ process and PEC/$S_2O_8^{2-}$ process. Obviously, the addition of $S_2O_8^{2-}$ largely enhanced the TOC removal in the PEC process.

To optimize the conditions for PEC/$S_2O_8^{2-}$ process, the effect of $S_2O_8^{2-}$ concentration and current density on the decomplexation of Cu complexes and Cu recovery was investigated. Figure 2(a) displays the residual ratio of Cu complexes and

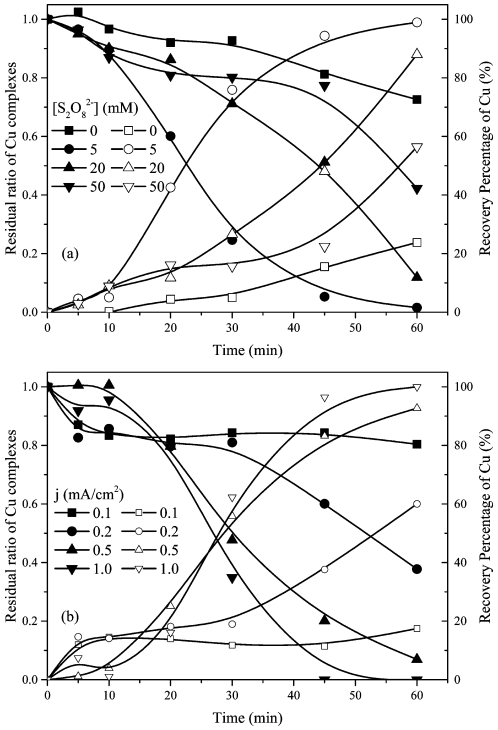

Figure 2. (a) Effect of $S_2O_8^{2-}$ concentration on the PEC process (current density, 0.2 mA/cm^2); (b) Effect of current density on the PEC/$S_2O_8^{2-}$ process (($Na_2S_2O_8$), 10 mM) ((Cu–EDTA), 0.5 mM; initial solution pH, 3.0; current density, 0.2 mA/cm^2).

recovery percentage of Cu as a function of time during the PEC/$S_2O_8^{2-}$ process with different $S_2O_8^{2-}$ concentrations. The decomplexation ratios of Cu complexes at the initial $S_2O_8^{2-}$ concentration of 0 mM, 5 mM, 20 mM and 50 mM are 27.4%, 98.4%, 88.1%, and 57.7%, respectively. The best performance in the decomplexaiton process of Cu complexes was obtained at the initial $S_2O_8^{2-}$ concentration of 5 mM. A similar trend for the Cu recovery is observed. Figure 2(b) investigated the effect of current density on the performance of the PEC/$S_2O_8^{2-}$ process. Corresponding to the current density of 0.1 mA/cm^2, 0.2 mA/cm^2, 0.5 mA/cm^2 and 1.0 mA/cm^2, the decomplexation ratios of Cu complexes are 19.6%, 62.2%, 93.1%, and 100%, and the recovery percentages of Cu are 17.5%, 60.0%, 92.7%, and 100%. It can be seen that the increase of the current density significantly enhanced the decomplexaiton of Cu complexes and Cu recovery.

Additionally, it is notable from Figure 2 that the decomposition of Cu complexes and Cu recovery can be divided into two phases. In the initial phase, the Cu complexes decom-

DOI: 10.1021/acs.est.6b00632
Environ. Sci. Technol. XXXX, XXX, XXX−XXX

plexaiton and Cu recovery proceeded at a low rate. After that, the rate rapidly increased. The transition point varied with the $S_2O_8^{2-}$ concentration and current density. It can be seen from the Figure 2(a) that the transition points between these two stages appear at 5 min, 20 and 45 min, when the initial concentrations of $S_2O_8^{2-}$ are 5 mM, 20 mM and 50 mM, respectively. With higher concentration of $S_2O_8^{2-}$, the period of Cu complexes decomplexaiton with a low rate by this system remained longer. It should be point out here that the reaction rate stays relatively stable in the PEC process without $S_2O_8^{2-}$. In Figure 2(b), the rate increased at the point of 60 min, 30 min, 10 and 10 min with the current density of 0.1 mA/cm^2, 0.2 mA/cm^2, 0.5 mA/cm^2 and 1.0 mA/cm^2. It was clear that the reaction time of the initial stage with a slow reaction rate had a positive correlation with concentration of $S_2O_8^{2-}$, which was negative to the current density. The differences will be explained subsequently.

Acidification Induced by $S_2O_8^{2-}$ Oxidation. Effect of initial pH on the decomplexation of Cu complexes and Cu recovery in the PEC process and PEC/$S_2O_8^{2-}$ process was investigated. In the individual PEC process, Cu recovery obviously decreases under the alkaline and neutral condition (Supporting Information Figure SI-11(a)), which can be explained by the different adsorption ability of Cu^{2+} and EDTA on the anode and the variation of Cu−EDTA species with solution pH.[4] By contrast, the variation of initial solution pH has slight influence on the PEC/$S_2O_8^{2-}$ process (Supporting Information Figure SI-11(b)). It is obviously that the addition of $S_2O_8^{2-}$ benefitted the high efficiencies of Cu complexes decomplexation and Cu recovery under a wide pH range.

Furthermore, the distribution of Cu species was analyzed at various initial solution pH. With respect to the individual PEC process, as shown in Figure 3(a), under the initial solution pH of 3.0, 22.9% of Cu is removed from the solution and 21.1% is deposited on the cathode. It is noticed that the liberated Cu^{2+} ions prefer to deposit on the anode rather than to deposit on the cathode with the increase of the initial solution pH. Under the alkaline condition, the formation of the copper (hydro) oxides from the liberated Cu^{2+} ions became easier,[6] which would deposit onto the TiO_2 photoanode surface once the Cu complexes were completely destroyed. The copper (hydro)-oxides precipitated on the anode will occupy active sites or cause adverse effects on the generation of OH·, which inhibited the decomplexation of Cu complexes and Cu recovery.[30] By contrast, a different behavior was exhibited in the PEC/$S_2O_8^{2-}$ system with the variation of initial solution pH. While recovery percentages of Cu are 61.9%, 59.8%, and 53.2%, percentages of Cu precipitated on the anode are detected as 1.71%, 1.18%, and 0.511% respectively, corresponding to the initial solution pH of 3.0, 7.0, and 11.0 (Figure 3(a)). The liberated Cu ions were mainly deposited onto the cathode under all initial solution pH conditions. As shown in Figure 3(b), the solution pH values remain to be constant in the individual PEC process. By contrast, the solution pH rapidly decreases to about 2.1 in the PEC/$S_2O_8^{2-}$ process at various initial pH.

The redox potential of $SO_4^{\cdot-}$ was confirmed as 2.5−3.1 V,[14] while the potential of OH· was detected as 2.7 V in acid solution and 1.8 V in neutral solution.[13] Due to the narrow gap of redox potential between $SO_4^{\cdot-}$ and OH·, the interconversion from $SO_4^{\cdot-}$ to OH· occurred by the following reaction 4 and reaction 5.[31]

$$SO_4^{\cdot-} + OH^- \rightarrow OH\cdot + SO_4^{2-} \quad (4)$$

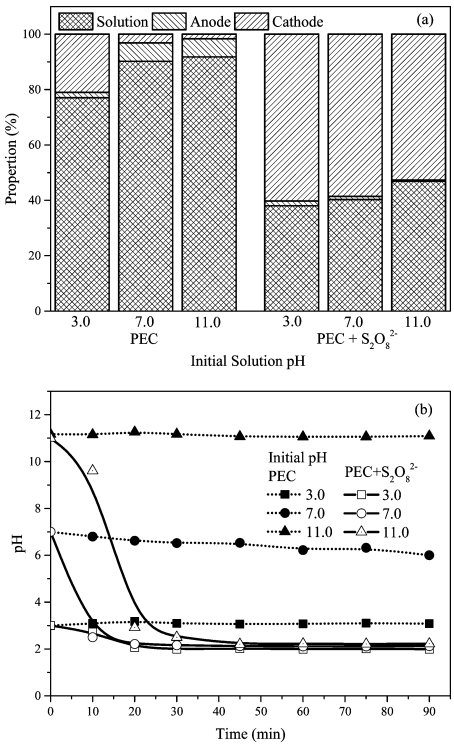

Figure 3. (a) The copper mass balance and (b) variation of the solution pH in the PEC process and the PEC/$S_2O_8^{2-}$ process under various initial solution pH. ((Cu−EDTA), 1.0 mM; ($Na_2S_2O_8$), 50 mM; current density, 0.2 mA/cm^2).

$$SO_4^{\cdot-} + H_2O \rightarrow OH\cdot + SO_4^{2-} + H^+ \quad (5)$$

According to the radicals quenching study, OH· played a dominant role in the PEC/$S_2O_8^{2-}$ process even in the acidic condition (Supporting Information Text SI-5). It was indicated that a large portion of $SO_4^{\cdot-}$ was transferred into OH· with the consumption of the OH^- or the production of H^+. As a result, the solution pH decreased at the initial phase. It should be pointed out here that the acidic condition was beneficial to the decomplexation process and Cu recovery process than the alkaline condition.[4]

It can be concluded that the $S_2O_8^{2-}$ ions played a double role in the PEC/$S_2O_8^{2-}$ process. On one hand, $SO_4^{\cdot-}$ radicals generated from the $S_2O_8^{2-}$ ions contributed to the enhanced destruction of Cu complexes. On the other hand, the rapid decrease of the system pH benefitted the further duestruction of Cu complexes and the subsequent cathodic reduction of liberated Cu^{2+} ions onto the cathode.

Involved Active Radicals. First, the active radicals in the UV/$S_2O_8^{2-}$, PEC and PEC/$S_2O_8^{2-}$ processes were analyzed using the ESR technique with the DMPO addition. The hyperfine splitting constants of DMPO radicals adducts of DMPO−OH and DMPO−SO_4 were representative of OH· and $SO_4^{\cdot-}$ radicals, respectively.[32,33] As shown in Figure 4(a), the signals of DMPO−SO_4 and DMPO−OH in the PEC/$S_2O_8^{2-}$

DOI: 10.1021/acs.est.6b00632
Environ. Sci. Technol. XXXX, XXX, XXX−XXX

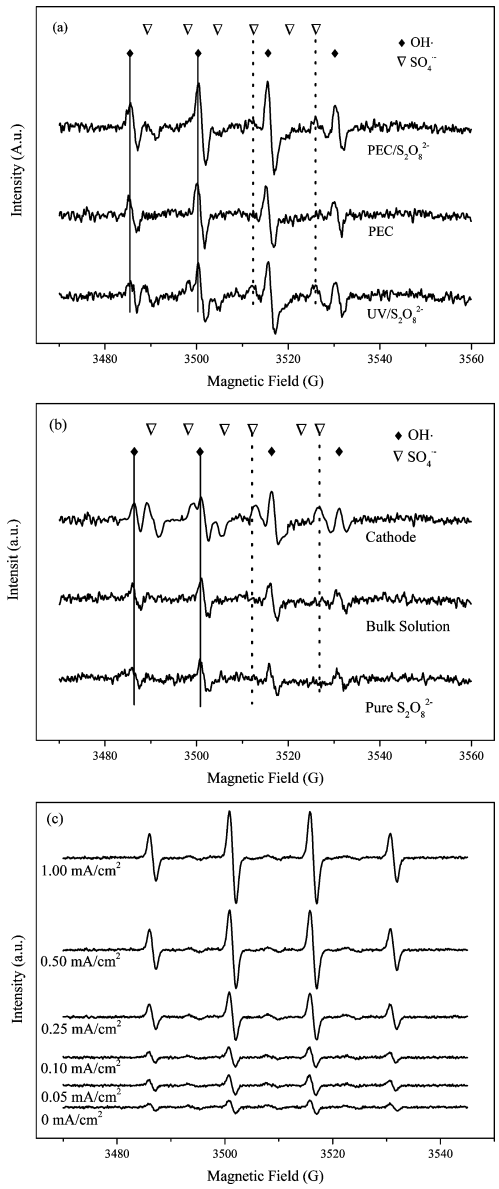

Figure 4. (a) DMPO spin-trapping ESR spectra recorded at ambient temperature in the PEC process, UV/$S_2O_8^{2-}$ process and PEC/$S_2O_8^{2-}$ process; (b) DMPO spin-trapping ESR spectra recorded at ambient temperature in the $S_2O_8^{2-}$ oxidation process and in the bulk solution and around the cathode of the EC/$S_2O_8^{2-}$ process; (c) Effect of the current density on the ESR signals of DMPO−OH at the solution pH of 10.0.

and UV/$S_2O_8^{2-}$ processes are observed, indicating the generation of $SO_4^{\cdot-}$ and OH· radicals. Furthermore, the signals intensities of DMPO−OH and DMPO−SO_4 in the PEC/$S_2O_8^{2-}$ process are stronger than that in the PEC process and that in UV/$S_2O_8^{2-}$ process, respectively. With respect to the EC/$S_2O_8^{2-}$ process, nearly no enhanced signal of DMPO−SO_4 and DMPO−OH in the bulk solution was observed (Figure 4(b)); it is interesting to observe that the obvious signals of DMPO−SO_4 around the cathode appear (Figure 4(b)). It was suggested that the $S_2O_8^{2-}$ can be activated into $SO_4^{\cdot-}$ by the cathodic reduction. To support this conclusion, the variation of radicals' production rate around cathode with increase of current density in the EC/$S_2O_8^{2-}$ process was investigated at the solution pH of 10.0, where the ESR signals of DMPO−OH can be regard as representative of total radicals due to nearly complete transformation of $SO_4^{\cdot-}$ to OH·.[31] As shown in Figure 4(c), high current density has a positive effect on the intensity of DMPO−OH signals, indicating that increasing current density can promote the cathodic activation of $S_2O_8^{2-}$ and was beneficial to the production of active radicals.

Activation of $S_2O_8^{2-}$ to $SO_4^{\cdot-}$ by UV irradiation has been largely investigated.[15,17] In our case, $SO_4^{\cdot-}$ in the bulk solution may be mainly induced by the UV activation process. It also has been recognized that $SO_4^{\cdot-}$ can be formed as a result of the electron transfer from the reductive materials, such as Fe^{2+}, Fe and other reducing organics to $S_2O_8^{2-}$.[15,34−39] In the EC system, the cathode also had the same ability to donate electron. Thus, the $SO_4^{\cdot-}$ may be generated from $S_2O_8^{2-}$ via a cathodic activation (reaction 6).

$$S_2O_8^{2-} + e^- \rightarrow SO_4^{\cdot-} + SO_4^{2-} \quad (6)$$

It has been reported that photogenerated electron of C_3N_4-photocatalysis can activate $S_2O_8^{2-}$ under visible light irradiation.[39] In the PEC/$S_2O_8^{2-}$ process, activation of $S_2O_8^{2-}$ by photogenerated electrons transferred to the cathode by bias potential may occur. In general, in the PEC/$S_2O_8^{2-}$ process, the cathodic activation and UV photolysis activation accelerated the production of active radicals, which were responsible for the enhanced performance of Cu complexes oxidation and Cu recovery.

A Proposed $S_2O_8^{2-}$ Enhanced Reaction Process. The electrochemical behaviors of Cu^{2+}, Cu−EDTA and $S_2O_8^{2-}$ in solution of 0.1 M Na_2SO_4 were investigated by linear sweep voltammetry. It can be seen from Figure 5(a) that the current intensity increases with the concentration of $S_2O_8^{2-}$ at the potential lower than 0.20 V, which indicates that the cathodic reduction of $S_2O_8^{2-}$ begins at the potential of 0.20 V vs Ag/AgCl. By contrast, the cathodic reduction of Cu^{2+} and Cu−EDTA begins at the potential of −0.02 V (Figure 5(b)) and −0.28 V (Figure 5(c)), respectively. The lower reduction potential of both Cu^{2+} and Cu−EDTA than $S_2O_8^{2-}$ indicated that $S_2O_8^{2-}$ was prior to be activated through reaction 6 on the cathode. Then, the cathodic reduction of the liberated Cu^{2+} ions occurred.

The residual ratio of $S_2O_8^{2-}$ and Cu recovery percentage in the PEC/$S_2O_8^{2-}$ process were investigated at a $S_2O_8^{2-}$ concentration of 5 mM and a Cu−EDTA concentration of 0.5 mM. The $S_2O_8^{2-}$ concentration decreases rapidly with a low rate of Cu recovery at the beginning of 10 min (Supporting Information Figure SI-12). After the $S_2O_8^{2-}$ concentration decreases to 1 mM, the Cu ions are removed rapidly.

Surface variation of the titanium cathode at the different reaction time in the PEC/$S_2O_8^{2-}$ process was characterized by SEM and EDS analysis. In comparison with that before the reaction (Supporting Information Figure SI-13 (a-I)), it can be seem from Supporting Information Figure SI-13 (a-II) that the nearly no copper can be observed on the surface of cathode at 10

DOI: 10.1021/acs.est.6b00632
Environ. Sci. Technol. XXXX, XXX, XXX−XXX

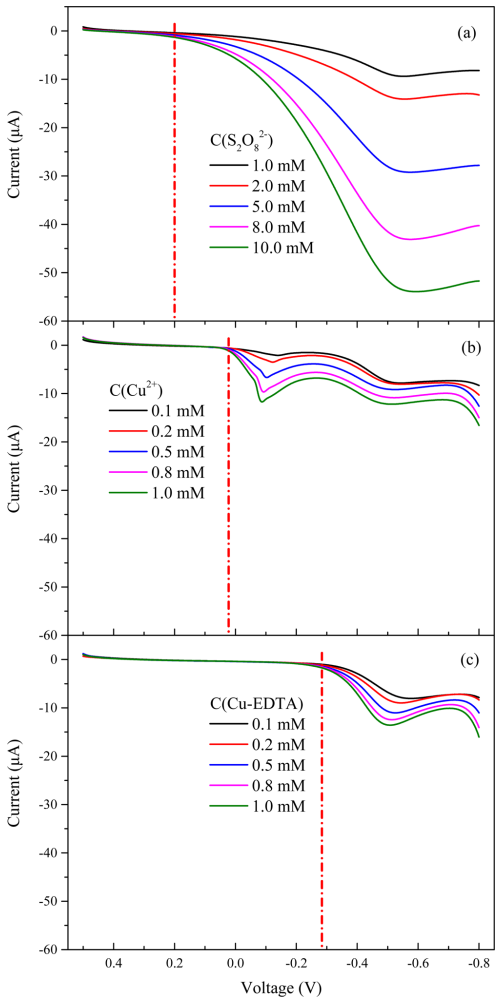

Figure 5. Linear sweep voltammetry of (a) $S_2O_8^{2-}$, (b) Cu^{2+} and (c) Cu−EDTA with various concentrations at the glassy carbon electrode in 0.1 M Na_2SO_4 (Solution pH, 3.0).

min. By contrast, as shown in Supporting Information Figure SM-13 (a-III), the cathode at 45 min is occupied with granular deposition. It can be seen from Supporting Information Figure SI-13 (b-I), (b-II) and (b-III) that the atomic percentage of Cu from the EDS analysis on the cathode is increased from 0.838% to 0.979% after 10 min' reaction. By contrast, it is increased to 14.41% at 45 min. The XPS analysis further confirmed the above results (shown in Figure 6(a)). XPS spectra in the Cu $2p_{3/2}$ region for the titanium cathode for the 45 min reaction are given in Figure 6(b). The signals are presented at 932.8 and 952.4 eV, which are assignable to the emissions from the Cu $2p_{3/2}$ and Cu $2p_{1/2}$ levels and respondent to the binding energies of Cu^0.[40] It is notable to point out that there is no signal at 934 eV, which is directly related to the presence of CuO species.

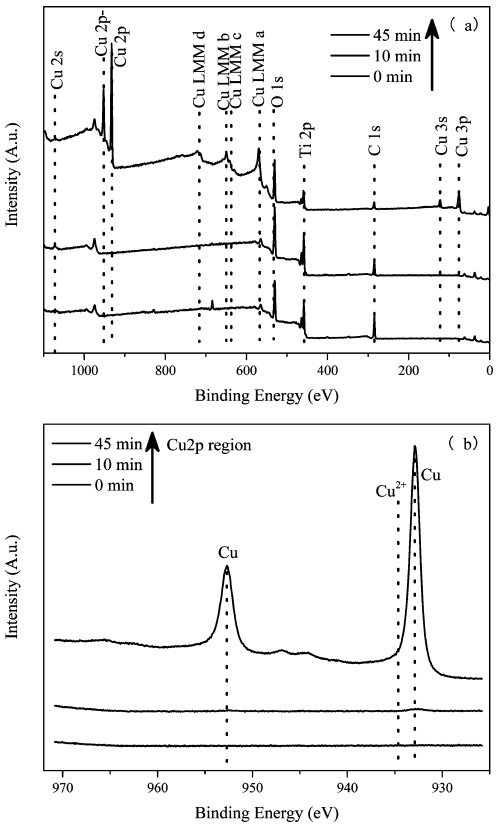

Figure 6. XPS analysis of the titanium cathode at the different reaction time in the PEC/$S_2O_8^{2-}$ process: (a) XPS full scan of the Titanium cathode; (b) XPS analysis in the Cu 2p region of the titanium cathode.

Summarily, as shown in Figure 7, at the beginning of the PEC/$S_2O_8^{2-}$ process, besides the PEC oxidation of Cu−EDTA, the

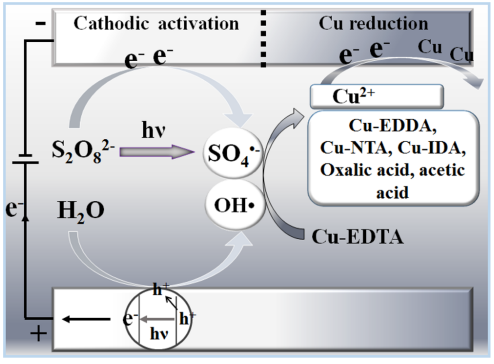

Figure 7. Schematic of the PEC/$S_2O_8^{2-}$ process.

DOI: 10.1021/acs.est.6b00632
Environ. Sci. Technol. XXXX, XXX, XXX−XXX

$SO_4^{\cdot-}$ was greatly generated through the cathodic activation and photolysis activation to enhance the decomplexation process of Cu−EDTA. As a result, the efficient decomplexation was achieved. The reduction of $S_2O_8^{2-}$ was prior to that of the liberated Cu^{2+} ions at the cathode. Once the $S_2O_8^{2-}$ ions were consumed, the cathodic reduction of liberated Cu^{2+} ions dominated the cathodic reaction. Meantime, the conversion of $SO_4^{\cdot-}$ to OH· rapidly contributed to the pH decrease, which was beneficial for the Cu^{2+} recovery. The liberated Cu^{2+} ions were efficiently deposited onto the cathode followed by the Cu^0 electroreduction.

Environmental Implications for Wastewater Treatments. This paper exhibited that activation of $S_2O_8^{2-}$ to $SO_4^{\cdot-}$ can be achieved by cathodic reduction and UV irradiation jointly in the PEC system, which largely increased the oxidation efficiency of the PEC process toward the destruction of Cu−EDTA and cathodic recovery of Cu ions across a wide range of pH conditions. In order to check the efficiency of PEC/$S_2O_8^{2-}$ process, a real electroplating effluent was treated by the PEC/$S_2O_8^{2-}$ process. The initial Cu^{2+} and TOC content were determined to be 65 mg/L and 244 mg/L, respectively. Due to many kinds of organics chelating agents in the effluent, the variation of TOC removal was used as a probe of the organics abatement level. As shown in Figure 8(a), with the increase of

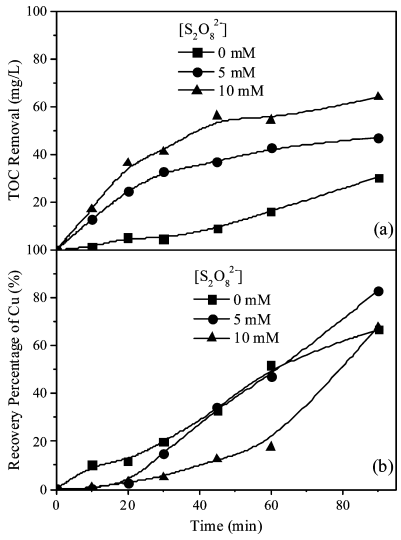

Figure 8. Effect of $S_2O_8^{2-}$ concentration on the (a) TOC removal and (b) Cu recovery in the PEC/$S_2O_8^{2-}$ process to treat an actual wastewater containing Cu−EDTA. (Cu, 65 mg/L; initial TOC, 244 mg/L; initial solution pH, 2.6; current density, 0.4 mA/cm^2).

$S_2O_8^{2-}$ concentration from 0 mM to 10 mM, the TOC removal was improved from 30.29 mg/L to 64.00 mg/L, indicating that the organics in the electroplating wastewater were efficiently abated in the PEC/$S_2O_8^{2-}$ process. At the same time, the percentage of Cu recovery in 90 min is as high as 82.8% with the addition of 5 mM $S_2O_8^{2-}$ (Figure 8(b)). This result furthermore demonstrated that the $S_2O_8^{2-}$ enhanced PEC process can achieved a fast destruction of Cu complexes with simultaneous Cu cathodic reduction.

Generally, penetrability of UV light due to the block of turbidity and chromaticity, as well as the NO_3^- of high concentration (Supporting Informsation Text SI-6), and the design of the PEC system should be considered carefully in the application of PEC/$S_2O_8^{2-}$ process. The impact of some ions in the real electroplating wastewater, such as Cl^- and SO_4^{2-}, on the PEC/$S_2O_8^{2-}$ process also was investigated. The SO_4^{2-} exhibited a limited effect on TOC removal and Cu recovery (Supporting Information Text SI-7). By contrast, an obvious negative influence was observed with the Cl^- addition into the PEC/$S_2O_8^{2-}$ process (Supporting Information Text SI-8). Besides the ions in the wastewater, the dissolved oxygen may also impede the $S_2O_8^{2-}$ activation and Cu recovery on the cathode due to its competition between O_2 with $S_2O_8^{2-}$ or Cu^{2+} on the cathode (Supporting Information Text SI-9). A pilot-scale experiment of the application of this PEC/$S_2O_8^{2-}$ process in treating the real electroplating wastewater containing heavy metal complexes with the simultaneous metal ions recovery will be performed to further optimize the reaction parameters and confirm its adaptation. And, a large-scale testing and engineering cost comparisons are necessary before PEC/$S_2O_8^{2-}$ process can be recommended for full scale applications.

■ ASSOCIATED CONTENT

Supporting Information

The Supporting Information is available free of charge on the ACS Publications website at DOI: 10.1021/acs.est.6b00632.

Additional information about the detection methods of total Cu complexes and $S_2O_8^{2-}$, procedure of Cu mass balance, proposed degradation pathway of Cu−EDTA, radicals quenching study, effect of NO_3^-, SO_4^{2-}, Cl^- and O_2 on the PEC/$S_2O_8^{2-}$ process, effect of initial solution pH on the PEC process and PEC/$S_2O_8^{2-}$ process, the variation of $S_2O_8^{2-}$ concentration and Cu^{2+}, characteristics of the cathode at different reaction time and qualities variation of the real electroplating wastewater (PDF)

■ AUTHOR INFORMATION

Corresponding Author

*Phone: +86-10-62849667; fax: +86-10-62849667; e-mail: zhaoxu@rcees.ac.cn.

Notes

The authors declare no competing financial interest.

■ ACKNOWLEDGMENTS

This work was supported by National Natural Science Foundation of China (No. 21377148, 51438011, 51222802).

■ REFERENCES

(1) Lopez-Munoz, M. J.; Aguado, J.; van Grieken, R.; Marugan, J. Simultaneous photocatalytic reduction of silver and oxidation of cyanide from dicyanoargentate solutions. *Appl. Catal., B* **2009**, *86*, 53−62.

(2) Pirkanniemi, K.; Metsdrinne, S.; Sillanpaa, M. Degradation of EDTA and novel complexing agents in pulp and paper mill process and waste waters by Fenton's reagent. *J. Hazard. Mater.* **2007**, *147*, 556−561.

(3) Tunay, O.; Kabdasli, N. I. Hydroxide precipitation of complexed metals. *Water Res.* **1994**, *28*, 2117−2124.

(4) Zhao, X.; Guo, L. B.; Zhang, B. F.; Liu, H. J.; Qu, J. H. Photoelectrocatalytic oxidation of Cu-II-EDTA at the TiO_2 electrode and simultaneous recovery of Cu-II by electrodeposition. *Environ. Sci. Technol.* **2013**, *47*, 4480−4488.

(5) Zhao, X.; Guo, L. B.; Hu, C. Z.; Liu, H. J.; Qu, J. H. Simultaneous destruction of Nickel (II)-EDTA with TiO_2/Ti film anode and

DOI: 10.1021/acs.est.6b00632
Environ. Sci. Technol. XXXX, XXX, XXX−XXX

electrodeposition of nickel ions on the cathode. *Appl. Catal., B* **2014**, *144*, 478−485.
(6) Zhao, X.; Zhang, J. J.; Qiao, M.; Liu, H. J.; Qu, J. H. Enhanced photoelectrocatalytic decomposition of copper cyanide complexes and simultaneous recovery of copper with a Bi_2MoO_6 electrode under visible light by EDTA/$K_4P_2O_7$. *Environ. Sci. Technol.* **2015**, *49*, 4567−4574.
(7) Sra, K. S.; Thomson, N. R.; Barker, J. F. Persistence of Persulfate in uncontaminated aquifer materials. *Environ. Sci. Technol.* **2010**, *44*, 3098−3104.
(8) Yuan, S. H.; Liao, P.; Alshawabkeh, A. N. Electrolytic manipulation of persulfate reactivity by iron electrodes for trichloroethylene degradation in groundwater. *Environ. Sci. Technol.* **2014**, *48*, 656−663.
(9) Liu, H. Z.; Bruton, T. A.; Doyle, F. M.; Sedlak, D. L. In situ chemical oxidation of contaminated groundwater by persulfate: decomposition by Fe(III)- and Mn(IV)-containing oxides and aquifer materials. *Environ. Sci. Technol.* **2014**, *48*, 10330−10336.
(10) Zhang, R. C.; Sun, P.; Boyer, T. H.; Zhao, L.; Huang, C. H. Degradation of pharmaceuticals and metabolite in synthetic human urine by UV, UV/H_2O_2, and UV/PDS. *Environ. Sci. Technol.* **2015**, *49*, 3056−3066.
(11) Deng, Y.; Ezyske, C. M. Sulfate radical-advanced oxidation process (SR-AOP) for simultaneous removal of refractory organic contaminants and ammonia in landfill leachate. *Water Res.* **2011**, *45*, 6189−6194.
(12) Neppolian, B.; Celik, E.; Choi, H. Photochemical oxidation of arsenic(III) to arsenic(V) using peroxydisulfate ions as an oxidizing agent. *Environ. Sci. Technol.* **2008**, *42*, 6179−6184.
(13) Buxton, G. V.; Greenstock, C. L.; Helman, W. P.; Ross, A. B. Critical-review of rate constants for reactions of hydrated electrons, hydrogen-atoms and hydroxyl radicals (•OH/•O^-) in aqueous-solution. *J. Phys. Chem. Ref. Data* **1988**, *17*, 513−886.
(14) Neta, P.; Huie, R. E.; Ross, A. B. Rate constants for reactions of inorganic radicals in aqueous-solution. *J. Phys. Chem. Ref. Data* **1988**, *17*, 1027−1284.
(15) Antoniou, M. G.; De La Cruz, A. A.; Dionysiou, D. D. Degradation of microcystin-LR using sulfate radicals generated through photolysis, thermolysis and e^- transfer mechanisms. *Appl. Catal., B* **2010**, *96*, 290−298.
(16) Hazime, R.; Nguyen, Q. H.; Ferronato, C.; Huynh, T. K. X.; Jaber, F.; Chovelon, J. M. Optimization of imazalil removal in the system UV/TiO_2/$K_2S_2O_8$ using a response surface methodology (RSM). *Appl. Catal., B* **2013**, *132*, 519−526.
(17) Fang, J. Y.; Shang, C. Bromate formation from bromide oxidation by the UV/Persulfate process. *Environ. Sci. Technol.* **2012**, *46*, 8976−8983.
(18) Johnson, R. L.; Tratnyek, P. G.; Johnson, R. O. Persulfate persistence under thermal activation conditions. *Environ. Sci. Technol.* **2008**, *42*, 9350−9356.
(19) Tsitonaki, A.; Petri, B.; Crimi, M.; Mosbaek, H.; Siegrist, R. L.; Bjerg, P. L. In situ chemical oxidation of contaminated soil and groundwater using persulfate: a review. *Crit. Rev. Environ. Sci. Technol.* **2010**, *40*, 55−91.
(20) Kronholm, J.; Huhtala, S.; Haario, H.; Riekkola, M. L. Oxidation of 4-chloro-3-methylphenol in pressurized hot water in liquid and vapor phases. *Adv. Environ. Res.* **2002**, *6*, 199−206.
(21) Lin, H.; Wu, J.; Zhang, H. Degradation of bisphenol A in aqueous solution by a novel electro/Fe^{3+}/peroxydisulfate process. *Sep. Purif. Technol.* **2013**, *117*, 18−23.
(22) Avetta, P.; Pensato, A.; Minella, M.; Malandrino, M.; Maurino, V.; Minero, C.; Hanna, K.; Vione, D. Activation of persulfate by irradiated magnetite: implications for the degradation of phenol under heterogeneous photo-Fenton-like conditions. *Environ. Sci. Technol.* **2015**, *49*, 1043−1050.
(23) Zhang, T.; Chen, Y.; Wang, Y.; Le Roux, J.; Yang, Y.; Croué, J. Efficient peroxydisulfate activation process not relying on sulfate radical generation for water pollutant degradation. *Environ. Sci. Technol.* **2014**, *48*, 5868−5875.
(24) Lei, Y.; Chen, C. S.; Tu, Y. J.; Huang, Y. H.; Zhang, H. Heterogeneous degradation of organic pollutants by persulfate activated by CuO-Fe_3O_4: mechanism, stability, and effects of pH and bicarbonate ions. *Environ. Sci. Technol.* **2015**, *49*, 6838−6845.
(25) Anipsitakis, G. P.; Dionysiou, D. D. Transition metal/UV-based advanced oxidation technologies for water decontamination. *Appl. Catal., B* **2004**, *54*, 155−163.
(26) Shang, J.; Li, W.; Zhu, Y. F. Structure and photocatalytic characteristics of TiO_2 film photocatalyst coated on stainless steel webnet. *J. Mol. Catal. A: Chem.* **2003**, *202*, 187−195.
(27) Wang, A.; Qu, J. H.; Ru, J.; Liu, H. J.; Ge, J. T. Mineralization of an azo dye acid red 14 by electro-Fenton's reagent using an activated carbon fiber cathode. *Dyes Pigm.* **2005**, *65*, 227−233.
(28) Ma, W. H.; Huang, Y. P.; Li, J.; Cheng, M. M.; Song, W. J.; Zhao, J. C. An efficient approach for the photodegradation of organic pollutants by immobilized iron ions at neutral pHs. *Chem. Commun.* **2003**, *9*, 1582−1583.
(29) Yang, Y.; Pignatello, J. J.; Ma, J.; Mitch, W. A. Comparison of halide impacts on the efficiency of contaminant degradation by sulfate and hydroxyl radical-based advanced oxidation processes (AOPs). *Environ. Sci. Technol.* **2014**, *48*, 2344−2351.
(30) Zhao, X.; Guo, L. B.; Qu, J. H. Photoelectrocatalytic oxidation of Cu-EDTA complex and electrodeposition recovery of Cu in a continuous tubular photoelectrochemical reactor. *Chem. Eng. J.* **2014**, *239*, 53−59.
(31) Liang, C.; Su, H. W. Identification of sulfate and hydroxyl radicals in thermally activated persulfate. *Ind. Eng. Chem. Res.* **2009**, *48*, 5558−5562.
(32) Laine, D. F.; Blumenfeld, A.; Cheng, I. F. Mechanistic study of the ZEA organic pollutant degradation system: Evidence for H_2O_2, HO center dot, and the homogeneous activation of O-2 by Fe(II)EDTA. *Ind. Eng. Chem. Res.* **2008**, *47*, 6502−6508.
(33) Danilczuk, M.; Schlick, S.; Coms, F. D. Cerium(III) as a stabilizer of perfluorinated membranes used in fuel cells: In situ detection of early events in the ESR resonator. *Macromolecules* **2009**, *42*, 8943−8949.
(34) Liang, C. J.; Bruell, C. J.; Marley, M. C.; Sperry, K. L. Persulfate oxidation for in situ remediation of TCE. II. Activated by chelated ferrous ion. *Chemosphere* **2004**, *55*, 1225−1233.
(35) Anipsitakis, G. P.; Dionysiou, D. D. Radical generation by the interaction of transition metals with common oxidants. *Environ. Sci. Technol.* **2004**, *38*, 3705−3712.
(36) Fang, G. D.; Gao, J.; Dionysiou, D. D.; Liu, C.; Zhou, D. M. Activation of persulfate by quinones: Free radical reactions and implication for the degradation of PCBs. *Environ. Sci. Technol.* **2013**, *47*, 4605−4611.
(37) Drzewicz, P.; Perez-Estrada, L.; Alpatova, A.; Martin, J. W.; El-Din, M. G. Impact of peroxydisulfate in the presence of zero valent iron on the oxidation of cyclohexanoic acid and naphthenic acids from oil sands process-affected Water. *Environ. Sci. Technol.* **2012**, *46*, 8984−8991.
(38) Rodriguez, S.; Vasquez, L.; Costa, D.; Romero, A.; Santos, A. Oxidation of orange G by persulfate activated by Fe(II), Fe(III) and zero valent iron (ZVI). *Chemosphere* **2014**, *101*, 86−92.
(39) Tao, Y.; Ni, Q.; Wei, M.; Xia, D.; Li, X.; Xu, A. Metal-free activation of peroxymonosulfate by g-C_3N_4 under visible light irradiation for the degradation of organic dyes. *RSC Adv.* **2015**, *5*, 44128−44136.
(40) Abdulla-Al-Mamun, M.; Kusumoto, Y. New simple synthesis of Cu-TiO_2 nanocomposite: Highly enhanced photocatalytic killing of epithelia carcinoma (heLa) cells. *Chem. Lett.* **2009**, *38*, 826−827.

DOI: 10.1021/acs.est.6b00632
Environ. Sci. Technol. XXXX, XXX, XXX−XXX

Publication II

Liu, S.S., Zhao, X., Zeng, H.B., Wang, Y.B., Qiao, M., and Guan, W.

Enhancement of Photoelectrocatalytic Degradation of Diclofenac with Persulfate Activated by Cu Cathode

Reprinted with permission from
Chemical Engineering Journal
Vol. 320, pp. 168-177, 2017

Chemical Engineering Journal 320 (2017) 168–177

Contents lists available at ScienceDirect

Chemical Engineering Journal

journal homepage: www.elsevier.com/locate/cej

Enhancement of photoelectrocatalytic degradation of diclofenac with persulfate activated by Cu cathode

Shanshan Liu [a,b], Xu Zhao [a,*], Huabin Zeng [a,b], Yanbin Wang [a], Meng Qiao [a], Wei Guan [a,c]

[a] Key Laboratory of Drinking Water Science and Technology, Research Center for Eco-Environmental Sciences, Chinese Academy of Sciences, Beijing 100085, China
[b] University of Chinese Academy of Sciences, Beijing 100049, China
[c] Chongqing Key Laboratory of Environmental Materials & Remediation Technologies, Chongqing University of Arts and Sciences, Chongqing 402160, China

HIGHLIGHTS

- Photoelectro-oxidation of diclofenac was largely enhanced with persulfate addition.
- Cu_2O was identified at copper cathode by in situ Raman technique.
- Activation mechanism of persulfate to $SO_4^{\cdot-}$ at copper cathode was proposed.

GRAPHICAL ABSTRACT

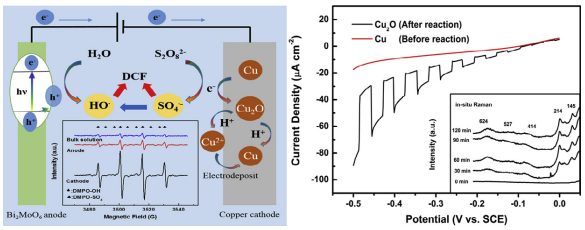

ARTICLE INFO

Article history:
Received 21 December 2016
Received in revised form 1 March 2017
Accepted 14 March 2017
Available online 18 March 2017

Keywords:
Photoelectrocatalysis
Persulfate
Cu cathode
Cu_2O
Diclofenac

ABSTRACT

In this work, persulfate ($S_2O_8^{2-}$, PS) was introduced to the photoelectrocatalytic (PEC) system, which consisted of a γ-Bi_2MoO_6 photoanode and a copper foil cathode (Bi_2MoO_6/Cu/PEC/PS system). Significant enhancement of diclofenac sodium (DCF) degradation efficiency was observed in this system under visible light irradiation. At an applied bias of 1.5 V and initial solution pH of 5.62, the removal efficiency of DCF with an initial concentration of 10 mg/L was increased from 19.4% in the PEC process to 86.3% in the PEC process with 10 mM PS addition. The pseudo-first-order kinetic rate constant of DCF degradation was increased from 0.1112 h^{-1} to 1.0498 h^{-1}. Active free radicals involving $SO_4^{\cdot-}$ and $HO^{\cdot}$ were produced in this process, which were confirmed by electron spin resonance analysis. Furthermore, the surface variation of copper foil cathode was characterized by FE-SEM, GI-XRD, XPS and in situ Raman spectroscopy. It was demonstrated that Cu_2O formed on the surface in the reaction process with the $S_2O_8^{2-}$ addition, which was further confirmed by the photoelectrochemical analysis of the cathode. The surface Cu(0)–Cu(I)–Cu(II)–Cu(0) redox cycle of cathode was proposed, which was responsible for the persulfate activation, leading to the generation of free radicals. This work may provide a new perspective on the combined utilization of different technologies for catalytic contaminant removal.

1. Introduction

Pharmaceuticals and personal care products (PPCPs) have received an increasing attention of their occurrence and transfer in aquatic systems and soils over the past few years [1,2]. Diclofenac sodium (DCF), which is considered as a common non-steroidal anti-inflammatory drug and meanwhile, a persistent toxic pollutant, may produce adverse effect on animal kidney, liver and cause renal lesions [3,4]. Due to its low biodegradability, DCF cannot be effectively removed by conventional biochemical processes [5]. In recent years, the application of UV, UV/H_2O_2 and ozonation treatments in its degradation was largely investigated. For instance, it

* Corresponding author at: P.O. Box 2871, 18 Shuangqing Road, Haidian District, Beijing 100085, PR China.
E-mail address: zhaoxu@rcees.ac.cn (X. Zhao).

http://dx.doi.org/10.1016/j.cej.2017.03.047
1385-8947/

has been proved that DCF could be removed effectively by UV irradiation with H_2O_2 addition [2,6], and ozonation technology also achieved a complete conversion of chlorine to ions and 32% mineralization of DCF for 1.5 h treatment [7].

Photoelectrocatalytic (PEC) oxidation process in which a small positive potential is applied on the semiconductor photoanode has proven to be more efficient than single photocatalytic process [8]. In PEC system, the application of a small external bias decreases the recombination rate of photogenerated electron-hole pairs and thus increases the photocatalytic activity of the semiconductor photocatalyst [9]. It has been largely investigated on the application of PEC processes in degrading refractory organics in aquatic system and water splitting recently [10]. In a PEC system, the semiconductor film electrode is usually used as the photoanode for organics oxidation, while the role of the cathode beyond a counter electrode is not fully exploited. Studies about cathode utilization such as reticulated vitreous carbon as a counter electrode for H_2O_2 generation to enhance PEC oxidation were reported [11]. But the amount of generated H_2O_2 via the cathodic reduction is limited due to the low applied bias used in PEC system. Therefore, it is desired to simultaneously improve the oxidation efficiency of organic contaminants and cathode utilization in the PEC system.

Recently, sulfate radical ($SO_4^{\cdot-}$) based processes have been paid more attention on the removal of organic contaminants. It has been proved that persulfate ($S_2O_8^{2-}$, PS) can be activated to generate sulfate radicals with a redox potential of 2.5 ~ 3.1 V which can efficiently decompose organics in water [12]. Generally, persulfate can be activated by physical means such as heating [13], UV irradiation [14] and microwave [15] as shown in Eq. (1).

$$S_2O_8^{2-} + \text{Heat}/h\nu/\text{Microwave} \rightarrow 2SO_4^{\cdot-} \quad (1)$$

Driven by the need of overcoming the drawback of above physical means, transition metal activation (Eq. (2)) has an advantage on high efficiency without high energy consumption and could be achieved under room temperature. For example, Fe(0) [16], Fe (II) [17] and Ag(I) [18] could be used as PS activators.

$$S_2O_8^{2-} + M^{n+} \rightarrow SO_4^{\cdot-} + SO_4^{2-} + M^{n+1} \quad (2)$$

Owing to its rich abundance and high catalytic efficiency, copper-based catalyst has attracted a particular attention nowadays. PS activation by copper ion was proven to be efficient for propachlor degradation [19]. Zhang et al. discovered that magnetic $CuFe_2O_4$ spinel showed high activity on inducing peroxymonosulfate (PMS) activation; iopromide as target contaminant can be removed completely within 10 min at the PMS dosage of 20 μM [20]. It was also reported that almost 100% phenol was removed in 120 min with addition of 5 mM PS and 0.3 g/L CuO-Fe_3O_4 composite catalyst [21]. Above studies propose that the Cu(II)–Cu(III)–Cu(II) redox cycle activates PS to form free radicals. However, Zhang suggested that peroxydisulfate (PDS) activation can be achieved not relying on sulfate radical generation but electrons rearrangement of PDS [22]. These results indicate the high efficiency of copper-based catalysts for the PS activation through different mechanisms.

To further improve the contaminant degradation efficiency, above two techniques are considered to be combined. Fu et al. investigated the response surface methodology (RSM) on optimising the photoelectrocatalytic degradation of fulvic acid (FA) [23]. A. A. El-Zomrawy reported photoelectrocatalytic degradation of dye with ammonium persulfate (APS) addition [24]. However, the mechanism remained unclear about the interaction between PS and PEC reaction. Zeng et al. reported that PS was added to a photoelectrocatalytic system driven by UV light in order to enhance the Cu-EDTA decomplexation and Cu recovery [25]. This paper indicated the PS activation through cathodic electron and served as a bridge between two techniques. To the best of our knowledge, there have been no published work about the PS activation through cathode itself in PEC system under visible light irradiation.

Herein, Cu cathode was used in a PEC system to activate PS and to improve the PEC degradation efficiency of target contaminant, DCF. In situ Raman spectroscopy combined with photoelectrochemical analysis was employed to analyze the copper cathode variation and generation of Cu_2O on the surface was confirmed. The variation of copper species was investigated in detail. In this variation process, PS was activated and free radicals such as $HO^{\cdot}$ and $SO_4^{\cdot-}$ were produced, which were responsible for the enhanced degradation efficiency of DCF. The activation mechanism was investigated in details.

2. Material and methods

2.1. Chemicals

Sodium persulfate ($Na_2S_2O_8$, 98 + % purity) and sodium sulfite (Na_2SO_3, 98.5% purity) were bought from Acros Organics. Diclofenac sodium ($C_{14}H_{10}Cl_2NNaO_2$, 98% purity) was procured from TOKYO Chemical Industry Co.,Ltd. Sodium sulfate (Na_2SO_4, 99% purity), Bismuth(III) nitrate pentahydrate ($Bi(NO_3)_3{\cdot}5H_2O$, 99% purity), Molybdenum oxide (MoO_3, 99.5% purity), Diethylenetriaminepentaacetic acid ($C_{14}H_{23}N_3O_{10}$, 99.0 + % purity), Diethanolamine ($C_4H_{11}NO_2$, 98–102% purity), sodium acetate (CH_3COONa, 99% purity) and acetic acid (CH_3COOH, 99.8% purity) were all purchased from Sinopharm Chemical Reagent Co.,Ltd. The 5,5-dimethyl-1-pyrrolidine N-oxide (DMPO) was obtained from Aladdin, China. The copper foil was bought from Beijing Heng Li Ti Co.,Ltd. All reagents used were at least analytical grade and without further purification. All solutions were prepared to required concentration in Milli-Q water (ρ = 18.2 MΩ·cm).

2.2. Experimental section

Degradation experiments were carried out in a rectangular quartz reactor with DCF solution (120 mL, 10 mg/L). The PEC reaction was driven by an electrochemical workstation (CHI 660E; Shanghai Chenhua Instruments Co.,Ltd, Shanghai, China) connected with a working photoelectrode (the γ-Bi_2MoO_6 film deposited onto the Indium-tin oxide glass, active area of 13 cm^2), a counter electrode (copper foil, active area of 13 cm^2) and a reference electrode (saturated calomel electrode). The visible light source was from a Xe lamp (PLS-SXE300; Beijing PerfectLight Co., Ltd, Beijing, China) with a UV cutoff filter (λ > 420 nm). Linear sweep voltammetry (LSV) was also conducted in a single-compartment with Na_2SO_4 electrolyte, three electrode cell on the same workstation. Electrochemical impedance spectra (EIS, presented in Supplementary material) were measured at 0 V (vs. open circuit potential) on an electrochemical workstation (Interface 1000, Gamry, America). The initial pH (pH_0) adjustments were achieved by moderate addition of H_2SO_4 (0.1 M) or NaOH (0.1 M). Samples were taken from the reactor every 30 min and filtered through 0.22 μm membrane prior to analysis.

As reported in our previous work [26], γ-Bi_2MoO_6 film was deposited onto indium tin oxide (ITO) substrate from an amorphous heteronuclear complex solution by dip-coating method. Before each experiment, the anode film was rinsed by Milli-Q water and the copper foil used as a cathode was rinsed by hydrochloric acid, cleaned with 800-grit sandpapers to remove any rusts or solid deposits and double rinsed with Milli-Q water.

2.3. Analytical procedures

The concentration of DCF was determined by high performance liquid chromatography (HPLC; Shimadzu LC-20AT, Tokyo, Japan) with a C18 (250 mm × 4.6 mm × 5 μm) reversed-phase column (GL Sciences Inc., Tokyo, Japan) and a UV detector. The mobile phase was a mixture of acetate buffer (pH = 5.0) and methanol (V/V = 40/60) with a flow rate of 1 mL/min. The injection volume was set as 20 μL.

For the intermediates identification, samples were filtered and analyzed by UPLC-Q-TOF-MS (ACQUITY UPLC, Quattro Premier XE, Waters, America) with C18 (50 mm × 2.1 mm × 1.7 μm) reversed-phase column. The mobile phase contained A (0.2% formic acid in water) and B (0.1% formic acid in acetonitrile) at the flow rate of 0.3 mL/min. The gradient was 90% A for 1 min, linearly increasing to 95% B for 8 min, 95% B and 5% A for 5 min, decreasing back to 90% A and maintaining for 1 min. The mass spectrometer was operated with negative electrospray ionization recorded from 50 to 1000 *m/z*.

The mineralization of DCF was measured with an Elementar vario TOC analyzer (Germany). The pH adjustment was completed on PHS-3E. The metal ions were quantified by inductively coupled plasma-optical emission spectrometer (ICP-OES, Optima 8300, PerkinElmer, America).

The surface morphology of electrodes was characterized by field emission-scanning electron microscope (FE-SEM; HITACHI SU8020, Tokyo, Japan). The X-ray diffraction (XRD) patterns of electrodes were recorded on an X-ray diffractometer (XPert Pro MPD) with a Cu Kα radiation. X-ray photoelectron spectroscopy (XPS) was measured on ESCALAB 250Xi (Thermo Fisher Scientific) to determine the chemical state of copper. In situ Raman spectroscopic studies were performed with a confocal Raman microscope (LabRAM HR 800, Horiba, Tokyo, Japan), equipped with an Ar laser (514 nm) and a 40× objective.

For the involved radical studies, experiments were detected on Bruker A300-10/12 (Germany) using DMPO as trapping agent. The measurements were conducted using a radiation of 9.85 GHz (X band) with center field of 3512.170 G, modulation frequency of 100 kHz, sweep width of 200 G, sweep time of 81.92 s, time constant of 40.96 ms, and microwave power of 21 MW at room temperature.

3. Results and discussion

3.1. Characterization of γ-Bi_2MoO_6 film anode

XRD pattern and SEM image of γ-Bi_2MoO_6 were shown in Fig. 1 (a). The peaks of prepared electrode are in conformity with the standard Bi_2MoO_6 (JCPDS: 21–0102). Both the sharpness of XRD reflections and small half peak width clearly demonstrate that the synthesized γ-Bi_2MoO_6 film is highly crystalline. The cell parameters are a = 5.50 Å, b = 16.24 Å, c = 5.49 Å and the principal crystalline phase is orthorhombic structure. As Fig. 1(a) inset graph shows, the film consists of small particles with a porous structure. In recent years, Bi-based photocatalysts are getting more and more attention [27,28]. The electrochemical behavior of photoanode was also investigated by LSV in solution with 0.05 M Na_2SO_4 at a potential range from 0.0 V to 1.5 V (vs. SCE). As shown in Fig. 1(b), the Bi_2MoO_6 electrode shows a strong photocurrent under visible light irradiation. The transient photocurrent response of prepared Bi_2MoO_6 electrode was examined. As shown in Fig. 1(c), the photocurrent with good reproducibility for prepared photoanode is observed when irradiated by visible light. After several cycles, the current remains stable and this indicates that the electrode photoresponse is repeatable and reversible. Under 1 V applied bias,

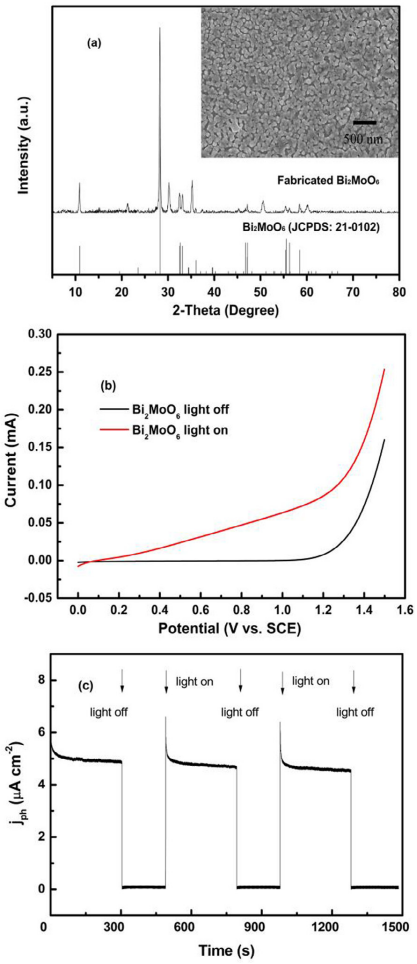

Fig. 1. XRD pattern and SEM image (inset) (a), LSV curves at a potential range of 0.0 to 1.5 V (vs. SCE) (b) and the transient photocurrent response (c) of the prepared Bi_2MoO_6 electrode. Conditions: [Na_2SO_4] = 0.05 M, λ > 420 nm.

the photocurrent density of electrode is 5 μA·cm^{-2}. The optical property of prepared anode was conducted by UV–Vis diffuse reflectance spectroscopy and presented in Supplementary material (Fig. S1). The bandgap of the prepared γ-Bi_2MoO_6 is determined to be 2.58 eV and it exhibits a strong ability to utilize the visible portion of solar spectrum. The above result demonstrated that the prepared photoanode represented a good response to visible light.

3.2. Enhancement performance for DCF degradation

As shown in Fig. 2(a), only 19.4% of DCF is removed in 2 h in the PEC system using Bi_2MoO_6 as photoanode and Cu as cathode, and

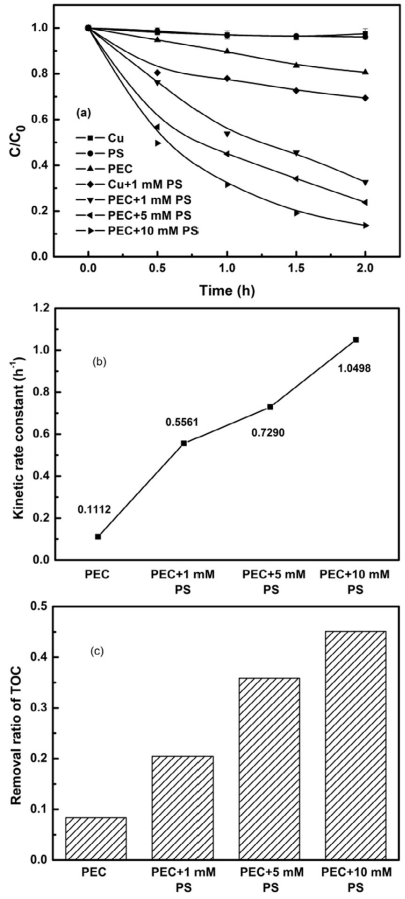

Fig. 2. Effect of PS concentration on the DCF removal (a), kinetic rate constants (b) and removal ratio of TOC (c). Conditions: [DCF] = 10 mg/L; applied bias, 1.5 V; pH_0, 5.62.

the removal efficiency of DCF by PS or copper alone is negligible. When copper itself is put into the solution with 1 mM PS, 30.6% of DCF is removed. Interestingly, a remarkable enhancement of DCF removal is observed with the addition of 1 mM PS into the PEC process, and nearly 70% DCF is removed in 2 h. Meanwhile, the effect of PS concentration on the DCF degradation was examined. It is observed that the removal efficiency of DCF increases with the PS concentration. With 10 mM PS, 86.3% DCF is removed. All these results indicate that the combination of PS and PEC process is an efficient way to degrade the target contaminant from water.

The kinetic investigations exhibit that the degradation reaction of DCF follows a pseudo-first-order kinetics equation and the rate constant versus the concentration of PS is shown in Fig. 2(b). It is estimated to be 0.1112 h^{-1} (R^2 = 0.993) in the PEC system without the addition of PS. By contrast, corresponding to PS concentration of 1, 5 and 10 mM, the rate constants are 0.5561 h^{-1} (R^2 = 0.992), 0.7290 h^{-1} (R^2 = 0.995) and 1.0498 h^{-1} (R^2 = 0.987), respectively. These results strongly confirm the enhancement of DCF degradation efficiency in PEC process with the PS addition.

With respect to TOC variation, in PEC system, the TOC removal ratio is less than 10%. As shown in Fig. 2(c), when 1, 5 and 10 mM PS is added to the solution, it increases to 20.5%, 35.9% and 45.1%, respectively. It is demonstrated that DCF can be degraded more thoroughly in the PEC process with an increasing addition of PS.

3.3. Influence of applied bias and initial pH

The effect of applied bias on the DCF removal in PEC process was investigated with 1 mM PS addition. As illustrated in Fig. 3(a), the degradation efficiency of DCF increases with the increasing applied potential. For example, when the applied bias increases from 0 V to 0.5 V, the removal ratio of DCF increases from 17.3% to 25.3%. As the potential is increased to 2 V, a 72.4% removal of DCF is achieved within 2 h. It can be seen from Fig. 3(b) that the kinetic rate constant increases as the applied bias increases. When the applied bias increases from 0 V to 2 V, the rate constant increases from 0.0912 h^{-1} (R^2 = 0.980) to 0.6431 h^{-1} (R^2 = 0.990).

The increased degradation efficiency is due to firstly, the increased bias promotes the separation of the photogenerated electron-hole pairs and reduces their recombination possibility [29]. As a result, the photocatalytic oxidation of DCF at the photoanode is increased [30,31]. Secondly, as shown in Fig. 3(c), the copper concentration in the solution decreases obviously when the applied bias increases to be 2 V. It is clear that the increased applied bias is beneficial to the cathodic reduction of the liberated copper ions in PEC system within a certain range. The Cu cathodic leakage and reduction in the long-term run was also evaluated (Text S1, Fig. S2).

The effect of pH_0 on the DCF removal and solution pH variation in the PEC process were illustrated in Fig. 4. As shown in Fig. 4(a), when the pH_0 increases from 5.62, 7.00 to 10.00, the removal ratio of DCF decreases from 67.4%, 64.5% to 46.3% at 2 h. As shown in the inset graph of Fig. 4(a), the degradation rate of DCF is well fitted with a pseudo-first-order reaction model at each initial solution pH and the kinetic rate constants are determined to be 0.5561 h^{-1} (R^2 = 0.992), 0.4882 h^{-1} (R^2 = 0.982) and 0.3217 h^{-1} (R^2 = 0.987), respectively.

Thus, it is clear that the rate of DCF degradation efficiency decreases with an increase of pH_0. DCF has a pKa of 4.0, it deprotonates in the pH_0 range of 5.62 to 10.0 thus is always negative charged. Therefore, the effect from the charge interaction between electrode and DCF can be excluded. There may be some other factors which influence the DCF degradation in this system. From the view of free radicals, the redox potential of $SO_4^{\cdot-}$ is confirmed as 2.5 ~ 3.1 V, even higher than $HO^{\cdot}$ (potential of $HO^{\cdot}$ is about 2.7 V in acid solution and 1.8 V in neutral solution) [32–35]. As shown in Eq. (3), the conversion of $SO_4^{\cdot-}$ to $HO^{\cdot}$ occurs easily in alkaline conditions [36]. Therefore, more $SO_4^{\cdot-}$ are generated at acid conditions, which may be partly responsible for the efficient DCF degradation under acid conditions.

$$SO_4^{\cdot-} + OH^- \rightarrow SO_4^{2-} + HO^{\cdot} \quad k = (6.5 \pm 1.0) \times 10^7 M^{-1} s^{-1} \tag{3}$$

Moreover, PS was reported to be further catalyzed under acid conditions according to the literature [37] indicated by Eqs. (4) and (5):

$$S_2O_8^{2-} + H^+ \rightarrow HS_2O_8^- \tag{4}$$

$$HS_2O_8^- \rightarrow SO_4^{\cdot-} + SO_4^{2-} + H^+ \tag{5}$$

On the other hand, solution pH may affect the generation of Cu species and the liberation of copper ions in solution. As shown in Fig. 4(b), the leached copper concentration is decreased from acid

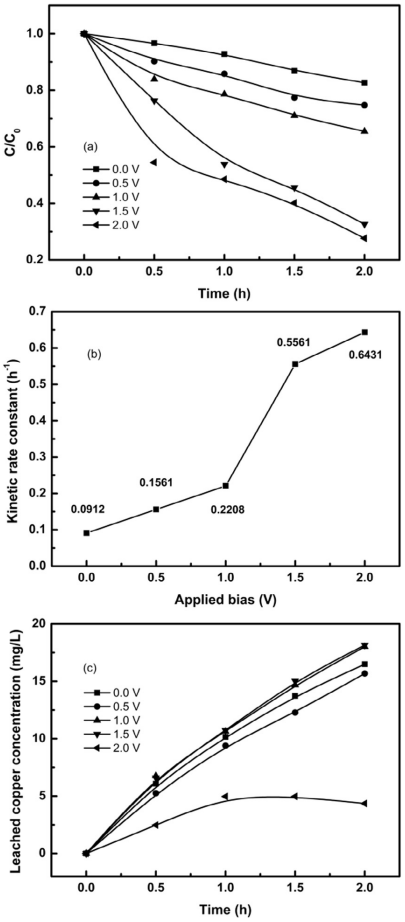

Fig. 3. Effect of applied bias on the DCF removal (a), kinetic rate constants (b) and leached copper concentration (c) in PEC system. Conditions: [DCF] = 10 mg/L; [PS] = 1 mM; pH_0, 5.62.

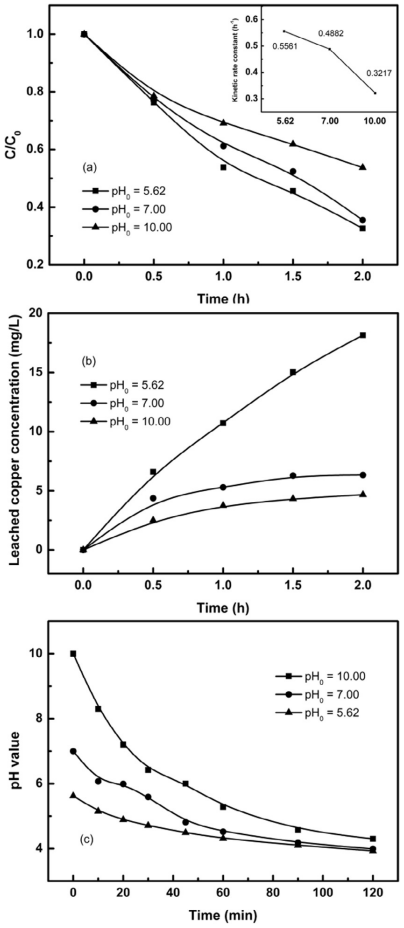

Fig. 4. Effect of pH_0 on the DCF removal (a), leached copper ions concentration (b) and pH variation (c) during the reaction in the PEC system. Conditions: [DCF] = 10 mg/L; applied bias, 1.5 V; [PS] = 1 mM.

to alkaline conditions. Copper ions in alkaline conditions are inclined to precipitate. By contrast, acid condition is beneficial to copper electrodeposition [38], which will be discussed subsequently.

The pH variations with the reaction evolution under different conditions were shown in Fig. 4(c). It can be observed that the solution pH decreases as the reaction proceeds under both acid and alkaline conditions. This phenomenon is caused by the acidification stems from the transformation of $SO_4^{\cdot-}$ to $HO^{\cdot}$, which consumes OH^- in the solution according to Eq. (3). The result was consistent with the research reported by Gu et al. [37].

3.4. Involved active radicals

According to previous literatures [14,22], there are two major proposed mechanisms to explain the PS activation process: radical processes and nonradical processes. In most cases, it was illustrated that $SO_4^{\cdot-}$ and $HO^{\cdot}$ were produced in the process of activation which was responsible for the pollutant degradation [16,39]. As shown in Fig. 5(a), $SO_4^{\cdot-}$ and $HO^{\cdot}$ are both detected at the Cu cathode and Bi_2MoO_6 anode in our PEC system. In PEC system, the photoanode produces electron-hole pairs and the holes can move to the surface of semiconductor to react with water and form $HO^{\cdot}$ [30]. The detected $HO^{\cdot}$ at the anode stem from this process. It can be concluded that the relative intensity of free radicals generated at the cathode is much higher than those generated at the anode and in the bulk solution. The above results indicate that free radicals are produced in this PS activation process and it mainly occurs at the surface of the copper cathode in this PEC system.

In order to investigate the role of Cu foil cathode in the generation process of free radicals, the control experiments were conducted by using Ti, Fe and Co foil as cathodes (the ESR analyses

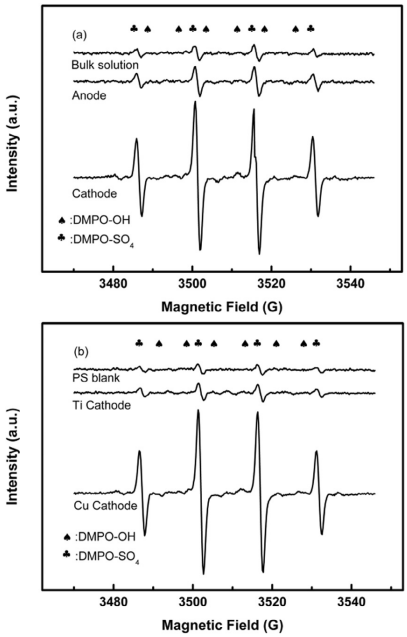

Fig. 5. Comparison of ESR spectrum in bulk solution, at the anode and at the cathode in Bi_2MoO_6/Cu/PEC/PS system (a); Comparison of ESR spectrum in aqueous solution, at Ti cathode and at Cu cathode in PEC system (b). Conditions: Applied bias, 1.5 V; [PS] = 5 mM; pH_0, 5.62.

of Fe, Co cathodes were shown in Fig. S3). As shown in Fig. 5(b), the peak intensities of $HO^{\cdot}$ and $SO_4^{\cdot-}$ generated at the Cu cathode are obviously higher than other metal cathodes. Some literatures demonstrate that photogenerated electrons could activate PS in the photocatalytic process [40,41]. In our case, the photogenerated electrons transferred to the cathode is limited for activating PS. Meanwhile, the Cu cathode plays the key role in activating PS. The effects of PS concentration, applied bias and pH_0 on ESR signals of $SO_4^{\cdot-}$ and $HO^{\cdot}$ are further investigated in detail. As illustrated in Fig. S4(a)-(b), as the PS concentration and applied bias increases, the peak intensities of $HO^{\cdot}$ and $SO_4^{\cdot-}$ at the Cu cathode increase which leads to an increased degradation efficiency of DCF. As shown in Fig. S4(c), more free radicals may exist in the form of $HO^{\cdot}$ in alkaline conditions according to Eq. (3) as stated.

3.5. Characterizations of the Cu cathode variation

It was noticed that the fresh copper foil cathode became dark red with the addition of PS during the PEC reaction. The surface change of copper cathode was firstly checked using the FE-SEM technique. As shown in Fig. 6, the surface of copper foil is relatively smooth and uniform before the PEC reaction. The scratches observed are caused by copper pretreatment by sandpaper polish. However, the smooth surface is destroyed with the generation of porous structure at the PEC reaction time of 0.5 and 1 h. With the reaction evolution, this structure can be always observed and nearly covers the copper surface fully at 2 h.

Furthermore, copper cathode samples at various times in the PEC reaction with PS addition were analyzed by GI-XRD. This technique has a smaller incident angle of 0.2° and it could obtain a more intense signal than conventional XRD from surface in order to reduce the effect of Cu substrate. As shown in Fig. 7, before the PEC reaction, no other peaks except copper are observed. After one hour, peaks at $2\theta = 36.4°$, 42.3° and 61.4° are obviously observed, which are corresponded well with Cu_2O (JCPDS: 78-2076). Moreover, the peak intensity of Cu_2O increases with the reaction evolution. It is demonstrated that some reactions may occur on the copper foil, leading to the formation of Cu_2O.

In addition, XPS technique was used to determine the variation of the copper valence. It can be clearly seen from Fig. 8(a) that nearly no change of the major elements on the copper surface is observed after the PEC reaction. As shown in Fig. 8(b), before the

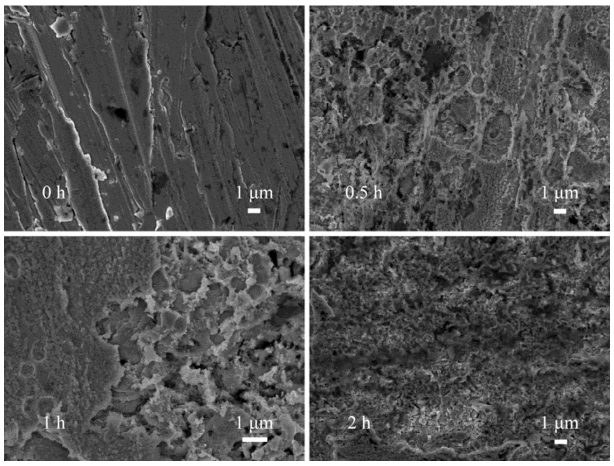

Fig. 6. FE-SEM images of copper foil at various time in Bi_2MoO_6/Cu/PEC/PS system. Conditions: [DCF] = 10 mg/L; applied bias, 1.5 V; [PS] = 5 mM; pH_0, 5.62.

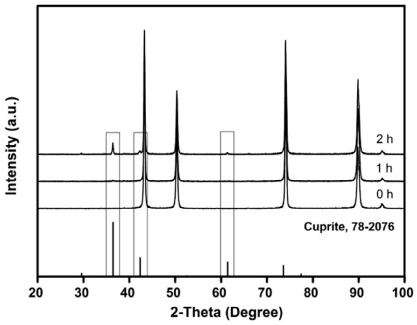

Fig. 7. GI-XRD patterns of copper foil at various times in Bi_2MoO_6/Cu/PEC/PS system. Conditions: [DCF] = 10 mg/L; applied bias, 1.5 V; [PS] = 5 mM; pH_0, 5.62.

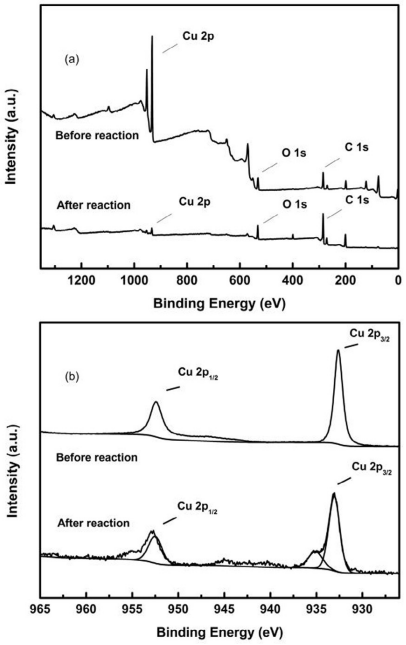

Fig. 8. XPS full scan spectra of copper cathode before and after reaction (a); XPS Cu 2p spectra of the copper cathode before and after reaction (b). Conditions: [DCF] = 10 mg/L; applied bias, 1.5 V; [PS] = 5 mM; pH_0, 5.62.

reaction, the major Cu $2p_{3/2}$ peaks centered at 932.6 eV and major Cu $2p_{1/2}$ peaks centered at 952.45 eV are assigned to zero-valent copper [42,43]. After the reaction, there are three peaks related to copper valence appearing in the graph. The binding energies are 933.05, 952.5 and 935.08 eV, respectively. The major Cu $2p_{3/2}$ peak centered at 933.05 eV is assigned to Cu [44]. In addition, the major Cu $2p_{1/2}$ peak centered at 952.5 eV is assigned to Cu_2O [45]. Combined with XRD analysis, this evidence once again indicates that Cu(I) generates on the copper foil cathode in the PEC

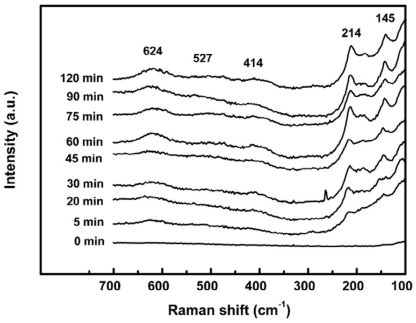

Fig. 9. In situ Raman spectroscopic analysis of the copper cathode in the PEC reaction process. Conditions: Applied bias, 1.5 V; [PS] = 5 mM; pH_0, 5.62.

process. In addition, a major Cu $2p_{3/2}$ peak centered at 935.08 eV is also detected and it is assigned to Cu^{2+} [46].

The variation of the copper foil cathode during the PEC reaction was further examined by in situ Raman spectroscopy. As shown in Fig. 9, no obvious peak is observed at 0 min, demonstrating that the copper remains metallic. Five peaks at 145, 214, 414, 527 and 624 cm^{-1} appear at 5 min, which are assigned to Cu_2O [47]. The intensity of these peaks remains low before the first 30 min and enhances gradually from 30 min to 120 min. Besides, in situ Raman spectra of copper foil under different pH_0 are compared which are shown in Fig. S5. It can be concluded that pH_0 do not have an

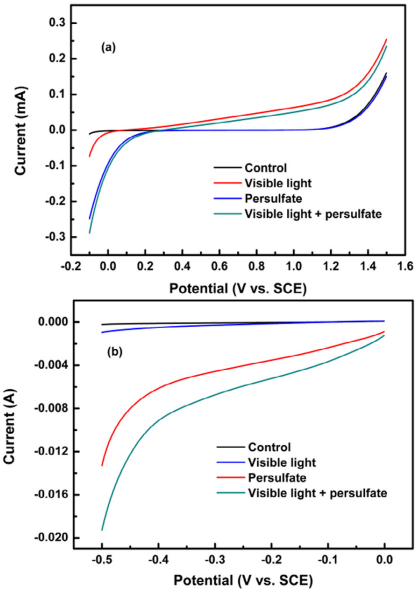

Fig. 10. LSV curves of Bi_2MoO_6 (a) and Cu_2O (b) electrode in the presence and absence of visible light irradiation and persulfate in Na_2SO_4 electrolyte solution. Conditions: [PS] = 5 mM; [Na_2SO_4] = 5 mM; $\lambda > 420$ nm; scan rate = 10 mV/s.

obvious influence on the generation of Cu_2O. From above, the generation of Cu_2O in the reaction process is confirmed.

3.6. Photoelectrochemical analysis

Photoelectrochemical characteristics of the Bi_2MoO_6 electrode and Cu_2O electrode were further discussed in the presence and absence of the persulfate by LSV measurements. As shown in Fig. 10(a), under visible light irradiation, the Bi_2MoO_6 photoanode shows a significant enhancement in photocurrent response. A slight difference was observed in the presence or absence of persulfate. In Fig. 10(b), the photoelectrochemical performance of the generated Cu_2O on the Cu cathode was presented. Under visible light irradiation, an enhancement of current is observed and the generated Cu_2O shows a good response to visible light with a p-type semiconductor characterization. Furthermore, it is clear that the current is largely increased with the persulfate addition both in the dark and under visible light irradiation, which indicated the interaction between generated Cu_2O and persulfate.

The IPCE plots and EIS Nyquist plots were shown in Fig. S6. IPCE increases slightly with the increase of persulfate concentration using the copper foil as cathode (Fig. S6(a)). As shown in Fig. S6(b), the arc radius of the Bi_2MoO_6 photoanode without visible light irradiation is larger than that with visible light irradiation. Smaller arc radius implies a higher efficiency of charge transfer. But the arc radius of system with persulfate is nearly similar with the system without persulfate under visible light irradiation. Above results demonstrate that the introduction of persulfate to this PEC system do not obviously change the transfer efficiency of photogenerated electron-hole pairs.

3.7. Identification of intermediates and proposed reaction pathways

The main intermediates of DCF in the reaction were identified by UPLC-Q-TOF-MS. A possible reaction pathway was proposed in Fig. 11. Besides DCF itself, there were four intermediates identified in the reaction (the structures were in Table S1 and the mass spectra were shown in Fig. S7). We formulated these detected products from P1 to P4, respectively. The MS spectrum of DCF shows a molecular ion peak at 294 m/z and 250 m/z. The loss of 44 could be attributed to CO_2 loss, which is consistent with previous studies about DCF. The MS spectrum of P1 shows a strong peak at 177 m/z. Previous studies reported that peak at 161 m/z might be the major product in the degradation process of DCF [48]. P1 might be the product derived from addition reaction with OH. In the mass spectrum of P2, the fragments are 228, 264 and 310 m/z. The most

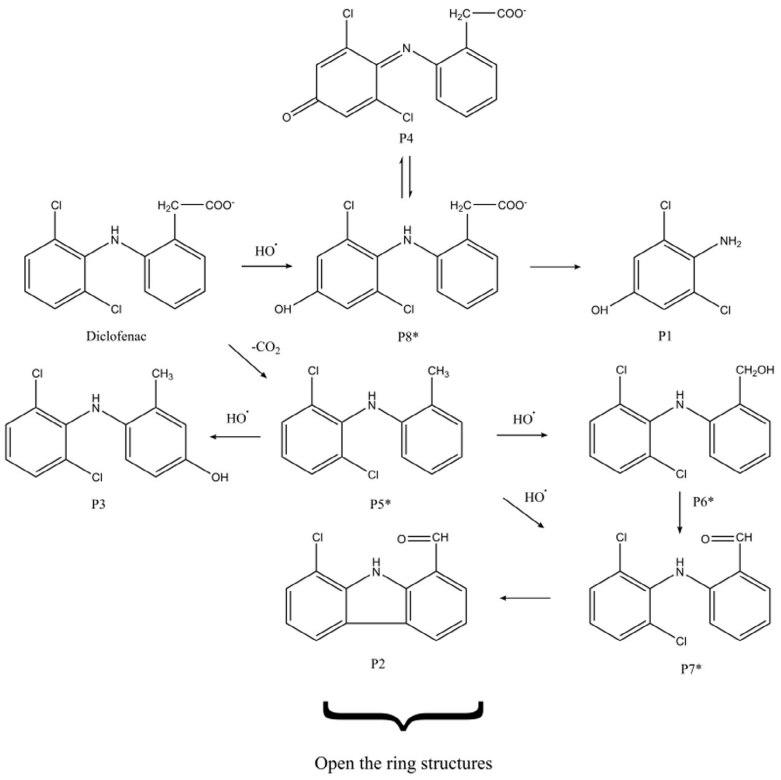

Fig. 11. Proposed degradation pathways of DCF in the Bi_2MoO_6/Cu/PEC/PS system (intermediates with * were deduced).

important fragment 228 *m*/*z* corresponds to the loss of HCl from fragment 264 *m*/*z*. The fragment 264 *m*/*z* corresponds to the loss of OH and CH_2 groups from 310 *m*/*z*. In the mass spectrum of P3, the most important fragment is 266 *m*/*z* and it corresponds to the loss of CO_2 from 310 *m*/*z*. P1 can be formed by cleavage of C-N bond from P8*. There is an interchange between P4 and P8*. P5* results from decarboxylation of DCF. P3 and P6* possess the same elemental compositions and they are derived from hydroxylation as a result of HO· attack. P2 is probably obtained by dehalogenation and oxidation of P6*. It can be concluded that most of the identified intermediates are generated by the attack of HO· in the reaction. This result is consistent with the ESR analyses and it is demonstrated that the main oxidizing species are HO· in this system.

3.8. A proposed enhanced mechanism

The above results indicated that HO· and $SO_4^{\cdot-}$ were produced from the copper foil cathode with the addition of PS; and Cu_2O was generated during the PEC reaction process. Considering the above analyses, a proposed reaction process was expressed by Eqs. (6)–(9) and Scheme S1.

$$Cu(s) - e^- \rightarrow Cu^+(s) \quad (6)$$

$$S_2O_8^{2-} + e^- \rightarrow SO_4^{\cdot-} + SO_4^{2-} \quad (7)$$

$$Cu_2O(s) + 2H^+ \rightarrow Cu^{2+}(aq) + Cu(s) + H_2O \quad (8)$$

$$Cu^{2+}(aq) + 2e^- \rightarrow Cu(s) \quad (9)$$

As illustrated in Scheme S1, PS could be activated by receiving an electron from the copper when PS was added into the PEC system. As a result, $SO_4^{\cdot-}$ and HO· were generated, which were responsible for DCF oxidation. Meanwhile, Cu_2O was generated on the surface of copper cathode. In order to test its activation capacity for PS, the Cu_2O thin film was prepared with an electrodeposition method on ITO glass [49]. As shown in Fig. S8, there is nearly no removal of DCF observed by the prepared Cu_2O film with addition of 1 mM PS. It is known that Cu_2O is more inclined to undergo disproportionation reaction, leading to the generation of Cu and Cu^{2+} in acid conditions. Cu^{2+} absorbed on the surface according to XPS results may diffuse into the solution. In the meantime, Cu^{2+} could be deposited onto the copper surface again by cathodic reduction, which benefited the copper recycle between electrode and solution. This copper recovery process can be confirmed by the compared experiments between PEC system and chemical oxidation system in which copper just puts into solution with PS and DCF. The leached copper ion concentration in PEC system is 37% fewer than in chemical oxidation process when the PS and copper dosage is definite. This result demonstrates that the leached copper ions can be recovered by the cathodic reduction in the PEC system. In a word, the copper surface redox cycle of Cu(0)–Cu(I)–Cu(II)–Cu(0) would be probably responsible for the PS activation in this system.

3.9. Stability analysis

In order to evaluate the reproducibility of the system, the experiments were conducted for three times. As shown in Fig. 12, the removal efficiency of DCF does not change significantly in each cycle (67%, 72% and 71%, respectively). The final removal efficiency remains steady and consistent in the three cycles. From the above results, the system shows high reproducibility for DCF removal.

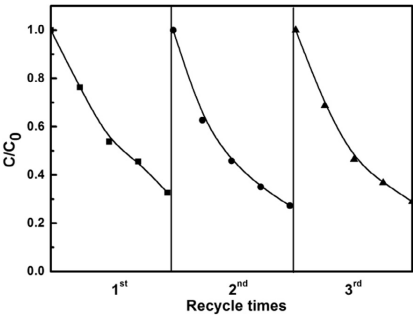

Fig. 12. The residual rate of DCF for cycles. Conditions: [DCF] = 10 mg/L; applied bias, 1.5 V; [PS] = 1 mM; pH_0, 5.62.

4. Conclusions

In summary, DCF can be efficiently removed in the PEC system with γ-Bi_2MoO_6 as photoanode and copper as cathode with the PS addition. The generation of hydroxyl radicals and sulfate radicals was detected, which was responsible for the enhanced DCF degradation. It was deduced that the copper provided electrons to PS with the generation of Cu_2O on the surface and PS was activated in this process. Then Cu(I) disproportionated in the acid solution, leading to the production of Cu(0) and Cu(II). Cu(II) was deposited onto the copper again by the cathodic reduction. Above results of this study showed the PS oxidation catalyzed with copper cathode may be an available method for contaminant removal. This work also provides a new perspective towards PS activation and efficient utilization of the cathode in the PEC system.

Acknowledgements

The authors gratefully acknowledge financial support from National Natural Science Foundation of China (No. 21377148, 51438011), Natural Science Foundation of Yongchuan, Chongqing (Ycstc, 2014ac4001).

Appendix A. Supplementary data

Supplementary data associated with this article can be found, in the online version, at http://dx.doi.org/10.1016/j.cej.2017.03.047.

References

[1] T. Heberer, Occurrence, fate, and removal of pharmaceutical residues in the aquatic environment: a review of recent research data, Toxicol. Lett. 131 (2002) 5–17.
[2] I. Kim, N. Yamashita, H. Tanaka, Photodegradation of pharmaceuticals and personal care products during UV and UV/H_2O_2 treatments, Chemosphere 77 (2009) 518–525.
[3] W. Chen, X. Li, Z. Pan, S. Ma, L. Li, Effective mineralization of Diclofenac by catalytic ozonation using Fe-MCM-41 catalyst, Chem. Eng. J. 304 (2016) 594–601.
[4] C. Martinez, M. Canle L, M.I. Fernandez, J.A. Santaballa, J. Faria, Aqueous degradation of diclofenac by heterogeneous photocatalysis using nanostructured materials, Appl. Catal. B-Environ. 107 (2011) 110–118.
[5] D. Stuelten, S. Zuehlke, M. Lamshoeft, M. Spiteller, Occurrence of diclofenac and selected metabolites in sewage effluents, Sci. Total Environ. 405 (2008) 310–316.
[6] I. Kim, H. Tanaka, Photodegradation characteristics of PPCPs in water with UV treatment, Environ. Int. 35 (2009) 793–802.
[7] D. Vogna, R. Marotta, A. Napolitano, R. Andreozzi, M. d'Ischia, Advanced oxidation of the pharmaceutical drug diclofenac with UV/H_2O_2 and ozone, Water Res. 38 (2004) 414–422.

[8] T. An, H. Sun, G. Li, H. Zhao, P.K. Wong, Differences in photoelectrocatalytic inactivation processes between E-coli and its isogenic single gene knockoff mutants: Destruction of membrane framework or associated proteins?, Appl Catal. B-Environ. 188 (2016) 360–366.

[9] X. Meng, Z. Zhang, X. Li, Synergetic photoelectrocatalytic reactors for environmental remediation: a review, J. Photochem. Photobiol. C-Photochem. Rev. 24 (2015) 83–101.

[10] H. Yu, S. Chen, X. Quan, H. Zhao, Y. Zhang, Silicon nanowire/TiO_2 heterojunction arrays for effective photoelectrocatalysis under simulated solar light irradiation, Appl. Catal. B-Environ. 90 (2009) 242–248.

[11] X.Z. Li, H.S. Liu, Development of an E-H_2O_2/TiO_2 photoelectrocatalytic oxidation system for water and wastewater treatment, Environ. Sci. Technol. 39 (2005) 4614–4620.

[12] G.P. Anipsitakis, D.D. Dionysiou, Degradation of organic contaminants in water with sulfate radicals generated by the conjunction of peroxymonosulfate with cobalt, Environ. Sci. Technol. 37 (2003) 4790–4797.

[13] H. Gao, J. Chen, Y. Zhang, X. Zhou, Sulfate radicals induced degradation of Triclosan in thermally activated persulfate system, Chem. Eng. J. 306 (2016) 522–530.

[14] Y. Zhang, J. Zhang, Y. Xiao, V.W.C. Chang, T.-T. Lim, Kinetic and mechanistic investigation of azathioprine degradation in water by UV, UV/H_2O_2 and UV/persulfate, Chem. Eng. J. 302 (2016) 526–534.

[15] S.Y. Yang, P. Wang, X. Yang, G. Wei, W.Y. Zhang, L. Shan, A novel advanced oxidation process to degrade organic pollutants in wastewater: microwave-activated persulfate oxidation, J. Environ. Sci. 21 (2009) 1175–1180.

[16] P. Drzewicz, L. Perez-Estrada, A. Alpatova, J.W. Martin, M.G. El-Din, Impact of peroxydisulfate in the presence of zero valent iron on the oxidation of cyclohexanoic acid and naphthenic acids from oil sands process-affected water, Environ. Sci. Technol. 46 (2012) 8984–8991.

[17] S. Rodriguez, L. Vasquez, D. Costa, A. Romero, A. Santos, Oxidation of Orange G by persulfate activated by Fe(II), Fe(III) and zero valent iron (ZVI), Chemosphere 101 (2014) 86–92.

[18] G.P. Anipsitakis, D.D. Dionysiou, Radical generation by the interaction of transition metals with common oxidants, Environ. Sci. Technol. 38 (2004) 3705–3712.

[19] C.S. Liu, K. Shih, C.X. Sun, F. Wang, Oxidative degradation of propachlor by ferrous and copper ion activated persulfate, Sci. Total Environ. 416 (2012) 507–512.

[20] T. Zhang, H. Zhu, J.-P. Croue, Production of sulfate radical from peroxymonosulfate induced by a magnetically separable $CuFe_2O_4$ spinel in water: efficiency, stability, and mechanism, Environ. Sci. Technol. 47 (2013) 2784–2791.

[21] Y. Lei, C.-S. Chen, Y.-J. Tu, Y.-H. Huang, H. Zhang, Heterogeneous degradation of organic pollutants by persulfate activated by CuO-Fe_3O_4: mechanism, stability, and effects of pH and bicarbonate ions, Environ. Sci. Technol. 49 (2015) 6838–6845.

[22] T. Zhang, Y. Chen, Y. Wang, J. Le Roux, Y. Yang, J.-P. Croue, Efficient peroxydisulfate activation process not relying on sulfate radical generation for water pollutant degradation, Environ. Sci. Technol. 48 (2014) 5868–5875.

[23] J. Fu, Y. Zhao, Q. Wu, Optimising photoelectrocatalytic oxidation of fulvic acid using response surface methodology, J. Hazard. Mater. 144 (2007) 499–505.

[24] A.A. El-Zomrawy, Kinetic studies of photoelectrocatalytic degradation of Ponceau 6R dye with ammonium persulfate, J. Saudi Chem. Soc. 17 (2013) 397–402.

[25] H. Zeng, S. Liu, B. Chai, D. Cao, Y. Wang, X. Zhao, Enhanced photoelectrocatalytic decomplexation of Cu-EDTA and Cu recovery by persulfate activated by UV and cathodic reduction, Environ. Sci. Technol. 50 (2016) 6459–6466.

[26] X. Zhao, J. Qu, H. Liu, C. Hu, Photoelectrocatalytic degradation of triazine-containing azo dyes at gamma-Bi_2MoO_6 film electrode under visible light irradiation (λ> 420 nm), Environ. Sci. Technol. 41 (2007) 6802–6807.

[27] L.W. Zhang, T.G. Xu, X. Zhao, Y.F. Zhu, Controllable synthesis of Bi_2MoO_6 and effect of morphology and variation in local structure on photocatalytic activities, Appl. Catal. B-Environ. 98 (2010) 138–146.

[28] J. Tian, P. Hao, N. Wei, H. Cui, H. Liu, 3D Bi_2MoO_6 nanosheet/TiO_2 nanobelt heterostructure: enhanced photocatalytic activities and photoelectochemistry performance, ACS Catal. 5 (2015) 4530–4536.

[29] F. Liang, Y. Zhu, Enhancement of mineralization ability for phenol via synergetic effect of photoelectrocatalysis of g-C_3N_4 film, Appl. Catal. B-Environ. 180 (2016) 324–329.

[30] R. Daghrir, P. Drogui, D. Robert, Photoelectrocatalytic technologies for environmental applications, J. Photochem. Photobiol. A-Chem. 238 (2012) 41–52.

[31] C. Adams, Y. Wang, K. Loftin, M. Meyer, Removal of antibiotics from surface and distilled water in conventional water treatment processes, in: J. Environ. Eng.-ASCE 128 (2002) 253–260.

[32] G.R. Peyton, The free-radical chemistry of persulfate-based total organic-carbon analyzers, Mar. Chem. 41 (1993) 91–103.

[33] A. Ahmad, X. Gu, L. Li, S. Lu, Y. Xu, X. Guo, Effects of pH and anions on the generation of Reactive Oxygen Species (ROS) in nZVI-rGo-activated persulfate system, Water Air Soil Pollut. 226 (2015) 369.

[34] G.V. Buxton, C.L. Greenstock, W.P. Helman, A.B. Ross, Critical-review of rate constants for reactions of hydrated electrons, hydrogen-atoms and hydroxyl radicals (.OH/.O-) in aqueous-solution, J. Phys. Chem. Ref. Data 17 (1988) 513–886.

[35] P. Neta, R.E. Huie, A.B. Ross, Rate constants for reactions of inorganic radicals in aqueous-solution, J. Phys. Chem. Ref. Data 17 (1988) 1027–1284.

[36] E. Hayon, A. Treinin, J. Wilf, Electronic spectra, photochemistry, and autoxidation mechanism of the sulfite-bisulfite-pyrosulfite systems. The SO_2^-, SO_3^-, SO_4^-, and SO_5^- radicals, J. Am. Chem. Soc. 94 (1972) 47–57.

[37] X. Gu, S. Lu, L. Li, Z. Qiu, Q. Sui, K. Lin, Q. Luo, Oxidation of 1,1,1-Trichloroethane stimulated by thermally activated persulfate, Ind. Eng. Chem. Res. 50 (2011) 11029–11036.

[38] X. Zhao, L. Guo, B. Zhang, H. Liu, J. Qu, Photoelectrocatalytic oxidation of Cu-II-EDTA at the TiO_2 electrode and simultaneous recovery of Cu-II by electrodeposition, Environ. Sci. Technol. 47 (2013) 4480–4488.

[39] O.S. Furman, A.L. Teel, R.J. Watts, Mechanism of base activation of persulfate, Environ. Sci. Technol. 44 (2010) 6423–6428.

[40] Y. Tao, Q. Ni, M. Wei, D. Xia, X. Li, A. Xu, Metal-free activation of peroxymonosulfate by g-C_3N_4 under visible light irradiation for the degradation of organic dyes, RSC Adv. 5 (2015) 44128–44136.

[41] S. Song, L. Xu, Z. He, J. Chen, X. Xiao, B. Yan, Mechanism of the photocatalytic degradation of C.I. Reactive Black 5 at pH 12.0 using $SrTiO_3$/CeO_2 as the catalyst, Environ. Sci. Technol. 41 (2007) 5846–5853.

[42] C.D. Wagner, Chemical shifts of Auger lines, and the Auger parameter, Faraday Discuss. Chem. Soc. 60 (1975) 291–300.

[43] A.C. Miller, G.W. Simmons, Copper by XPS, Surf. Sci. Spectra 2 (1993) 55–60.

[44] J. Haber, T. Machej, L. Ungier, J. Ziolkowski, ESCA studies of copper oxides and copper molybdates, J. Solid State Chem. 25 (1978) 207–218.

[45] J.G. Jolley, G.G. Geesey, M.R. Hankins, R.B. Wright, P.L. Wichlacz, Auger electron and X-ray photoelectron spectroscopic study of the biocorrosion of copper by alginic acid polysaccharide, Appl. Surf. Sci. 37 (1989) 469–480.

[46] R.P. Vasquez, $CuCl_2$ by XPS, Surf. Sci. Spectra 2 (1993) 160–164.

[47] D. Ren, Y. Deng, A.D. Handoko, C.S. Chen, S. Malkhandi, B.S. Yeo, Selective electrochemical reduction of carbon dioxide to ethylene and ethanol on copper (I) oxide catalysts, ACS Catal. 5 (2015) 2814–2821.

[48] H. Cheng, D. Song, H. Liu, J. Qu, Permanganate oxidation of diclofenac: the pH-dependent reaction kinetics and a ring-opening mechanism, Chemosphere 136 (2015) 297–304.

[49] P. Wang, H. Wu, Y.M. Tang, R. Amal, Y.H. Ng, Electrodeposited Cu_2O as photoelectrodes with controllable conductivity type for solar energy conversion, J. Phys. Chem. C 119 (2015) 26275–26282.

Publication III

Zeng, H.B., Zhao, X., Zhao, F.P., Park, Y., and Sillanpää, M.

Accelerated Fe^{3+}/Fe^{2+} Cycle Using Atomic H* on Pd/Al_2O_3: A Novel Mechanism for an Electrochemical System with Particle Electrode for Iron Sludge Reduction in the Fe^{2+}/Peroxydisulfate Oxidation Process

Reprinted with permission from
Chemical Engineering Journal
Vol. 382, pp. 122972, 2019

Chemical Engineering Journal 382 (2020) 122972

Contents lists available at ScienceDirect

Chemical Engineering Journal

journal homepage: www.elsevier.com/locate/cej

Accelerated Fe^{3+}/Fe^{2+} cycle using atomic H* on Pd/Al_2O_3: A novel mechanism for an electrochemical system with particle electrode for iron sludge reduction in the Fe^{2+}/peroxydisulfate oxidation process

Huabin Zeng[a,*], Xu Zhao[b], Feiping Zhao[a], Yuri Park[a], Mika Sillanpää[a]

[a] Department of Green Chemistry, School of Engineering Science, Lappeenranta-Lahti University of Technology LUT, Sammonkatu 12, FI-50130 Mikkeli, Finland
[b] State Key Laboratory of Environmental Aquatic Chemistry, Research Center for Eco-Environmental Sciences, Chinese Academy of Sciences, Beijing 100085, China

HIGHLIGHTS

- In Pd-EF system, $SO_4^{\cdot -}$ and ·OH were continuously produced with addition of trace iron.
- Iron sludge reduction was achieved via accelerating the Fe^{2+}/Fe^{3+} cycle.
- Atomic Hydrogen played a dominant role in the cycle of Fe^{2+}/Fe^{3+}.
- The performance of Pd-EF system can be further enhanced by N_2 sparging.

GRAPHICAL ABSTRACT

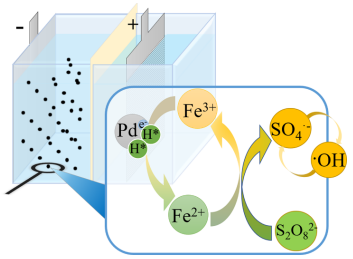

ARTICLE INFO

Keywords:
Fe^{2+}/PDS process
Pd/Al_2O_3
Atomic H*
Iron cycle
Iron sludge reduction

ABSTRACT

The high cost associated with the disposal of iron sludge in Fe^{2+} activated oxidation systems significantly limits their widespread use. In this study, we constructed a trace iron-based peroxydisulfate (PDS) oxidation system (Pd-EFP) using Pd/Al_2O_3 as the particle electrode and externally added PDS as an oxidant. At an initial solution pH of 3.0 and a current density of 3.33 mA/cm^2, with the addition of 10 mM PDS, 50 mg Pd/Al_2O_3, and 2 mg/L Fe ions, 80.12% of 180 μM benzoic acid (BA) was degraded within 120 min. The Pd/Al_2O_3 catalyst provided sufficiently large surface area for atomic H* production from the adsorption of electrogenerated H_2 or H^+ conversion via electro-induction on the Pd/Al_2O_3 surface, which subsequently accelerated the transformation from Fe^{3+} to Fe^{2+}. Using this method, organics could be degraded by both $SO_4^{\cdot -}$ and ·OH via the Fe^{2+}-activated PDS process. In the Pd-EFP process, the optimal dosage of Fe ions was determined to be 36 μM (2 mg/L). Correspondently, the optimal current density and PDS concentration in the Pd-EFP system were 3.33 mA/cm^2 and 20 mM, respectively. Furthermore, degradation of BA was efficiently promoted by the N_2 atmosphere, which could steer the reaction on the surface of Pd/Al_2O_3 in the right direction toward Fe^{3+} reduction by atomic H*, by dispelling accumulated H_2 above the reaction liquid and suppressing oxygen reduction. Finally, the Pd/Al_2O_3

Abbreviations: BA, Benzoic acid; PDS, Peroxydisulfate; Fe^{2+}/PDS process, PDS oxidation process activated by Fe^{2+}; Fe^{3+}/PDS process, PDS oxidation process activated by Fe^{3+}; Electro/Fe^{3+}/PDS, PDS oxidation with addition of Fe^{3+} and applying current; Pd/Fe^{3+}/PDS, PDS oxidation process with the addition of Fe^{3+} and Pd/Al_2O_3 catalyst; Electro/Pd/PDS, PDS oxidation process with the addition of the Pd/Al_2O_3 catalyst and applying current; Electro/Pd/Fe^{3+}, Fe^{3+} oxidation process with the addition of the Pd/Al_2O_3 catalyst and applying current; Pd-EFP system, Pd/Al_2O_3-enhanced electro/ Fe^{3+}/PDS oxidation process; XRD, X-ray diffraction; AOPs, Advanced oxidation processes; 3D, Three-dimensional; ESR, Electron spin resonance; ICP-OES, Inductively coupled plasma-optical emission spectroscopy; TBA, Tert-butyl alcohol; H_2/Pd/PDS, PDS oxidation process with the addition of the Pd/Al_2O_3 catalyst in an atmosphere of H_2

* Corresponding author.
E-mail address: Huabin.zeng@lut.fi (H. Zeng).

https://doi.org/10.1016/j.cej.2019.122972
Received 14 June 2019; Received in revised form 18 September 2019; Accepted 25 September 2019
Available online 27 September 2019

catalyst was found to be durable in the Pd-EFP system according to reusability experiments and X-ray diffraction patterns of the fresh and used Pd/Al_2O_3 catalyst. This research provides an environmentally benign system for recycling Fe^{3+} in Fe^{2+}/PDS processes and for suppressing iron sludge production.

1. Introduction

By producing strongly oxidising ·OH, advanced oxidation processes (AOPs) are appealing treatment options for removing non-biodegradable, recalcitrant and toxic organic contaminants from water [1–4]. Among AOPs, the Fenton reaction (reaction (1)) has been widely applied in wastewater treatments for its high oxidation ability, low operating cost, and controllability [5]. In parallel to the Fenton reaction, the reaction between Fe^{2+} and peroxydisulfate (PDS, $S_2O_8^{2-}$) (Fe^{2+}/PDS reaction, reaction (2)) shares similar advantages with the Fenton reaction while sulfate radical ($SO_4^{\cdot -}$) demonstrate a longer lifetime than hydroxyl radical (·OH) in water [6–14].

$$Fe^{2+} + H_2O_2 \rightarrow Fe^{3+} + {\cdot}OH + OH^- \quad (1)$$

$$Fe^{2+} + S_2O_8^{2-} \rightarrow Fe^{3+} + SO_4^{\cdot -} + SO_4^{2-} \quad (2)$$

$$S_2O_8^{2-} + SO_4^{\cdot -} \rightarrow S_2O_8^{\cdot -} + SO_4^{2-} \quad (3)$$

$$Fe^{3+} + S_2O_8^{2-} \rightarrow Fe^{2+} + S_2O_8^{\cdot -} \quad (4)$$

$$2S_2O_8^{2-} + 2H_2O \rightarrow 3SO_4^{2-} + SO_4^{\cdot -} + O_2^{\cdot -} + 4H^+ \quad (5)$$

$$S_2O_8^{2-} + 2H_2O \rightarrow 2SO_4^{2-} + HO_2^- + 4H^+ \quad (6)$$

$$Fe^{3+} + O_2^{\cdot -} \rightarrow Fe^{2+} + O_2 \quad (7)$$

The activation of PDS with dissolved Fe ions as a catalyst has some intrinsic drawbacks [15]. As shown in reaction (2), one mole of added Fe^{2+} only produce one mole of radicals. Although Fe^{2+} can be regenerated via reactions (4) and (7), the regeneration rate of Fe^{2+} remains far lower than their consumption rate via reaction (2) [12,13]. For efficient production of $SO_4^{\cdot -}$, engineers normally choose to add more Fe^{2+}. The separation of Fe ions as ferric oxyhydroxides is required before discharging treated wastewater into natural waters, resulting in the production of iron sludge. Correspondently, the high cost of the disposal of iron sludge significantly limits the widespread use of the Fe^{2+}/PDS reaction. Although PDS oxidation processes initiated by heterogeneous catalysts have the potential to avoid iron sludge formation, the application of some of these catalysts leads to problems, such as leaching of metal ions into the acidic solution [16]. Furthermore, other efforts to accelerate the transformation of Fe^{3+} into Fe^{2+} have been undertaken. Hydroxylamine in the Fenton process and the Fe^{2+}/PMS process is reported to enhance the Fe^{3+}/Fe^{2+} redox cycles, which leads to steady Fe^{2+} recovery and significantly activated H_2O_2/PMS with a small addition of Fe ions (1 mg/L) [17,18]. Hydroxylamine is degraded in oxidation processes, but it also introduces NO_2^-/NO_3^- into the wastewater. Anett et al. explored H_2/Pd pairs as a reductant/catalyst to achieve the fast regeneration of Fe^{3+} back to Fe^{2+} and an accelerated catalytic Fenton reaction with traces of iron [9]. It can be concluded from these studies that the continuous regeneration of Fe^{2+} occurs in the presence of a reductive substance.

Based on its excellent performance in the reductive dechlorination of various by-products, electrochemical systems with Pd-modified particle electrodes, namely three-dimensional (3D) electrochemical systems, are also promising systems for the acceleration of Fe^{3+}/Fe^{2+} recycling [21,22]. Pd catalysts have the unique ability to activate H_2 to form continuously adsorbed atomic H*, which has been confirmed to be a strong reducing agent in catalytic reduction process [23]. Furthermore, compared to an electro-reduction system with a traditional two-dimensional (2D) cathode, a 3D electrochemical system provides a larger surface area and more active sites, significantly improving the electro-reduction capacity [24,25]. In the work by Qin et al., it was deduced that Fe^{2+} continuously came from the reduction of Fe^{3+} by chemisorbed atomic H* on Au/Pd particle electrodes [26]. However, no direct evidence was provided in their study and, to our knowledge, no study has quantified the accelerating effect of a 3D electrochemical system on Fe^{2+} regeneration and sludge reduction.

In this work, benzoic acid (BA) was used as a probe for $SO_4^{\cdot -}$ and ·OH because BA is highly reactive with these two radicals [27,28]. First, a trace iron-based electro/Fe^{3+}/PDS system was constructed using Pd/Al_2O_3 as the particle electrode and by externally added PDS as the oxidant. The oxidation performance of this new system was assessed by comparing it with other systems and the radicals in this process were confirmed via electron spin resonance (ESR) analysis and quenching experiments. Thereafter, the influencing factors such as PDS concentration, current density, iron concentration and gas atmosphere were investigated to evaluate the radical utilisation efficiency. Finally, the stability of Pd/Al_2O_3 was studied and the application potential of this system was discussed.

2. Experimental section

2.1. Chemicals and materials

Benzoic acid (BA), sodium peroxydisulfate (PDS), ferric sulfate ($Fe_2(SO_4)_3$), sodium sulfate ($NaSO_4$), methanol, tert-butyl alcohol (TBA), and 5,5-dimethyl-1-pyrroline N-oxide (DMPO) were purchased from Sigma Aldrich (Finland).

The Pd/Al_2O_3 catalyst was purchased from Sigma Aldrich (Finland), which had 10% Pd loading on Al_2O_3.

2.2. Experimental procedures

The solutions in this study were prepared using deionised (DI) water (resistivity of 18.2 MΩ, Arium® Pro System). The solution pH was adjusted using either 100 mM NaOH or 50 mM H_2SO_4.

Experiments were conducted in a two-cell electrochemical reactor, a schematic diagram of which is presented in Fig. SM-2 (Supplementary Material). Before the reactor was used, N_2 was used to flush out the air in the cathode cell. The hydrogen produced from the cathode was sealed in the cathode cell during the experiment. To prevent further oxidation of BA in the sample, an ethanol solution was added once the sample was removed from the reactor.

2.3. Analytical methods

The concentration of BA was measured by high-performance liquid chromatography (HPLC, Shimadzu LC-20AD, Tokyo, Japan) using a C18 column and ultraviolet detector. The mobile phase was maintained at a flow rate of 1.0 mL/min with a constant ratio (50:50) of 25 mM acetic acid and methanol; the temperature of the column was kept at 35 °C, and the maximum absorption wavelength at 228 nm was selected. The PDS concentration was determined colorimetrically using potassium titanium oxalate solution at a wavelength of 352 nm using an ultraviolet spectrophotometer (Lambda 45, PerkinElmer). This detection method was described in detail by Zeng et al. [29]. The Pd leaching concentration was analysed by inductively coupled plasma-optical emission spectroscopy (ICP Agilent 5110).

The formation of reactive oxygen radicals was identified using an electron spin resonance (ESR) spectrometer (CMS 8400, Adani). For the ·OH and $SO_4^{\cdot -}$ measurements, the sample was immediately mixed with DMPO to form adducts. The phase composition of the synthesised

catalyst was studied using an X-ray diffractometer (XRD, PANalytical) using Co-Kα radiation (λ = 0.1789 nm, at 40 kV and 40 mA) over a 2θ range of 10–120° with a step size of 0.02° and scan speed of 2°/min.

3. Results and discussion

3.1. Enhancement of the Electro/Fe^{2+}/PDS process using Pd/Al_2O_3

Initially, we conducted an experiment to degrade BA (C_0 = 180 μM) in a Pd/Al_2O_3-enhanced electro/Fe^{3+}/PDS system (Pd-EFP system), *i.e.* in addition to PDS (10 mM) and Fe^{3+} (2 mg or 36 μM), the reaction suspension contained Pd/Al_2O_3 as the particle electrode catalyst and cathode (3.33 mA/cm^2, pH of 3.0, and N_2 atmosphere). As shown in Fig. 1a, 80.12% of BA was degraded within 120 min. The Pd/Al_2O_3 catalyst in this experiment showed almost no adsorption towards BA or Fe ions.

To clarify the role of PDS, the cathode, Pd/Al_2O_3 catalyst, and Fe^{3+} in the oxidation process, control experiments were conducted by excluding each component. Zero degradation of BA occurred in the absence of PDS (electro/Pd/Fe^{3+} system), which obviously played the role of oxidant in the Pd-EFP system. The addition of the Pd/Al_2O_3 catalyst in the Fe^{3+}/PDS system also had a negligible effect on the degradation of BA (Pd/Fe^{3+}/PDS system). To our surprise, 2.87% of BA was degraded in the electro/Fe^{3+}/PDS system. According to the aforementioned discussion, Fe^{3+} could be reduced on the cathode directly and then led to the subsequent activation of PDS [19]. The low reduction efficiency of Fe^{3+} could be ascribed to the occupation of active sites by H^+ and subsequent H_2 evolution on the cathode (Fig. SM-3a). This was verified by the large amount of bubbles near the cathode. According to the research reported by Anett, generated H_2 can be chemically adsorbed by the Pd/Al_2O_3 catalyst and converted into a strongly reducing agent (Pd-H*) (reaction (8)), which can reduce Fe^{3+} [9]. To verify our hypothesis for our system, we investigated the variation of the Fe^{2+} concentration in the Pd-EFP system in the absence of BA and PDS (Fig. 1b). Because the recycling of Fe^{3+}/Fe^{2+} was too fast to detect the variation of the Fe^{2+} concentration, we increased the initial concentration of Fe ions ten-fold. In the absence of the Pd/Al_2O_3 catalyst, no variation in the iron species was observed. With the addition of 50 mg of Pd/Al_2O_3 in the electrochemical cell, 360 μM of Fe^{3+} could be totally reduced, and Fe^{2+} were formed in only 1 min. The results strongly supported our hypothesis that the cathode played the role of electron donor by electro-generating H_2.

$$\equiv Pd\text{-}H_2 \rightarrow 2\equiv Pd\text{-}H^* \quad (8)$$

In summary, this new system exhibited continuously strong oxidation ability when we applied PDS as the oxidant, a cathode as an electron donor, Pd/Al_2O_3 particles for the catalytic reduction of Fe^{3+}, and Fe ions as the one-electron transferring medium. Based on this, it is reasonable to divide the Pd-EFP system into a two-stage process: an accelerated Fe^{3+}/Fe^{2+} cycle on the Pd/Al_2O_3 particle electrode and a subsequent Fe^{2+}/PDS oxidation process in the bulk solution.

3.2. Active radical analysis

ESR spectroscopy with the spin-trapping reagent of DMPO was applied to directly confirm the generation of radicals. The hyperfine splitting constants for the DMPO radical adducts of DMPO·-OH and DMPO·-SO_4 were representative of ·OH and $SO_4^{\cdot -}$, respectively [13,30–32]. In this study, as shown in Fig. 2a, we observed no signal for the Fe^{3+}/PDS system. For the Pd-EFP system, as we predicted, slight signals for DMPO·-SO_4 adducts suggested the generation of $SO_4^{\cdot -}$. Moreover, a typical four-line ESR spectrum with an intensity of 1:2:2:1 was detected, which indicated the emergence of ·OH.

It is obvious that $SO_4^{\cdot -}$ came from the PDS activation via *in situ*-generated Fe^{2+} (reaction (2)) in the Pd-EFP system. The redox potential of $SO_4^{\cdot -}$ was confirmed to be 2.5–3.1 V, while the 2.7 V potential of · OH was detected in acidic solution [33,34]. Due to the narrow gap of potentials between the two radicals, ·OH could be generated via fast transformation from $SO_4^{\cdot -}$ (reaction (9)) [12].

$$SO_4^{\cdot -} + H_2O \rightarrow SO_4^{2-} + \cdot OH + H^+ \quad (9)$$

Quenching experiments were further conducted to check the importance of $SO_4^{\cdot -}$ and ·OH in the oxidation process. Ethanol is well known to be an efficient scavenger for ·OH and $SO_4^{\cdot -}$ due to its high reaction constant with these two radicals [34]. As shown in Fig. 2b, the degradation of BA was significantly inhibited in the presence of ethanol. More specifically, 80.12% BA was degraded without ethanol within 120 min. With the addition of 0.18 M ethanol, only 30.80% BA degradation was observed; with a further increase in the ethanol concentration to 1.8 M, the degradation of BA was reduced to 22.82%. The inhibitory effect of ethanol on the BA degradation indicated that $SO_4^{\cdot -}$ and its symbiotic radical (·OH) were the main oxidation species in the Pd-EFP system.

The reductive effect of Pd-based catalysts in the electrochemistry system has been extensively investigated [21,22,35,36]. Direct electron transfer and atomic H* may be both involved in the accelerated recycling process of Fe^{3+}/Fe^{2+}. For a better understanding of the accelerated iron recycling process, we further clarified the importance of the two reductive mechanisms in the reduction process of Fe^{3+}. Tert-butyl alcohol (TBA) is reported to be an efficient scavenging agent of atomic H* [21]. To minimise the systematic error, the initial Fe^{3+}

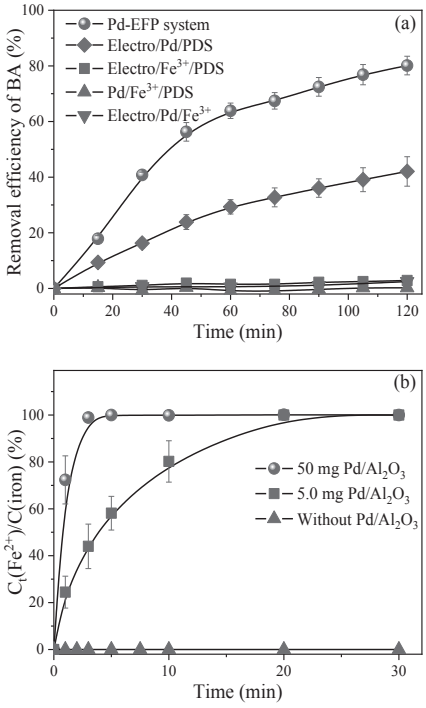

Fig. 1. (a) Degradation efficiency of BA in various systems ([BA], 180 μM; [PDS], 10 mM; [Fe^{3+}], 36 μM; [Pd/Al_2O_3], 50 mg/120 mL; current density, 3.33 mA/cm^2; initial solution pH, 3.0); (b) Reduction ratio of Fe^{3+} in the Pd-EFP system (initial solution pH, 3.0; C(Fe ions), 360 μM).

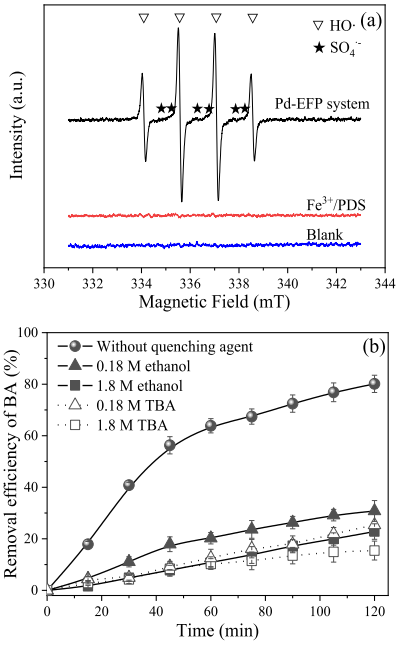

Fig. 2. (a) ESR spectra of DMPO·-OH and DMPO·-SO_4 formed in various systems. (b) Effect of scavengers on the BA degradation in the Pd-EFP system ([BA], 180 μM; [PDS], 10 mM; [Fe^{3+}], 36 μM; [Pd/Al_2O_3], 50 mg/120 mL; current density, 3.33 mA/cm^2; initial solution pH, 3.0).

concentration was increased to 360 μM, while the Pd/Al_2O_3 catalyst was set to only 5.0 mg/120 mL. As shown in Fig. 3, strong inhibition of Fe^{3+} reduction occurred with TBA addition (36 mM and 360 mM). We further fitted the process with pseudo-first-order kinetics. As shown in Fig. 3 (insert), with TBA additions of 36 mM and 360 mM, the reduction kinetics constant decreased by 77.81% and 83.97%, respectively. The sharp decrease in the Fe^{3+} reduction rate suggested the main role of atomic H* rather than direct electron transfer on the Pd/Al_2O_3 particle electrode (reaction (10), Fig. SM-3b), which is identical to the catalytic property of Pd as an atomic H* keeper.

$$\equiv Pd\text{-}H^* + Fe^{3+} \rightarrow \equiv Pd + H^+ + Fe^{2+} \quad (10)$$

TBA is also an effective screening agent for ·OH because it exhibits a low reactivity towards $SO_4^{\cdot -}$ [34]. Consequently, the inhibitory effect of TBA on organic degradation is normally not stronger than that of ethanol for normal oxidation processes. Interestingly, the screening effect of TBA on BA degradation in our system was stronger than the influence of ethanol (Fig. 2b) [18]. This contradiction can be ascribed to the simultaneous inhibition of both ·OH and atomic H*. The results further confirmed the importance of atomic H* for the reduction of Fe^{3+}.

Atomic H* may originate from the adsorption of electrogenerated H_2 or H^+ conversion via electro-induction on the Pd surface [9]. Plenty of atomic H* in the bulk solution accelerated the transformation of Fe^{3+} to Fe^{2+} considerably. The Pd-EFP system provided continuous Fe^{2+} for the Fe^{2+}/PDS oxidation process. Thus, organics could be degraded by both $SO_4^{\cdot -}$ and ·OH from the Fe^{2+}-activated PDS process.

3.3. Sludge production

Fe ions bridged as a single electron-transferring medium between the electron-donor and PDS-oxidation process. Additionally, Fe ions are significant for this system because they are removed from water as a sludge, which is the focus of our research. We then investigated the effect of varying the initial iron concentration on the efficiency of BA. As shown in Fig. 4, with the addition of 180 μM Fe^{3+} (10 mg/L), the degradation efficiency of BA was determined to be 86.89% within 120 min. When we further decreased the initial Fe^{3+} concentration to 36 μM (2 mg/L), the removal efficiency was kept at 80.12%.

To quantitatively compare the iron sludge production in various systems, we standardized the iron sludge production by dividing the iron dosage (C_0(Fe)) by the organic removal (ΔC(pollutant)) in the Fe^{2+}/PDS process. Depending on the organic contaminants, the ratio varied from 5.1 to 238 for the Fe^{2+}/PDS process (Table 1) [37–43]. As shown in reactions 2–7, one mole of Fe^{2+} can produce one mole of ·OH, which can subsequently oxidize up to one mole of organics. Thus, a ratio of C(Fe)/ΔC(pollutant) in the Fe^{2+}-activated PDS process below 1.0 indicates the recycling of Fe ions in the system. We checked the C(Fe)/ΔC(BA) in the Fe^{2+}/PDS oxidation process of BA (Table 1), and the ratio was 87.2 when the ratio was decreased to 0.2 in the Pd-EFP system, suggesting trace production of iron sludge in the post-treatment process.

For conventional Fenton processes or Fe^{2+}/PDS processes, excess Fe^{2+} has been reported to have a detrimental effect on the oxidation of contaminants owing to their quenching effect toward ·OH and $SO_4^{\cdot -}$ (reactions 11–12). According to studies on Fe^{2+}/PDS processes (Table 1), an optimal ratio of C(Fe)/C(PDS) for organic degradation has generally been determined to be in the range of 0.16–1.0 [37–43]. With higher Fe^{2+} addition than the optimal dosage, excess Fe^{2+} will result in decreasing the degradation efficiency of organics. We checked the BA degradation in the Fe^{2+}/PDS system, and the optimal ratio was obtained when the iron concentration was 1.5 times the PDS concentration (Fig. SM-4). In the Pd-EFP process, the Fe^{2+}/PDS ratio was no more than 0.0036, indicating that Fe^{2+} was mainly used for PDS activation instead of radical quenching. The addition of trace iron not only benefited the post treatment of the dissolved iron, but also improved the contaminant oxidation efficiency of the Fe^{2+}/PDS process [9,7].

$$Fe^{2+} + \cdot OH \rightarrow Fe^{3+} + OH^- \quad (11)$$

$$Fe^{2+} + SO_4^{\cdot -} \rightarrow Fe^{3+} + SO_4^{2-} \quad (12)$$

Another mechanism for decreasing the iron dosage in the Fe^{2+}-activating oxidation process is the reduction of Fe^{3+} on the cathode (reaction (13)), which has been widely investigated for the electro-

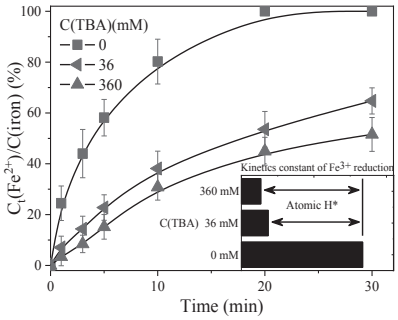

Fig. 3. Fe^{2+} concentration variation in the Pd-EFP system without PDS and BA ([Fe^{3+}], 360 μM; [Pd/Al_2O_3], 50 mg/120 mL; current density, 3.33 mA/cm^2; initial solution pH, 3.0).

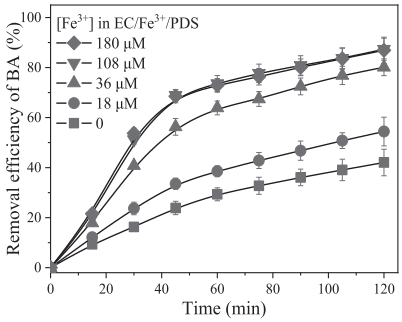

Fig. 4. Effect of initial Fe^{3+} addition on the removal efficiency of BA in the Pd-EFP system ([BA], 180 μM; [PDS], 10 mM; [Pd/Al_2O_3], 50 mg/120 mL; current density, 3.33 mA/cm^2; initial solution pH, 3.0).

Table 1
A comparison of pollutant concentration, iron dosage and PDS dosage in the Fe^{2+}/PDS system.

ΔC(pollutant)	C(Fe)	C(PDS)	C(Fe)/ ΔC(pollutant)	C(Fe)/ C(PDS)	
40 μM	1.6 mM	2 mM	40	0.16	[37]
10 μM	0.4 mM	0.4 mM	40	1	[38]
4.2 μM	1 mM	5 mM	238	0.2	[39]
0.7 mM	3.6 mM	5 mM	5.1	0.72	[40]
0.84 mM	5.8 mM	20 mM	6.9	0.29	[40]
0.8 mM	8.1 mM	35 mM	10.13	0.23	[40]
25 μM	0.25 mM	1 mM	10	0.25	[41]
50 μM	4 mM	4 mM	80	1	[42]
32 μM	2 mM	2 mM	62.5	1	[43]
172 μM	15 mM	10 mM	87.2	1.5	Fe^{2+}/PDS
144 μM	36 μM	10 mM	0.25	0.0036	Pd-EFP

Fenton process. By accurately controlling the applied potential on the cathode, such as graphite or carbon felt, fast reduction of Fe^{3+} can be achieved.

$$Fe^{3+} + e^- \rightarrow Fe^{2+} \quad (13)$$

To better compare the performance of this new system and electro-Fenton system on the iron sludge reduction, the iron concentration in electro-Fenton processes are summarised in Table SM-1. Obviously, the electro-Fenton process requires iron dosages according to the different cathode materials. To continuously provide Fe^{2+} and activate H_2O_2, iron concentrations are required to be higher than 0.2 mM (11.2 mg/L). In contrast, the iron dosage was 36 μM (2 mg/L) in the Pd-EFP system (limitation of Fe in EU and US). The further decrease in the need for iron can be ascribed to the strong reduction ability of atomic H* and large surface area of the Pd/Al_2O_3 catalyst.

3.4. Radical consumption analysis

The effects of the applied current density and PDS concentration were investigated to optimize the parameters and explore side reactions. As shown in Fig. 5a, under a current density of 0.66 mA/cm^2, the degradation efficiency of BA was only 20.63% within 120 min. With an increase in the current density to 3.33 mA/cm^2, the degradation efficiency was improved to 80.12%. Interestingly, a further increase in the current density to 6.66 mA/cm^2 led to a counterproductive effect on BA degradation.

With the increase in the current density, the applied voltage increased and hydrogen bubbles were produced faster, both of which were beneficial to the production of atomic H* on the Pd/Al_2O_3. Thus, as a reductant, atomic H* on the catalyst can act not only as an accelerator of iron recycling but also as a possible quenching agent for ·OH and $SO_4^{\cdot -}$ (reactions 14–15). The adverse effect of current density beyond 3.33 mA/cm^2 verified the hypothesis, *i.e.* in our system, the optimal current density was 3.33 mA/cm^2.

$$\equiv Pd\text{-}H^* + \cdot OH \rightarrow \equiv Pd + H^+ + OH^- \quad (14)$$

$$\equiv Pd\text{-}H^* + SO_4^{\cdot -} \rightarrow \equiv Pd + H^+ + SO_4^{2-} \quad (15)$$

Similar to the effect of current density on the performance of BA degradation, BA removal was enhanced with an increase in the PDS concentration from 2 to 20 mM; however, a further increase of PDS concentration adversely affected the degradation efficiency of BA (Fig. 5b). This was due to the fact that more $SO_4^{\cdot -}$ was generated at higher PDS concentrations, but excessive PDS consumed $SO_4^{\cdot -}$ via reaction (3) [44].

3.5. Effect of the gas atmosphere

The gas atmosphere above the cathodic cell is another parameter that affects the reaction on the Pd/Al_2O_3. We concluded that atomic H* is the main species responsible for Fe^{3+} reduction. It has been found that dissolved oxygen can compete with Fe^{3+} for the reaction with atomic H* (reaction (16)) [45,46]. Given the inhibition of dissolved oxygen on atomic H*, oxygen should be prevented in the cathodic cell [47].

$$4\equiv Pd\text{-}H^* + O_2 \rightarrow 4\equiv Pd + 2H_2O \quad (16)$$

In the study by Anett et al., increasing concentration of H_2 above the

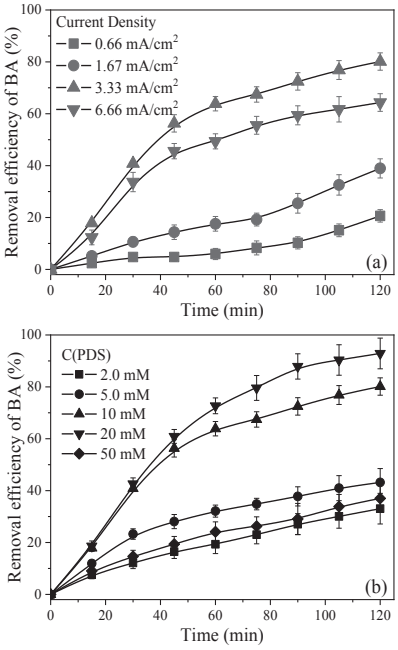

Fig. 5. Effect of current density (a) and initial PDS addition (b) on the removal efficiency of BA in the Pd-EFP system ([BA], 180 μM; [PDS], 10 mM; [Fe^{3+}], 36 μM; [Pd/Al_2O_3], 50 mg/120 mL; current density, 3.33 mA/cm^2; initial solution pH, 3.0).

cathode cell was found to be beneficial to accelerate Fe^{3+} recycling owing to the reductive effect of activated H_2 on the Pd/Al_2O_3 catalyst [9]. By slowly feeding N_2 and H_2, we checked the performance of the Pd-EFP process on BA degradation in N_2 and H_2 atmospheres (Fig. 6a). Compared with the *in situ* electro-generated H_2 atmosphere, pure N_2 provided a better atmosphere for the performance of the Pd-EFP system on BA degradation. Interestingly, PDS in the H_2 atmosphere initially displayed a higher degradation rate than in the N_2 atmosphere, but almost no degradation of BA occurred after a retention time of 40 min. This variation can be ascribed to the quick degradation of PDS in the pure H_2 atmosphere. As shown in Fig. 6b, the PDS was degraded quickly in the pure H_2 atmosphere, while N_2 and electro-generated H_2 atmospheres showed a relatively slow degradation rate towards PDS. The results indicated a two-electron transfer from H_2 to PDS via reaction (17) rather than one-electron transfer from atomic H* to Fe^{3+}, which suppresses the oxidation process via a Pd-H*→Fe^{3+}/Fe^{2+}→PDS/$SO_4^{\cdot -}$→BA mechanism. To confirm this hypothesis, we checked BA degradation in the H_2/Pd/PDS system, and PDS was completely consumed with zero degradation of BA.

$$\equiv Pd\text{-}H_2 + S_2O_8^{2-} \rightarrow \equiv Pd + 2H^+ + 2SO_4^{2-} \quad (17)$$

By dispelling accumulated H_2 above the reaction liquid and suppressing the oxygen reduction, N_2 atmosphere could steer the reaction on the surface of Pd/Al_2O_3 in the right direction toward Fe^{3+} reduction by atomic H*, further leading to efficient organic degradation.

3.6. Application potential analysis

The aforementioned results indicated that Pd/Al_2O_3 particles, as a famous H* keeper, showed high performance for iron recycling and reduction of iron sludge production in the Fe^{2+}/PDS process. According to our catalyst dosage study, even with the addition of only 10 mg Pd/Al_2O_3 catalyst per 120 mL of reaction liquid in the Pd-EFP system, BA degradation could reach the level of 60% (Fig. SM-5). However, the stability of the particle electrode is a crucial issue owing to the high cost of noble metals. The Pd/Al_2O_3 catalyst has been extensively used in chemical industries owing to its high stability and outstanding catalytic efficiency [23]. We also monitored the catalyst stability by recycling the Pd/Al_2O_3 catalyst in the Pd-EFP system five times. As shown in Fig. 7a, the degradation efficiencies were kept relatively stable between 80.56% and 83.19%, indicating relatively high stability. Simultaneously, the Pd concentration in the effluent was lower than the detection limit of ICP-OES (0.01 mg/L). The variation in the catalytic activity on the Pd/Al_2O_3 catalyst in the Pd-EFP process was evaluated using XRD analysis. XRD patterns of the fresh and used Pd/Al_2O_3 catalyst were recorded, as shown in Fig. 7b, where diffraction peaks assigned to (1 1 1), (2 0 0), and (3 1 1) of metallic Pd were observed. The obtained results demonstrated that Pd/Al_2O_3 is stable and could be effectively used for a long period of time, which can produce a considerable economic benefit.

For practical application, the initial solution pH and the variation of the solution pH with the reaction progress are also important [48,49]. Owing to the acidification effect of the PDS decomposition process (reaction (17)), the Pd-EFP process was confirmed to be an efficient system even with an initial solution pH of 10.0 (Text SM-2).

The Pd-EFP process successfully produced a continuous Fe^{2+}/PDS process with trace amounts of Fe ions. However, this also resulted in some drawbacks, such as a low oxidation rate, high cost for catalyst preparation, and subsequent recovery of the Pd/Al_2O_3 catalyst. The catalyst dosage analysis revealed that the Pd-EFP process exhibited oxidation capacity even when we used a Pd catalyst dosage of 10 mg/120 mL (Fig. SM-5). Furthermore, in the research field of electrocatalytic dechlorination, various functional materials have been developed that possess new characteristics while maintaining their capacity as an atomic H* keeper, and they are good alternatives as particle electrodes in this system. To further decrease the Pd dosage in the Pd-EFP system, the catalytic activity of atomic H* formation can be enhanced by changing the morphology so that the Pd(1 1 1) facet and defect sites on the Pd crystal are highly active [50,51]. It has been found that Pd-supported multi-walled nanotubes can act as an excellent H* producer in a 3D electrocatalytic process with only 0.5% loading of Pd [22]. A bimetal catalyst (Pd/In) has also showed strong reductive capacity in a 3D electrochemical process [21]. This research points out the novel approach of reducing the iron sludge in the Fe^{2+}-activated peroxide process by accelerating the transformation from Fe^{3+} to Fe^{2+} using surface-bound atomic H* on Pd/Al_2O_3. Other atomic H* keeper materials should be tested to evaluate the application value of this technology in the future.

4. Conclusion

In this study, a trace-iron based electro/Fe^{3+}/PDS system was constructed using Pd/Al_2O_3 as the particle electrode and by externally added PDS as the oxidant. At an initial solution pH of 3.0, with the addition of 10 mM PDS, 50 mg Pd/Al_2O_3, and 2 mg/L Fe ions, 80.12% of 180 μM BA was degraded within 120 min. Mechanistic studies showed that the ·OH and $SO_4^{\cdot -}$ from Fe^{2+}-activated PDS were responsible for the BA degradation, whereas atomic H* was mainly responsible for Fe^{3+} reduction to Fe^{2+}. In the Pd-EFP process, the optimal dosage of Fe ions was determined to be 36 μM (2 mg/L) because the extra addition of more than 2 mg/L Fe ions had a positive but negligible influence on BA degradation. Correspondently, the optimal current density and PDS concentration in the Pd-EFP system were found to be 3.33 mA/cm^2 and 20 mM, respectively. A higher current density

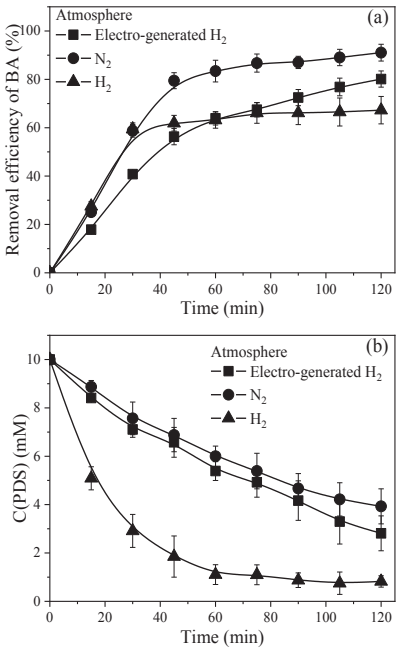

Fig. 6. Effect of gas atmosphere in a cathode cell on BA degradation (a) and PDS consumption (b) in the Pd-EFP system ([BA], 180 μM; [PDS], 10 mM; [Fe^{3+}], 36 μM; [Pd/Al_2O_3], 50 mg/120 mL; current density, 3.33 mA/cm^2; initial solution pH, 3.0).

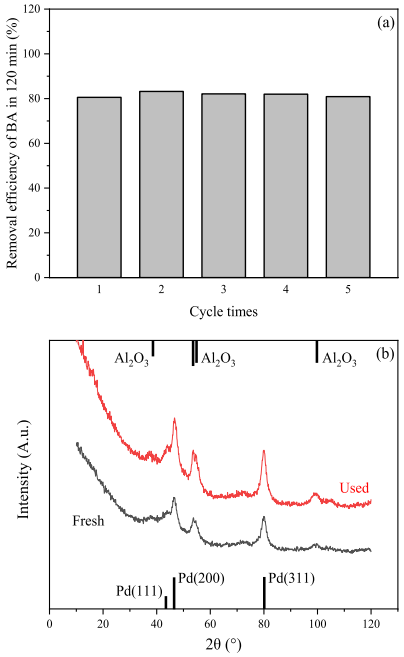

Fig. 7. (a) The degradation efficiency of BA in the Pd-EFP system for five recycling times ([BA], 180 μM; [PDS], 10 mM; [Fe^{3+}], 36 μM; current density, 3.33 mA/cm^2; initial solution pH, 3.0, reaction time, 120 min) (b) XRD spectra of the fresh and used Pd/Al_2O_3 catalysts.

or higher PDS concentration had a quenching effect on $SO_4^{\cdot-}$. The Pd-EFP process is efficient for BA degradation at various initial solution pH levels. Furthermore, the degradation of BA was also efficiently promoted by the N_2 atmosphere, which could steer the reaction on the surface of Pd/Al_2O_3 in the right direction toward Fe^{3+} reduction by atomic H* by dispelling accumulated H_2 above the reaction liquid and suppressing oxygen reduction. Finally, catalyst reusability experiments and the XRD pattern of fresh and used Pd/Al_2O_3 catalyst indicated that the Pd/Al_2O_3 catalyst maintained its high durability in the Pd-EFP system.

Declaration of Competing Interest

The authors declare that they have no known competing financial interests or personal relationships that could have appeared to influence the work reported in this paper.

Acknowledgements

The authors are grateful to the Academy of Finland and the European Union for funding this project.

Appendix A. Supplementary data

Supplementary data to this article can be found online at https://doi.org/10.1016/j.cej.2019.122972.

References

[1] B.C. Hodges, E.L. Cates, J.H. Kim, Challenges and prospects of advanced oxidation water treatment processes using catalytic nanomaterials, Nat. Nanotechnol. 13 (2018) 642–650, https://doi.org/10.1038/s41565-018-0216-x.
[2] L. Li, C. Lai, F. Huang, M. Cheng, G. Zeng, D. Huang, B. Li, S. Liu, M. Zhang, L. Qin, M. Li, J. He, Y. Zhang, L. Chen, Degradation of naphthalene with magnetic bio-char activate hydrogen peroxide: synergism of bio-char and Fe-Mn binary oxides, Water Res. 160 (2019) 238–248, https://doi.org/10.1016/j.watres.2019.05.081.
[3] C. Zhou, P. Xu, C. Lai, C. Zhang, G. Zeng, D. Huang, M. Cheng, L. Hu, W. Xiong, X. Wen, L. Qin, J. Yuan, W. Wang, Rational design of graphic carbon nitride co-polymers by molecular doping for visible-light-driven degradation of aqueous sulfamethazine and hydrogen evolution, Chem. Eng. J. 359 (2019) 186–196, https://doi.org/10.1016/j.cej.2018.11.140.
[4] C. Zhou, D. Huang, P. Xu, G. Zeng, J. Huang, T. Shi, C. Lai, C. Zhang, M. Cheng, Y. Lu, A. Duan, W. Xiong, M. Zhou, Efficient visible light driven degradation of sulfamethazine and tetracycline by salicylic acid modified polymeric carbon nitride via charge transfer, Chem. Eng. J. 370 (2019) 1077–1086, https://doi.org/10.1016/j.cej.2019.03.279.
[5] J.J. Pignatello, E. Oliveros, A. MacKay, Advanced oxidation processes for organic contaminant destruction based on the Fenton reaction and related chemistry, Crit. Rev. Environ. Sci. Technol. 36 (2006) 1–84, https://doi.org/10.1080/10643380500326564.
[6] T. Olmez-Hanci, I. Arslan-Alaton, Comparison of sulfate and hydroxyl radical based advanced oxidation of phenol, Chem. Eng. J. 224 (2013) 10–16, https://doi.org/10.1016/j.cej.2012.11.007.
[7] I.M. Kolthoff, A.I. Medalia, H.P. Raaen, The reaction between ferrous iron and peroxides. IV. Reaction with potassium persulfate[1a], J. Am. Chem. Soc. 73 1733–1739 (1951), https://doi.org/10.1021/ja01148a089.
[8] H. Kusic, I. Peternel, S. Ukic, N. Koprivanac, T. Bolanca, S. Papic, A.L. Bozic, Modeling of iron activated persulfate oxidation treating reactive azo dye in water matrix, Chem. Eng. J. 172 (2011) 109–121, https://doi.org/10.1016/j.cej.2011.05.076.
[9] A. Georgi, M.V. Polo, K. Crincoli, K. Mackenzie, F.D. Kopinke, Accelerated catalytic Fenton reaction with traces of iron: an Fe-Pd-multicatalysis approach, Environ. Sci. Technol. 50 (2016) 5882–5891, https://doi.org/10.1021/acs.est.6b01049.
[10] R. Woods, I. Kolthoff, E.J. Meehan, Arsenic(IV) as an intermediate in the induced oxidation of arsenic(III) by the iron(II)-persulfate reaction, J. Am. Chem. Soc. 86 (1964) 1698–1700, https://doi.org/10.1021/ja01063a011.
[11] H.Z. Liu, T.A. Bruton, F.M. Doyle, D.L. Sedlak, In situ chemical oxidation of contaminated groundwater by persulfate: decomposition by Fe(III)- and Mn(IV)-containing oxides and aquifer materials, Environ. Sci. Technol. 48 (2014) 10330–10336, https://doi.org/10.1021/es502056d.
[12] C.J. Liang, H.W. Su, Identification of sulfate and hydroxyl radicals in thermally activated persulfate, Ind. Eng. Chem. Res. 48 (2009) 5558–5562, https://doi.org/10.1021/ie9002848.
[13] O.S. Furman, A.L. Teel, R.J. Watts, Mechanism of base activation of persulfate, Environ. Sci. Technol. 44 (2010) 6423–6428, https://doi.org/10.1021/es1013714.
[14] W.P. Kwan, B.M. Voelker, Decomposition of hydrogen peroxide and organic compounds in the presence of dissolved iron and ferrihydrite, Environ. Sci. Technol. 36 (2002) 1467–1476, https://doi.org/10.1021/es011109p.
[15] A. Rastogi, S.R. Al-Abed, D.D. Dionysiou, Effect of inorganic, synthetic and naturally occurring chelating agents on Fe(II) mediated advanced oxidation of chlorophenols, Water Res. 43 (2009) 684–694, https://doi.org/10.1016/j.watres.2008.10.045.
[16] M. Hartmann, S. Kullmann, H. Keller, Wastewater treatment with heterogeneous Fenton-type catalysts based on porous materials, J. Mater. Chem. 20 (2010) 9002–9017, https://doi.org/10.1039/C0JM00577K.
[17] L.W. Chen, J. Ma, X.C. Li, J. Zhang, J.Y. Fang, Y.H. Guan, P.C. Xie, Strong enhancement on Fenton oxidation by addition of hydroxylamine to accelerate the ferric and ferrous iron cycles, Environ. Sci. Technol. 45 (2011) 3925–3930, https://doi.org/10.1021/es2002748.
[18] J. Zou, J. Ma, L.W. Chen, X.C. Li, Y.H. Guan, P.C. Xie, C. Pan, Rapid acceleration of ferrous iron/peroxymonosulfate oxidation of organic pollutants by promoting Fe(III)/Fe(II) cycle with hydroxylamine, Environ. Sci. Technol. 47 (2013) 11685–11691, https://doi.org/10.1021/es4019145.
[19] Y.Y. Chu, Y. Qian, W.J. Wang, X.L. Deng, A dual-cathode electro-Fenton oxidation coupled with anodic oxidation system used for 4-nitrophenol degradation, J. Hazard. Mater. 199 (2012) 179–185, https://doi.org/10.1016/j.jhazmat.2011.10.079.
[21] H.C. Lan, R. Mao, Y.T. Tong, Y.Z. Liu, H.J. Liu, X.Q. An, R.P. Liu, Enhanced electroreductive removal of bromate by a supported Pd-In bimetallic catalyst: kinetics and mechanism investigation, Environ. Sci. Technol. 50 (2016) 11872–11878, https://doi.org/10.1021/acs.est.6b02822.
[22] X.Y. She, Q. Yang, F.B. Yao, Y. Zhong, W.C. Ren, F. Chen, J. Sue, Y.H. Ma, Z.Y. Fe, D.B. Wang, X.M. Li, Electrocatalytic hydrodechlorination of 4-chlorophenol on Pd supported multi-walled carbon nanotubes particle electrodes, Chem. Eng. J. 358 (2019) 903–911, https://doi.org/10.1016/j.cej.2018.10.095.
[23] B.P. Chaplin, M. Reinhard, W.F. Schneider, C. Schuth, J.R. Shapley, T.J. Strathmann, C.J. Werth, Critical review of Pd-based catalytic treatment of priority contaminants in water, Environ. Sci. Technol. 46 (2012) 3655–3670, https://doi.org/10.1021/es204087q.
[24] R. Mao, X. Zhao, H.C. Lan, H.J. Liu, J.H. Qu, Graphene-modified Pd/C cathode and Pd/GAC particles for enhanced electrocatalytic removal of bromate in a continuous three-dimensional electrochemical reactor, Water Res. 77 (2015) 1–12, https://doi.

org/10.1016/j.watres.2015.03.002.
[25] J. Li, J. Yan, G. Yao, Y. Zhang, X. Li, B.J.C.E.J. Lai, Improving the degradation of atrazine in the three-dimensional (3D) electrochemical process using $CuFe_2O_4$ as both particle electrode and catalyst for persulfate activation, Chem. Eng. J. 361 (2018) 1317–1332, https://doi.org/10.1016/j.cej.2018.12.144.
[26] Y.H. Qin, M. Sun, H.J. Liu, J.H. Qu, AuPd/Fe_3O_4-based three-dimensional electrochemical system for efficiently catalytic degradation of 1-butyl-3-methylimidazolium hexafluorophosphate, Electrochim. Acta 186 (2015) 328–336, https://doi.org/10.1016/j.electacta.2015.10.122.
[27] M.E. Lindsey, M.A. Tarr, Quantitation of hydroxyl radical during Fenton oxidation following a single addition of iron and peroxide, Chemosphere 41 (2000) 409–417, https://doi.org/10.1016/S0045-6535(99)00296-9.
[28] P. Nate, V. Madhavan, H. Zemel, R. Fessenden, Rate constants and mechanism of reaction of $SO_4^{\cdot-}$ with aromatic compounds, J. Am. Chem. Soc. 99 (1977) 163–164, https://doi.org/10.1021/ja00443a030.
[29] H.B. Zeng, S.S. Liu, B.Y. Chai, D. Cao, Y. Wang, X. Zhao, Enhanced photoelectrocatalytic decomplexation of Cu-EDTA and Cu recovery by persulfate activated by UV and cathodic reduction, Environ. Sci. Technol. 50 (2016) 6459–6466, https://doi.org/10.1021/acs.est.6b00632.
[30] P.L. Zamora, F.A. Villamena, Theoretical and experimental studies of the spin trapping of inorganic radicals by 5,5-dimethyl-1-pyrroline N-oxide (DMPO). 3. Sulfur dioxide, sulfite, and sulfate radical anions, J. Phys. Chem. A 116 (2012) 7210–7218, https://doi.org/10.1021/jp3039169.
[31] C. Zhou, C. Lai, P. Xu, G. Zeng, D. Huang, C. Zhang, M. Cheng, L. Hu, J. Wan, Y. Liu, W. Xiong, Y. Deng, M. Wen, In situ grown AgI/$Bi_{12}O_{17}Cl_2$ heterojunction photocatalysts for visible light degradation of sulfamethazine: efficiency, pathway, and mechanism, ACS Sustain. Chem. Eng. 6 (2018) 4174–4184, https://doi.org/10.1021/acssuschemeng.7b04584.
[32] C. Zhou, C. Lai, P. Xu, G. Zeng, D. Huang, Z. Li, C. Zhang, M. Cheng, L. Hu, J. Wan, F. Chen, W. Xiong, R. Deng, Rational design of carbon-doped carbon nitride/$Bi_{12}O_{17}Cl_2$ composites: a promising candidate photocatalyst for boosting visible-light-driven photocatalytic degradation of tetracycline, ACS Sustain. Chem. Eng. 6 (2018) 6941–6949, https://doi.org/10.1021/acssuschemeng.8b00782.
[33] G.V. Buxton, C.L. Greenstock, W.P. Helman, A.B. Ross, Critical review of rate constants for reactions of hydrated electrons, hydrogen atoms and hydroxyl radicals ($\cdot OH/\cdot O^-$) in aqueous solution, J. Phys. Chem. Ref. Data 17 (1988) 513–886, https://doi.org/10.1063/1.555805.
[34] P. Neta, R.E. Huie, A.B. Ross, Rate constants for reactions of inorganic radicals in aqueous-solution, J. Phys. Chem. Ref. Data 17 (1988) 1027–1284, https://doi.org/10.1063/1.555808.
[35] X. Zhao, A. Li, R. Mao, H. Liu, J. Qu, Electrochemical removal of haloacetic acids in a three-dimensional electrochemical reactor with Pd-GAC particles as fixed filler and Pd-modified carbon paper as cathode, Water Res. 51 (2014) 134–143, https://doi.org/10.1016/j.watres.2013.12.028.
[36] J. Zhou, Z. Lou, J. Xu, X. Zhou, K. Yang, X. Gao, Y. Zhang, X. Xu, Enhanced electrocatalytic dechlorination by dispersed and moveable activated carbon supported palladium catalyst, Chem. Eng. J. 358 (2019) 1176–1185, https://doi.org/10.1016/j.cej.2018.10.098.
[37] X.X. Jiang, Y.L. Wu, P. Wang, H.J. Li, W.B. Dong, Degradation of bisphenol A in aqueous solution by persulfate activated with ferrous ion, Environ. Sci. Pollut. Res. 20 (2013) 4947–4953, https://doi.org/10.1007/s11356-013-1468-5.
[38] L. Bu, Z. Shi, S. Zhou, Modeling of Fe(II)-activated persulfate oxidation using atrazine as a target contaminant, Sep. Purif. Technol. 169 (2016) 59–65, https://doi.org/10.1016/j.seppur.2016.05.037.
[39] W. Shang, Z. Dong, M. Li, X. Song, M. Zhang, C. Jiang, F. Sun, Degradation of diatrizoate in water by Fe(II)-activated persulfate oxidation, Chem. Eng. J. 361 (2019) 1333–1344, https://doi.org/10.1016/j.cej.2018.12.139.
[40] A. Long, Y. Lei, H. Zhang, Degradation of toluene by a selective ferrous ion activated persulfate oxidation process, Ind. Eng. Chem. Res. 53 (2014) 1033–1039, https://doi.org/10.1021/ie402633n.
[41] Y.F. Rao, L. Qu, H. Yang, W. Chu, Degradation of carbamazepine by Fe(II)-activated persulfate process, J. Hazard. Mater. 268 (2014) 23–32, https://doi.org/10.1016/j.jhazmat.2014.01.010.
[42] S. Wang, J. Wang, Comparative study on sulfamethoxazole degradation by Fenton and Fe(II)-activated persulfate process, RSC Adv. 7 (2017) 48670–48677, https://doi.org/10.1039/C7RA09325J.
[43] L. Zhou, W. Zheng, Y. Ji, J. Zhang, C. Zeng, Y. Zhang, Q. Wang, X. Yang, Ferrous-activated persulfate oxidation of arsenic(III) and diuron in aquatic system, J. Hazard. Mater. 263 (2013) 422–430, https://doi.org/10.1016/j.jhazmat.2013.09.056.
[44] W.J. McElroy, S.J. Waygood, Kinetics of the reactions of the $SO_4^{\cdot-}$ radical with $SO_4^{\cdot-}$, $S_2O_8^{2-}$, H_2O and Fe^{2+}, J. Chem. Soc. Faraday Trans. 86 (1990) 2557–2564, https://doi.org/10.1002/chin.199044022.
[45] W. Xie, S. Yuan, X. Mao, W. Hu, P. Liao, M. Tong, A.N. Alshaulabkeh, Electrocatalytic activity of Pd-loaded Ti/TiO_2 nanotubes cathode for TCE reduction in groundwater, Water Res. 47 (2013) 3573–3582, https://doi.org/10.1016/j.watres.2013.04.004.
[46] R. Mao, N. Li, H.C. Lan, X. Zhao, H.J. Liu, J.H. Qu, M. Sun, Dechlorination of trichloroacetic acid using a noble metal-free graphene-Cu foam electrode via direct cathodic reduction and atomic H*, Environ. Sci. Technol. 50 (2016) 3829–3837, https://doi.org/10.1021/acs.est.5b05006.
[47] S. Yuan, Y. Fan, Y. Zhang, M. Tong, P. Liao, Pd-Catalytic In situ generation of H_2O_2 from H_2 and O_2 produced by water electrolysis for the efficient electro-Fenton degradation of rhodamine B, Environ. Sci. Technol. 45 (2011) 8514–8520, https://doi.org/10.1021/es2022939.
[48] Q. Ouyang, F. Kou, N. Zhang, J. Lian, G. Tu, Z. Fang, Tea polyphenols promote Fenton-like reaction: pH self-driving chelation and reduction mechanism, Chem. Eng. J. 366 (2019) 514–522, https://doi.org/10.1016/j.cej.2019.02.078.
[49] L. Hu, G. Zhang, M. Liu, Q. Wang, S. Dong, P. Wang, Application of nickel foam-supported Co_3O_4-Bi_2O_3 as a heterogeneous catalyst for BPA removal by peroxymonosulfate activation, Sci. Total Environ. 647 (2019) 352–361, https://doi.org/10.1016/j.scitotenv.2018.08.003.
[50] R. Liu, H. Zhao, X. Zhao, Z. He, Y. Lai, W. Shan, D. Bekana, G. Li, J. Liu, Defect sites in ultrathin Pd nanowires facilitate the highly efficient electrochemical hydrodechlorination of pollutants by H*(ads), Environ. Sci. Technol. 52 (2018) 9992–10002, https://doi.org/10.1021/acs.est.8b02740.
[51] P. Quaino, E. Santos, Hydrogen evolution reaction on palladium multilayers deposited on Au(111): a theoretical approach, Langmuir 31 (2015) 858–867, https://doi.org/10.1021/la503881y.

Publication IV

Zeng, H.B., Lan, H.C., An, X.Q., Repo, E., Park Y., Pastushok, O., Liu, H.J., and Qu, J.H.

Insight into Electroreductive Activation Process of Peroxydisulfate for Eliminating Organic Pollution: Essential Role of Atomic Hydrogen

Reprinted with permission from
Chemical Engineering Journal
Vol. 2021 (in press)

Journal Pre-proofs

Insight into Electroreductive Activation Process of Peroxydisulfate for Eliminating Organic Pollution: Essential Role of Atomic Hydrogen

Huabin Zeng, Huachun Lan, Xiaoqiang An, Eveliina Repo, Yuri Park, Olga Pastushok, Huijuan Liu, Jiuhui Qu

PII: S1385-8947(20)34467-3
DOI: https://doi.org/10.1016/j.cej.2020.128355
Reference: CEJ 128355

To appear in: *Chemical Engineering Journal*

Received Date: 25 September 2020
Revised Date: 30 November 2020
Accepted Date: 26 December 2020

Please cite this article as: H. Zeng, H. Lan, X. An, E. Repo, Y. Park, O. Pastushok, H. Liu, J. Qu, Insight into Electroreductive Activation Process of Peroxydisulfate for Eliminating Organic Pollution: Essential Role of Atomic Hydrogen, *Chemical Engineering Journal* (2020), doi: https://doi.org/10.1016/j.cej.2020.128355

Insight into Electroreductive Activation Process of Peroxydisulfate for Eliminating Organic Pollution: Essential Role of Atomic Hydrogen

Huabin Zeng,[a,b] Huachun Lan,[a*] Xiaoqiang An,[a] Eveliina Repo,[b] Yuri Park,[b] Olga Pastushok,[b] Huijuan Liu,[a] Jiuhui Qu[a]

[a] Center for Water and Ecology, State Key Joint Laboratory of Environment Simulation and Pollution Control, School of Environment, Tsinghua University, Beijing 100084, China

[b] Department of Separation Science, School of Engineering Science, Lappeenranta-Lahti University of Technology LUT, Sammonkatu 12, FI-50130 Mikkeli, Finland

*Corresponding author:

Center for Water and Ecology, State Key Joint Laboratory of Environment Simulation and Pollution Control,

School of Environment, Tsinghua University,

Beijing 100084, China

E-mail address: hclan@tsinghua.edu.cn

Table of Contents/Abstract Art

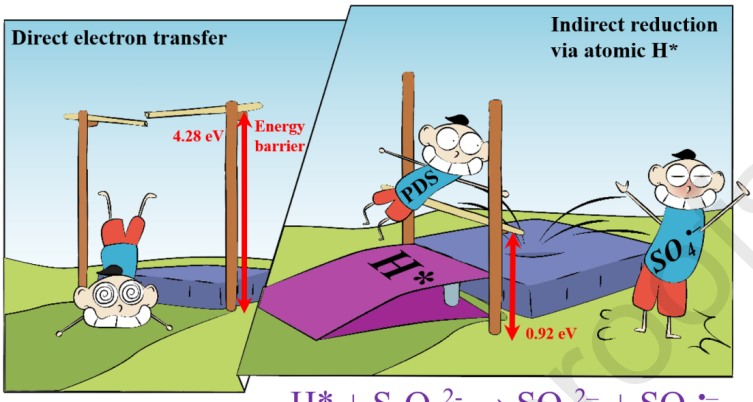

$$H^* + S_2O_8^{2-} \rightarrow SO_4^{2-} + SO_4^{\bullet-}$$

Abstract

Electrochemically activating peroxydisulfate (PDS) can eliminate organic pollution using electron as activator without the involvement of byproducts. Notwithstanding, the process suffered from long hydraulic retention time, and the activation regime remained unclear. Herein, using Pd/Al_2O_3 catalyst as particle electrode for initiating PDS oxidation in the cathodic cell can degrade various organic pollutants with varying the kinetic constants from 0.0256 min^{-1} to 0.0645 min^{-1}, which were at least 5-fold higher than that in previous studies. The reactive oxygen species were determined to be $SO_4^{\bullet-}$/$^{\bullet}OH$. These radicals were readily formed from the single-electron reduction of PDS by electro-induced atomic hydrogen (indirect reduction mechanism), while direct two-electron transfer from electro-generated H_2 to PDS consumed its oxidation capacity without yielding radical due to the higher energy barrier. Revealing the mechanism of electrochemically unleashing the oxidative power of PDS into $SO_4^{\bullet-}$ can rationalize the design of scalable electrode for PDS-based water purification.

Keywords: Organic pollution, peroxydisulfate, electroreductive activation, single electron transfer, atomic hydrogen

1. Introduction

By producing strongly oxidizing radicals, advanced oxidation processes (AOPs) were appealing treatment processes for degrading non-biodegradable, recalcitrant and toxic organic contaminants [1]. Recently, peroxydisulfate (PDS, $S_2O_8^{2-}$) attracted growing attention as a promising oxidant not only due to its chemical stability in the storage and transport periods but also owing to highly achievable radical formation yield [2]. Moreover, the produced sulfate radical ($SO_4^{\bullet-}$) demonstrated longer lifetime than hydroxyl radicals ($^{\bullet}OH$) in water (30 μs for $SO_4^{\bullet-}$ and 1 μs for $^{\bullet}OH$) [3], as well as less dependence of treatment efficiency on the operational parameters (e.g. pH, initial peroxide loading, and background constituents) [2]. These properties endowed the PDS with bright application perspective in the soil remediation and water treatment.

$$S_2O_8^{2-} + \text{energy} \rightarrow 2\ SO_4^{\bullet-} \quad (1)$$

$$S_2O_8^{2-} + M^{n+} \rightarrow M^{(n+1)+} + SO_4^{2-} + SO_4^{\bullet-} \quad (2)$$

$$S_2O_8^{2-} + e^- \rightarrow SO_4^{2-} + SO_4^{\bullet-} \quad (3)$$

For extending the application scenarios of PDS oxidation, the suitable activation approach for environmental problem has been a “holy grail” in these scientific researches [2]. Generally, the $S_2O_8^{2-}$ activation to $SO_4^{\bullet-}$ can be initiated by energy input (heat, microwave, or light) or single-electron transfer from transition metal catalysts (M=Fe, Co, Cu, Ag) (**reaction 1~2**) [4]. Among these approaches, the PDS activation by transition metal catalysts has been widely employed for application of PDS in *in-situ* chemical oxidation of polluted areas [5, 6]. In addition, the electrochemical activation of PDS via one-electron reduction on the cathode (**reaction 3**) attracted some attention [7-9], owing to the reagent-free property using electron as reductant without the involvement of byproducts, preventing the costly transportation and storage on the activators and

the downstream treatment for removing the byproducts, as well as reducing the dependence on the operating pH [9]. Meanwhile, remotely electrolytic manipulation toward the PDS activation theoretically allowed the environmental remediation process to be precisely controlled by tuning the applied potential [10, 11]. Despite these advantages, the degradation kinetics of most organic compounds (dinitrotoluene, aniline, and ciprofloxacin,) were much slower than those for PDS oxidation initiated by transition metal activators, and the process exhibited meaningful degradation only within an irrational time scale (more than 6 hours) [7-9]. More importantly, these works were confined to revealing the phenomena of heterolytically cleaving the peroxide bond for yielding $SO_4^{\bullet-}$ by single-electron injection from carbon cathode into PDS molecule (**reaction 3**). The studies never unravel the active sites for PDS reaction and key intermedia for single-electron transfer except in cases where pH-sensitive Fe^{2+}/Fe^{3+} bridged between electrode and PDS [12]. The insight into the electrochemical activation mechanism without iron will facilitate the rational design of an electro-AOP for efficiently utilizing PDS.

It has been well-documented that the electrocatalytic reduction of substrates can proceed through both direct electron transfer and indirect mechanism via atomic hydrogen (atomic H*) [13]. Depending on using the electrode surface or the electro-generated atomic H* as a platform for adsorption of substrates, the subsequent conversion may be steered towards the different routes with yielding different products. In our case, we were particularly intrigued by atomic H* due to its unique nature as a one-electron reductant. Especially, much lower redox potential of H^*/H^+ couple (E° = -2.1 V vs RHE) than that of Fe^{2+}/Fe^{3+} couple (E° = -0.77 V vs RHE) indicated that PDS reduction by atomic H* was thermodynamically feasible with $SO_4^{\bullet-}$ as reduction product (**Reaction 4**) [14, 15]. Among various materials for atomic H* generation, the most presentative ones were palladium (Pd) and its alloys, for their outstanding electronic property to form relatively

stable Pd-H* bond (Volmer reaction) [16], and depress the recombination of two atomic H* (Heyrovsky reaction), therefore to extend the retention time of atomic H* [17-19]. The lab-scale experiments using Pd-doping cathode (two-dimensional electrode, 2D electrode) or Pd-coating particle electrode (three-dimensional electrode, 3D electrode) have been deemed atomic-H*-rich systems for dechlorination of disinfection by-products and dehydrogenation of various unsaturated organics [20]. In comparison to 2D electrochemical system, the electroreduction system with 3D electrode theoretically provided more active sites for generating atomic H*, which may lead to higher kinetic constant of substrate reduction in the system.

$S_2O_8^{2-} + H^* \rightarrow H^+ + SO_4^{2-} + SO_4^{\bullet-}$ (4)

In this work, a 3D electroreduction system using commercial Pd/Al_2O_3 as particle electrode was applied for investigating the mechanism of PDS reduction. Meanwhile, externally added BA (50 μM) was employed as a probe for efficiently capturing $SO_4^{\bullet-}$ in the PDS decomposition process (k=1.2×10^9 $M^{-1}\cdot s^{-1}$) [12, 21], while it showed inertness to atomic H* produced on the Pd/Al_2O_3 [12]. The PDS decompositions via single-electron/two-electron reduction routes were clarified by electron spin resonance (ESR) analysis, quenching experiments, and density function theory (DFT) calculations. The involved parameters were optimized for accelerating PDS activation. Finally, the practical value of the system was further assessed by degrading various organic contaminants.

2. Experimental Section

2.1 Chemicals

A complete list of reagents is provided in **Text S1 (Supplementary Material)**.

2.2 Setup of batch Experiment

Solutions in this study were prepared using deionized (DI) water (resistivity 18.2 MΩ, arium® pro system). Solution pH regulation was performed using NaOH or H_2SO_4.

Experiments were conducted in a two-cell electrochemical reactor, a schematic diagram of which is presented in **Figure S1**. Before the reactor was used, N_2 was used to flush out the air in the cathodic cell. The liquid samples were preserved in the 1 M ethanol solution once the sample was taken from the reactor.

2.3 Analytical Method

The concentrations of model contaminants were measured by high-performance liquid chromatography (HPLC, Shimadzu LC-20AD, Tokyo, Japan) with a C18 column and ultraviolet detector, the temperature of column was kept at 30 ℃ and the mobile phase was maintained at a flow rate of 1.0 ml/min. Other analytical details about HPLC analysis of organic contaminants were presented in the **Table S1,** including mobile phase and detecting wavelengths.

The PDS concentration was determined colorimetrically using potassium titanium oxalate solution at a wavelength of 352 nm by ultraviolet spectrophotometer (lambda 45, PerkinElmer) and the detection method was described in detail by Zeng et al [22].

The formation of reactive oxygen species (ROS) was identified with an ESR spectrometer (CMS 8400, Adani). For $OH\cdot$ and $SO_4^{\cdot-}$ measurements, the sample was immediately mixed with DMPO to form adducts. The phase composition of the synthesised catalyst was studied by X-ray diffractometer (XRD, PANalytical), using Co-Kα radiation (λ=0.1789 nm, at 40 kV and 40 mA) over a 2θ range of 10~120° with a step size of 0.02° and scan speed of 2°/min.

2.4 DFT analysis

The surface of Pd (111) was built, where the vacuum space along the z-direction is set to be 20 Å, eliminating the interaction between two neighboring images. The bottom two atomic layers were fixed, the top three atomic layers were adequately relaxed for all surface systems. Then the atom, ion and molecular were adsorbed on the surface. The first-principles calculations in the framework

of DFT were carried out based on the Cambridge Sequential Total Energy Package (CASTEP) [23]. The exchange-correlation functional under the generalized gradient approximation (GGA) with norm-conserving pseudopotentials [24], and Perdew-Burke-Ernzerhof functional was adopted to describe the electron-electron interaction [25]. An energy cutoff of 750 eV was used and a k-point sampling set of 5×5×1 were tested to be converged. A force tolerance of 0.01 eV/Å, energy tolerance of 5.0×10^{-7} eV per atom and maximum displacement of 5.0×10^{-4} Å were considered. The transition states are calculated with the complete LST/QST search.

The adsorption energy of were calculated by: $\Delta E_A = E^*_A - E^* - E_A$

where E^*_A, E^* and E_A denote the energy of adsorbed system, clear surface and absorbed atom, ion or molecular, respectively [26].

3. Results and discussion

3.1 PDS Activation by Pd/Al_2O_3 in Electroreduction System.

The physicochemical properties of the Pd/Al_2O_3 catalyst and its corresponding substrate (α-Al_2O_3) were characterized by SEM, XPS, and XRD analysis. SEM results (**Fig. 1b**) presented that many flower-like particles were attached to the relatively smooth surface of the particle presented in **Fig. 1a** (SEM analysis of α-Al_2O_3 substrate). These particles can be determined to be dominant Pd^0 speciation (335.2 eV for Pd^0 $3d_{5/3}$ and 340.5 eV for Pd^0 $3d_{2/3}$) by XPS analysis (**Fig. 1c**) [27]. Meanwhile, the coverage of the Pd crystal on the surface slightly impaired the acquisition of Al_2O_3-involving signals (74.7 eV for Al^{3+} 2p and 351.6 eV for O^{2-} 1s, **Fig. 1c inset**) [28]. Furthermore, comparing the XRD results of Pd/Al_2O_3 catalyst with α-Al_2O_3 substrate revealed the face-centered cubic structure of coated Pd catalyst (**Fig. 1d**). The emerging peak of Pd/Al_2O_3 at 39.4° can be assigned to the Pd(111) of metallic Pd crystal.

Theoretically, the dominant exposure of the Pd(111) facet can provide ideal active sites for producing atomic H* [29]. The atomic H* provision capacity of Pd/Al_2O_3 catalyst was further evaluated by the cyclic voltammetry (CV) curves using Pd/Al_2O_3-coating glassy carbon electrode as working electrode (**Text S2**). With varying starting potentials from -0.65 V to -0.80 V during CV analysis, the generated H* species in the reduction stage were oxidized in oxidation stage. **Fig. 1e** exhibited two oxidation peaks in positive scans, located in the potential ranges of −0.30 to −0.10 V and −0.10 to 0.10 V. By the addition of atomic H* scavenger (2,4-dichlorophenol, 2,4-DCP) [18], the peak at -0.10 V can be assigned to adsorbed H^*_{ads} while the peak at -0.30 V referred to the oxidation of absorbed H^*_{abs}. As shown in **Fig. 1f**, the height of the oxidation peaks for these atomic H* (H^*_{abs} and H^*_{ads}) significantly increased with a decreasing starting potential. The results suggested that the Pd/Al_2O_3 catalyst had plenty of active sites for H*, indicative of good testing platform for PDS activation by atomic H*.

Then, we conducted an experiment in the cathodic compartment to investigate feasibility of BA degradation ($C_{initial}$=50 μM) and simultaneous decomposition of PDS ($C_{initial}$=20 mM) in the Pd/Al_2O_3-enhanced electroreduction system (Pd/ER/PDS system), *i. e.* in addition to a constant current applied on the cathode (100 mA), the reaction suspension contained Pd/Al_2O_3 as particle electrode (0.5 g/L catalyst, pH of 3.0, and deoxygenated atmosphere). As shown in **Fig. 2**, 45.08% of BA in the Pd/ER system was rapidly degraded at a first-order kinetic constant of 0.0097 min^{-1} (k_1, R^2=0.9965). For demonstrating the role of these elements, Pd/PDS system and ER/Pd system showed no performance on the BA degradation, ruling out the feasibility of PDS activation by Pd/Al_2O_3 and BA degradation by atomic H*. Aforementioned results revealed that a synergetic activation of PDS occurs between Pd catalyst and ER system within the time scale. Meanwhile, we monitored the variation of PDS concentration as a function of time. As we supposed above that

PDS may serve as an oxidant for organic degradation, simultaneous PDS decomposition was observed with a zero-order kinetic constant of 0.3002 mM·min^{-1} (k_0, R^2=0.9971).

3.2 ROS analysis

ESR analysis was employed directly identifying ROS for BA oxidation using DMPO as a spin-trapping reagent. As displayed in **Fig. 3a**, nine characteristic peaks of DMPO−H were observed in the Pd/ER system, indicative of atomic H* formation [13]. With the addition of PDS, both DMPO−SO_4 and DMPO−OH adducts were clearly detected whereas signals of DMPO−H disappeared, proving the occurrence of $SO_4^{\bullet-}$ and its symbiotic radical ($^{\bullet}$OH) in our system (**reaction 5**) [22]. It has been well-documented that atomic H* can be generated in the 3D electrochemical system that contained Pd-involved particle electrode [20, 30]. Similar to Fe^{2+} (most presentative single-electron medium for activation of peroxide compounds), atomic H* as a single-electron reductant can asymmetrically cleavage the peroxide bond in the $S_2O_8^{2-}$ ions and forms $SO_4^{\bullet-}$ for oxidizing BA (**reaction 6**). The quenching experiment using ethanol as a scavenger for both $SO_4^{\bullet-}$ and $^{\bullet}$OH further confirmed the dominant role of these radicals played in the BA degradation process (**Fig. 3b, Fig. S3a**) [12]. Comparing the inhibitory effects of ethanol and TBA on the BA degradation unraveled the importance of atomic H* on the PDS activation (**Fig. 3b, Fig. S4a**). As a quenching agent for $^{\bullet}$OH and atomic H*, TBA showed much lower reactivity with $SO_4^{\bullet-}$ (**Table S2**) [31]. Therefore, this should have suggested a slighter inhibition of organic abatement by TBA than that by ethanol in the $SO_4^{\bullet-}$-based oxidation process, as evidenced by other researchers [32]. However, our experiment batch for BA degradation with TBA addition demonstrated a lower k_1-value than that with the addition of ethanol in this system, which may arise from the simultaneous quenching on both oxidizing radical generation from atomic H* and BA oxidation by $^{\bullet}$OH. The abnormal results reflected the necessity of atomic H* for the PDS

activation.

$SO_4^{\bullet-} + OH^- \rightarrow SO_4^{2-} + {}^{\bullet}OH$ (5)

$\equiv Pd\text{-}H^* + S_2O_8^{2-} \rightarrow \equiv Pd + H^+ + SO_4^{2-} + SO_4^{\bullet-}$ (6)

$\equiv Pd\text{-}H^* + SO_4^{\bullet-} \rightarrow \equiv Pd + H^+ + SO_4^{2-}$ (7)

Based on the data in **Fig. 2**, the ratio of Δc(PDS)/Δc(BA) was estimated to be around 700, which was close to the values in the literatures [7-9], indicating a low utilization efficiency of PDS for oxidizing organics. The low utilization efficiency might be due that excess atomic H* may quench the generated $SO_4^{\bullet-}$ (**reaction 7**) and inhibit organics' decontamination (similar to excess Fe^{2+} in Fenton process) [33], or that oxidation capacity of PDS could be consumed by directly abstracting two-electrons via a non-radical approach. The monitoring on PDS decay supplied some evidences for this. As displayed in **Fig. 3b**, although TBA efficiently inhibited atomic H*, the TBA addition of various concentrations showed almost no influence on the PDS degradation. The result ruled out the mechanism for PDS consumption via a two-step reduction of two atomic H* and implied another PDS decomposition approach.

3.3 DFT analysis

For better elucidating the PDS decomposition on the Pd/Al_2O_3, DFT analysis was conducted to connect the decomposition approaches of PDS with two electroreduction routes. In the analysis, a hyphen stood for the states where two units bonded with each other, whereas the plug sign presented the separate state. A Pd(111) facet was constructed as the representative role of Pd/Al_2O_3 catalyst, since the facet was revealed as the most exposed crystal faces by XRD analysis. In the proposed indirect reduction mechanism via atomic H*, the H^+ ions were firstly adsorbed on the Pd atom with a Free Gibbs energy change (ΔG) of -1.324 eV, the negative value indicated that the physical adsorption step can proceed spontaneously (**Fig. 4**). Later, the adsorbed H^+ ion accepted

one electron from Pd catalyst, then was converted into atomic H* through the formation of Pd-H* bond (ΔG=0.232 eV). Subsequently, the $S_2O_8^{2-}$ ion in the bulk solution coupled with atomic H* on the Pd surface to form ≡Pd-H*-$S_2O_8^{2-}$ adduct (ΔG=-3.321 eV), followed by the formation of a transition state structure (TS1) (ΔG=0.916 eV). The drastic decrease of the Gibbs free energy for forming ≡Pd-H*-$S_2O_8^{2-}$ implied the strong bond between atomic H* and $S_2O_8^{2-}$. As shown in **Fig. S5**, charge density difference analysis revealed that the electron density around $S_2O_8^{2-}$ molecule went up with the formation of ≡Pd-H*-$S_2O_8^{2-}$ adduct while the electron density around Pd-H* went down, suggesting an obvious injection of electron into PDS from ≡Pd-H*. Meanwhile, the bond length of the peroxide bridge in the $S_2O_8^{2-}$ ions is stretched from 1.347Å to 1.498Å upon $S_2O_8^{2-}$ adsorption on the atomic H*, indicating the subsequent cleavage of peroxide bond and formation of the ≡Pd-HSO_4^- and desired $SO_4^{\bullet-}$. The step where TS1 was formed was confirmed as the determining step through the reaction channel, due to its highest positive ΔG among these elementary reactions (ΔG_{ds}) [19]. Only when the system overcame the uphill energy barrier, the reaction proceeded fluently. More specifically, the determining step became the "neck of the funnel" for kinetics of PDS activation by atomic H*, determining the kinetic constant for the whole process according to the Arrhenius equation [34].

We then investigated the PDS reduction via direct electron transfer and supposed $SO_4^{\bullet-}$ as the product. In this case, the Pd atoms can be directly employed as the active sites for the PDS adsorption (ΔG = –5.977 eV). With the optimization of the molecule model, the peroxide bond was cleaved and then converted into two less oxidative ≡Pd-$SO_4^{\bullet-}$ [35]. By single-electron transfer, PDS decomposition can be oriented towards $SO_4^{\bullet-}$, presenting highly oxidative capacity when the $SO_4^{\bullet-}$ de-adsorbed from the Pd catalyst. However, the ΔG_{ds} for this reaction channel (4.281 eV) was much higher than ΔG_{ds} for PDS activation by atomic H*, denying the direct electron transfer

mechanism for $SO_4^{\bullet-}$ production and confirming that the atomic H* can orient the PDS reduction towards desired $SO_4^{\bullet-}$. In contrast, if the product was supposed to be SO_4^{2-}, the ΔGds for the channel was just 0.539 eV, suggesting the reasonable reaction route for direct two-electron transfer mechanism.

PDS activation can be efficiently initiated by single-electron transfer, whereas it lost the total oxidation capacity via a two-electron abstraction approach. It can be concluded from the DFT results that the electrochemical system met the necessity for single-electron transfer using atomic H^* as "stepping stone" (indirect reduction mechanism), by contrast, the reduction via direct electron transfer approach tended to consecutively donate two electrons to the adsorbed PDS on the Pd catalyst.

3.4 Electron donor analysis

We optimized the parameters for PDS degradation and $SO_4^{\bullet-}$ production in the Pd/ER system. Original data were displayed in **Fig. S6~S8**, and involved kinetics constants were summarized in **Table 1**. The PDS decay exhibited proportional degradation rates to applied current, which directly refers to the H_2 yield in the system (**Batch No. 1~3**). The positive correlation can be explained by that the H_2 played the role as a two-electron donor in the process through direct electron transfer mechanism. By contrast, the k_0-value for PDS decay was revealed to be kept at a certain value (about 0.3000 $M \cdot min^{-1}$), even with varying PDS and Pd/Al_2O_3 dosage (**Batch No. 1, 4~8**). The independence of PDS decay on these two parameters indicates that the PDS reaction with H_2 occurs at an extremely high speed. Moreover, comparing these influence factors revealed that the PDS diffusion was not the rate-limiting step under these conditions. Interestingly, the BA degradation exhibited different trends towards these influence factors, which characterizes the $SO_4^{\bullet-}$ production in the process. Higher applied current (or applied potential) and higher Pd/Al_2O_3

dosage endowed the BA degradation process higher kinetic constant (k_1), while the k_1 remained unaffected by varying PDS concentration.

It was frequently mentioned in the literatures that atomic H* can be generated from the adsorptive dissociation of electro-generated H_2 (**reaction 8**) or H^+ reduction by capturing the Pd-trapping electron (electro-induced atomic H^*, **reaction 9**) in the 3D ER system [12, 30, 36, 37]. For clarifying the interaction of PDS with active hydrogen species, we purged H_2 into reaction liquid containing BA as $SO_4^{\bullet-}$ probe, PDS as oxidant, and Pd/Al_2O_3 as catalyst. By this way, we excluded the electro-induced atomic H* and deepened the insight into the H_2-initiated PDS degradation process (**Fig. 5**). Interestingly, the PDS was rapidly decomposed without variation of BA concentration, indicative of a non-radical process between PDS and active H_2. Unlike conventionally believed idea that H_2 reduced pollutants via dissociative formation of atomic H*, adsorbed H_2 molecule with assistance of Pd catalyst can directly act as a two-electron donor (H_2^*, **reaction 10**) without necessity to form atomic H* [18]. Additionally, we designed a three-cell electrochemical reactor where only electro-induced atomic H* occurred in the middle cell. In this case, the BA degradation at sacrifice of trace PDS suggested successful production of $SO_4^{\bullet-}$ via efficient activation of PDS by electro-induced atomic H*.

$$\equiv Pd + H_2 \rightarrow 2 \equiv Pd\text{-}H^* \quad (8)$$

$$\equiv Pd + e^- + H^+ \rightarrow \equiv Pd\text{-}H^* \quad (9)$$

$$\equiv Pd + H_2 \rightarrow \equiv Pd\text{-}H_2^* \quad (10)$$

Aforementioned statement clearly unraveled two electron donors for PDS attenuation in the 3D electroreduction system, one was H_2 that inactivated the PDS via direct two-electron transfer, the other was electro-induced atomic H* that allowed valid activation of PDS via single-electron transfer. The H_2 yield was decided by the applied current, while the atomic H* by electro-induction

theoretically depended on the electric field and concentration of particle electrode. Unfortunately, the electrical double layer near the electrode mostly attenuated the electricpotential, while only finite electricpotential difference was used for constructing the electric field, which was the driving force source for ions directional migration to form current. It was impossible to minimize the H_2 yield and increase the proportion of atomic H* by simply adjust the applied potential/current, further improving the PDS activation efficiency. By contrast, increasing the Pd/Al_2O_3 dosage to 1.0 g/L can readily induce higher $SO_4^{\bullet-}$ level by providing more active sites for yielding more atomic H*, simultaneously increasing the organic degradation kinetics and PDS utilization efficiency.

3.5 Application analysis

The research unraveled the mechanism for PDS activation in an electroreduction system, emphasizing the importance of the indirect reduction mechanism in the process. The H*/PDS system was further evaluated by degrading several model contaminants (10 μM). As shown in **Fig. 6a**, all these organics can be abated with removal efficiencies of more than 80% in 60 min. Fitting these degradation process with first-order kinetics unrevealed that the resultant kinetic constants **(Table S3)** were at least 5 times than that in previous researches about electrochemically activating PDS (**Table S4**) [7-9]. And different from traditionally transitional-metal-involved AOPs where high valent cationic (HVC, such as Fe(IV), Cr(V), Mn(III), Cu(III)) and radicals ($^{\bullet}OH$, $SO_4^{\bullet-}$) all got involved in oxidizing organics [38-42], the H*/PDS system theoretically avoided the generation of HVC. This can be confirmed by analyzing the degradation intermediate using methyl phenyl sulfoxide (PMSO) as model contaminant, due that PMSO was converted into methyl phenyl sulfone ($PMSO_2$) by HVC, while phenylsulfinic acid ($PhSO_2$) was produced from the radical oxidation (**Fig. S9**) [39]. The concentration of $PMSO_2$ was monitored in the PMSO

degradation process (**Fig. 6b**), the results revealed that nearly no signal of $PMSO_2$ appeared through the H*/PDS oxidation process. Excluding the HVC as ROS in the H*/PDS allowed engineers to controllably steer the decontamination process via a scheduled degradation route, while organics degradation (such as various sulfoxide contaminants) was possibly oriented to unexpected products by HVC in the PDS oxidation system [39, 43]. Additionally, different from the M^{n+}/PDS system, the H*-PDS system had less dependence on the solution pH (**Text S3**), because the atomic H* can be evolved from H^+ at acidic condition, while it came from the H_2O at alkaline/neutral solution [16]. Meanwhile, the acidification in the PDS-based oxidation process highly alleviated the possible effect of solution pH on the system.

The endurability of Pd/Al_2O_3 was monitored by recycling the catalyst in the H*/PDS system for 6 times. In these cycles, the performance on the BA degradation was kept at a high level (>80%) **(Fig. S10)**. Accordingly, nearly no dissolved Pd was detected by ICP-OES analysis, demonstrating no loss of active sites on the catalyst. Meanwhile, the XPS analysis (**Fig. S11a** and **S11b**, 335.8 eV for Pd^0 $3d_{5/2}$ and 341.1 eV for Pd^0 $3d_{3/2}$) revealed that the Pd on the used electrode was still kept at Pd^0 species, even after several cycles. The XRD results of the used electrode was also unraveled that the crystal face didn't change in the process (**Fig.S11c**). The excellent stability of Pd/Al_2O_3 catalyst, zero-addition property of transition metal catalyst, and pH-independent nature endowed the system with high potential for a ternary process of wastewater before the emission to the natural waters. However, taking the low efficiency of PDS activation into consideration, other materials with high performance on atomic H* generation and inhibition of direct electron transfer mechanism should be explored to reduce the PDS dosage and sulfate residue, and improve the application value of electro-activated PDS technology.

4. Conclusion

In this study, an electroreduction system for activating PDS and degrading organic contaminants was constructed using Pd/Al_2O_3 catalyst as particle electrode. The reactive oxygen species were determined to be $SO_4^{\bullet-}$/$^{\bullet}OH$ by ESR analysis, quenching experiments and PMSO degradation analysis. Furthermore, the single-electron reduction of PDS by electrogenerated atomic H* can readily form $SO_4^{\bullet-}$ (indirect reduction mechanism), through which the energy barrier (ΔG_{ds}) was determined to be only 0.92 eV by density functional theory analysis. By contrast, taking Pd-activated H_2 as electron donor, the PDS decomposition via direct electron transfer was unveiled difficult to yield $SO_4^{\bullet-}$ (ΔG_{ds}=4.28 eV), but smoothly steered towards inert SO_4^{2-} (ΔG_{ds}=0.54 eV). By optimizing the operation parameters to maximize the production of electro-induced atomic H*, the cathodic cell can efficiently activate PDS and degrade various organic pollutants with varying the kinetic constants from 0.0256 min^{-1} to 0.0645 min^{-1}, which were (5~15)-fold higher than that in previous studies. This research pointed out the importance of indirect reduction mechanism in the PDS activation process, which paved the way to rationally construct efficient materials for electrochemically activating PDS and subsequent decontamination of organic compounds by weakening the direct electron transfer and enhancing the atomic H*-mediated reduction mechanism.

Author information

Corresponding Author

Email: hclan@tsinghua.edu.cn. Tel: 86-10-62849160.

Notes

The authors declare no competing financial interest.

Supplementary Material

The Supplementary Material is available free of charge, including 4 Texts, 11 Figures, and 4 Tables.

Acknowledgements

The authors acknowledge financial support by National Natural Science Foundation of China (No. 51722811, 51978373).

References

[1] B.C. Hodges, E.L. Cates, J.H. Kim, Challenges and prospects of advanced oxidation water treatment processes using catalytic nanomaterials, Nat. Nanotechnol. 13 (2018) 642-650.

[2] J. Lee, U. von Gunten, J.-H. Kim, Persulfate-Based Advanced Oxidation: Critical Assessment of Opportunities and Roadblocks, Environ. Sci. Technol. 54 (2020) 3064-3081.

[3] P.D. Hu, M.C. Long, Cobalt-catalyzed sulfate radical-based advanced oxidation: A review on heterogeneous catalysts and applications, Appl. Catal. B-Environ. 181 (2016) 103-117.

[4] L.W. Matzek, K.E. Carter, Activated persulfate for organic chemical degradation: A review, Chemosphere 151 (2016) 178-188.

[5] G.P. Fan, L. Cang, G.D. Fang, D.M. Zhou, Surfactant and oxidant enhanced electrokinetic remediation of a PCBs polluted soil, Sep. Purif. Technol. 123 (2014) 106-113.

[6] F. Pardo, A. Santos, A. Romero, Fate of iron and polycyclic aromatic hydrocarbons during the remediation of a contaminated soil using iron-activated persulfate: A column study, Sci. Total Environ. 566 (2016) 480-488.

[7] L.W. Matzek, M.J. Tipton, A.T. Farmer, A.D. Steen, K.E. Carter, Understanding Electrochemically Activated Persulfate and Its Application to Ciprofloxacin Abatement, Environ. Sci. Technol. 52 (2018) 5875-5883.

[8] W.S. Chen, Y.C. Jhou, C.P. Huang, Mineralization of dinitrotoluenes in industrial wastewater by electro-activated persulfate oxidation, Chem. Eng. J. 252 (2014) 166-172.

[9] W.S. Chen, C.P. Huang, Mineralization of aniline in aqueous solution by electrochemical activation of persulfate, Chemosphere 125 (2015) 175-181.

[10] S.H. Yuan, P. Liao, A.N. Alshawabkeh, Electrolytic Manipulation of Persulfate Reactivity by Iron Electrodes for Trichloroethylene Degradation in Groundwater, Environ. Sci. Technol. 48 (2014) 656-663.

[11] A.I.A. Chowdhury, J.I. Gerhard, D. Reynolds, D.M. O'Carroll, Low Permeability Zone Remediation via Oxidant Delivered by Electrokinetics and Activated by Electrical Resistance Heating: Proof of Concept, Environ. Sci. Technol. 51 (2017) 13295-13303.

[12] H. Zeng, X. Zhao, F. Zhao, Y. Park, M. Sillanpää, Accelerated Fe^{3+}/Fe^{2+} Cycle using Atomic H* on Pd/Al_2O_3: A Novel Mechanism for an Electrochemical System with Particle Electrode for Iron Sludge Reduction in the Fe^{2+}/Peroxydisulfate Oxidation Process, Chem. Eng. J. (2019) 122972.

[13] R. Mao, N. Li, H.C. Lan, X. Zhao, H.J. Liu, J.H. Qu, M. Sun, Dechlorination of Trichloroacetic Acid Using a Noble Metal-Free Graphene-Cu Foam Electrode via Direct Cathodic Reduction and Atomic H*, Environ. Sci. Technol. 50 (2016) 3829-3837.

[14] J.-Y. Lee, J.G. Lee, S.-H. Lee, M. Seo, L. Piao, J.H. Bae, S.Y. Lim, Y.J. Park, T.D.J.N.c. Chung, Hydrogen-atom-mediated electrochemistry, Nat. Commun, 4 (2013) 2766.

[15] Y. Pan, H.R. Su, Y.T. Zhu, F.V. Molamahmood, M. Long, CaO_2 based Fenton-like reaction at neutral pH: Accelerated reduction of ferric species and production of superoxide radicals, Water Res. 145 (2018) 731-740.

[16] Y. Zheng, Y. Jiao, M. Jaroniec, S.Z. Qiao, Advancing the Electrochemistry of the Hydrogen-Evolution Reaction through Combining Experiment and Theory, Angew. Chem.-Int. Edit., 54 (2015) 52-65.

[17] A. Li, X. Zhao, Y. Hou, H. Liu, L. Wu, J. Qu, The electrocatalytic dechlorination of chloroacetic acids at electrodeposited Pd/Fe-modified carbon paper electrode, Appl. Catal. B-Environ. 111 (2012) 628-635.

[18] G.M. Jiang, M.N. Lan, Z.Y. Zhang, X.S. Lv, Z.M. Lou, X.H. Xu, F. Dong, S. Zhang, Identification of Active Hydrogen Species on Palladium Nanoparticles for an Enhanced Electrocatalytic Hydrodechlorination of 2,4-Dichlorophenol in Water, Environ. Sci. Technol. 51 (2017) 7599-7605.

[19] Y.J. Zhou, G. Zhang, Q.H. Ji, W. Zhang, J.Y. Zhang, H.J. Liu, J.H. Qu, Enhanced Stabilization and Effective Utilization of Atomic Hydrogen on Pd-In Nanoparticles in a Flow-through Electrode, Environ. Sci. Technol. 53 (2019) 11383-11390.

[20] X. Zhao, A. Li, R. Mao, H. Liu, J. Qu, Electrochemical removal of haloacetic acids in a three-dimensional electrochemical reactor with Pd-GAC particles as fixed filler and Pd-modified carbon paper as cathode, Water Res. 51 (2014) 134-143.

[21] P. Nate, V. Madhavan, H. Zemel, R. Fessenden, Rate constants and mechanism of reaction of $SO_4^{\cdot-}$ with aromatic compounds, J. Am. Chem. Soc. 99 (1977) 163-164.

[22] H.B. Zeng, S.S. Liu, B.Y. Chai, D. Cao, Y. Wang, X. Zhao, Enhanced Photoelectrocatalytic Decomplexation of Cu-EDTA and Cu Recovery by Persulfate Activated by UV and Cathodic Reduction, Environ. Sci. Technol. 50 (2016) 6459-6466.

[23] M.D. Segall, P.J.D. Lindan, M.J. Probert, C.J. Pickard, P.J. Hasnip, S.J. Clark, M.C. Payne, First-principles simulation: ideas, illustrations and the CASTEP code, J. Phys. Condens. Matter 14 (2002) 2717-2744.

[24] J.P. Perdew, K. Burke, M. Ernzerhof, Generalized gradient approximation made simple, Phys. Rev. Lett. 77 (1996) 3865-3868.

[25] D.R. Hamann, M. Schluter, C. Chiang, Norm-Conserving pseudopotentials, Phys. Rev. Lett. 43 (1979) 1494-1497.

[26] H.H. Li, Y. Wu, C. Li, Y.Y. Gong, L.Y. Niu, X.J. Liu, Q. Jiang, C.Q. Sun, S.Q. Xu, Design of Pt/t-ZrO_2/g-C_3N_4 efficient photocatalyst for the hydrogen evolution reaction, Appl. Catal. B-Environ., 251 (2019) 305-312.

[27] M.C. Militello, S. Simko, Elemental palladium by XPS, Surf. Sci. Spectra 3 (1994) 387-394.

[28] B.J. Tan, K.J. Klabunde, P.M.A. Sherwood, XPS studies of solvated metal atom dispersed (SMAD) catalysts. Evidence for layered cobalt-manganese particles on alumina and silica, J. Am. Chem. Soc. 113 (1991) 855-861.

[29] P. Quaino, E. Santos, Hydrogen Evolution Reaction on Palladium Multilayers Deposited on Au(111): A Theoretical Approach, Langmuir 31 (2015) 858-867.

[30] H.C. Lan, R. Mao, Y.T. Tong, Y.Z. Liu, H.J. Liu, X.Q. An, R.P. Liu, Enhanced Electroreductive Removal of Bromate by a Supported Pd-In Bimetallic Catalyst: Kinetics and Mechanism Investigation, Environ. Sci. Technol. 50 (2016) 11872-11878.

[31] C.J. Liang, H.W. Su, Identification of Sulfate and Hydroxyl Radicals in Thermally Activated Persulfate, Ind. Eng. Chem. Res. 48 (2009) 5558-5562.

[32] A. Rastogi, S.R. Ai-Abed, D.D. Dionysiou, Sulfate radical-based ferrous-peroxymonosulfate oxidative system for PCBs degradation in aqueous and sediment systems, Appl. Catal. B-Environ. 85 (2009) 171-179.

[33] V. Kavitha, K. Palanivelu, The role of ferrous ion in Fenton and photo-Fenton processes for the degradation of phenol, Chemosphere 55 (2004) 1235-1243.

[34] G.F. Wei, Y.H. Fang, Z.P. Liu, First Principles Tafel Kinetics for Resolving Key Parameters in Optimizing Oxygen Electrocatalytic Reduction Catalyst, J. Phys. Chem. C. 116 (2012) 12696-12705.

[35] Y. Feng, P.H. Lee, D.L. Wu, K.M. Shih, Surface-bound sulfate radical-dominated degradation of 1,4-dioxane by alumina-supported palladium (Pd/Al_2O_3) catalyzed peroxymonosulfate, Water Res. 120 (2017) 12-21.

[36] Y. Xu, H. Lin, Y.K. Li, H. Zhang, The mechanism and efficiency of MnO_2 activated persulfate process coupled with electrolysis, Sci. Total Environ., 609 (2017) 644-654.

[37] A. Georgi, M.V. Polo, K. Crincoli, K. Mackenzie, F.D. Kopinke, Accelerated Catalytic Fenton Reaction with Traces of Iron: An Fe-Pd-Multicatalysis Approach, Environ. Sci. Technol. 50 (2016) 5882-5891.

[38] H.Y. Dong, Y. Li, S.C. Wang, W.F. Liu, G.M. Zhou, Y.F. Xie, X.H. Guan, Both Fe(IV) and Radicals Are Active Oxidants in the Fe(II)/Peroxydisulfate Process, Environ. Sci. Technol. Lett. 7 (2020) 219-224.

[39] Z. Wang, J. Jiang, S.Y. Pang, Y. Zhou, C.T. Guan, Y. Gao, J. Li, Y. Yang, W. Qu, C.C. Jiang, Is Sulfate Radical Really Generated from Peroxydisulfate Activated by Iron(II) for Environmental Decontamination? Environ. Sci. Technol. 52 (2018) 11276-11284.

[40] H.Y. Dong, G.F. Wei, T.C. Cao, B.B. Shao, X.H. Guan, T.J. Strathmann, Insights into the Oxidation of Organic Cocontaminants during Cr(VI) Reduction by Sulfite: The Overlooked Significance of Cr(V), Environ. Sci. Technol. 54 (2020) 1157-1166.

[41] W.F. Liu, B. Sun, J.L. Qiao, X.H. Guan, Influence of Pyrophosphate on the Generation of Soluble Mn(III) from Reactions Involving Mn Oxides and Mn(VII), Environ. Sci. Technol. 53 (2019) 10227-10235.

[42] L.H. Wang, H.D. Xu, N. Jiang, Z.M. Wang, J. Jiang, T. Zhang, Trace Cupric Species Triggered Decomposition of Peroxymonosulfate and Degradation of Organic Pollutants: Cu(III) Being the Primary and Selective Intermediate Oxidant, Environ. Sci. Technol. 54 (2020) 4686-4694.

[43] C. Tai, J.F. Peng, J.F. Liu, G.B. Jiang, H. Zou, Determination of hydroxyl radicals in advanced oxidation processes with dimethyl sulfoxide trapping and liquid chromatography, Anal. Chim. Acta 527 (2004) 73-80.

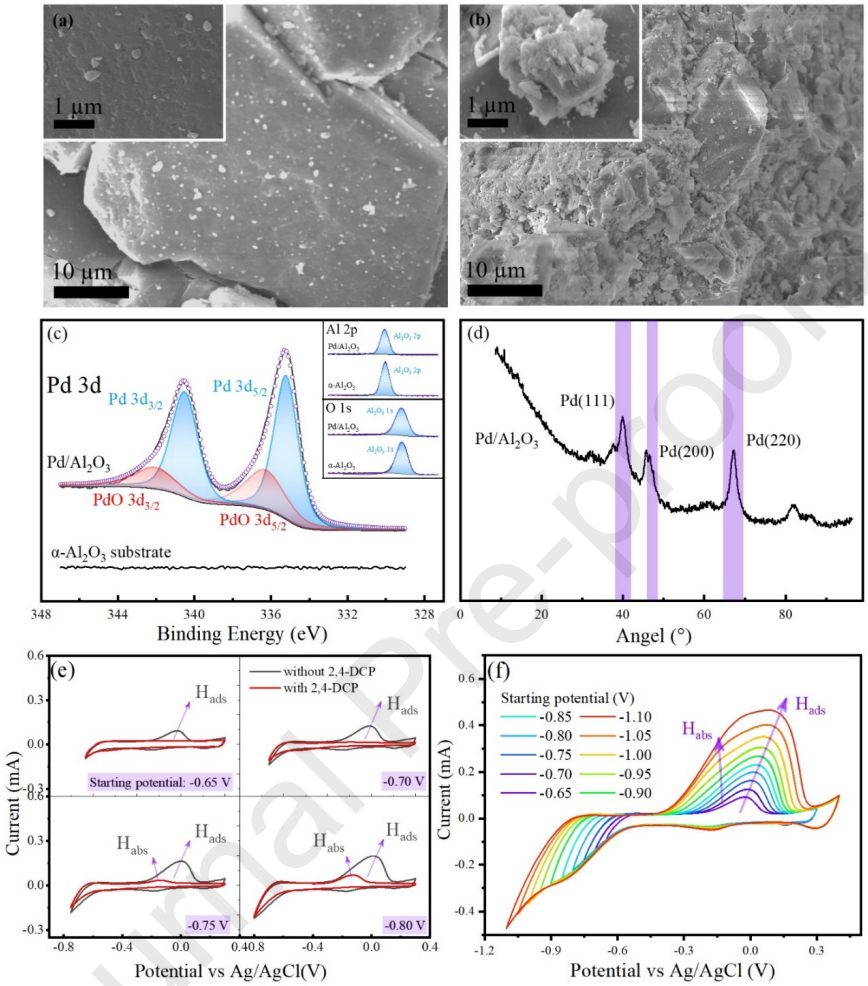

Fig. 1. SEM analyses of α-Al_2O_3 substrate (a) and Pd/Al_2O_3 catalyst (b); XPS analyses (c) and XRD analyses (d) of α-Al_2O_3 substrate and Pd/Al_2O_3 catalyst; (e) CVs of the Pd catalyst in N_2-saturated 50 mmol·L^{-1} Na_2SO_4 solution with and without 2,4-DCP under different starting potentials; (f) CVs of the Pd catalyst in N_2-saturated 50 mM Na_2SO_4 solution with different CV starting potentials: from −0.65 to −1.10 V. (scanning rate, 50 mV s^{-1}; solution pH, 7.0).

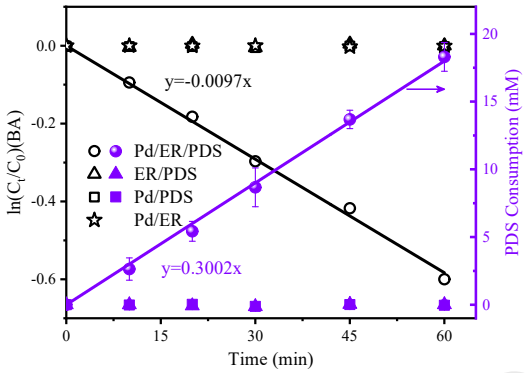

Fig. 2. BA degradation and PDS consumption in ER/PDS, Pd/PDS, Pd/ER and Pd/ER/PDS process. (BA, 50 μM; PDS, 20 mM; Pd/Al_2O_3, 0.5 g/L; Applied current, 0.10 A; initial solution pH, 3.0; deoxygenated atmosphere)

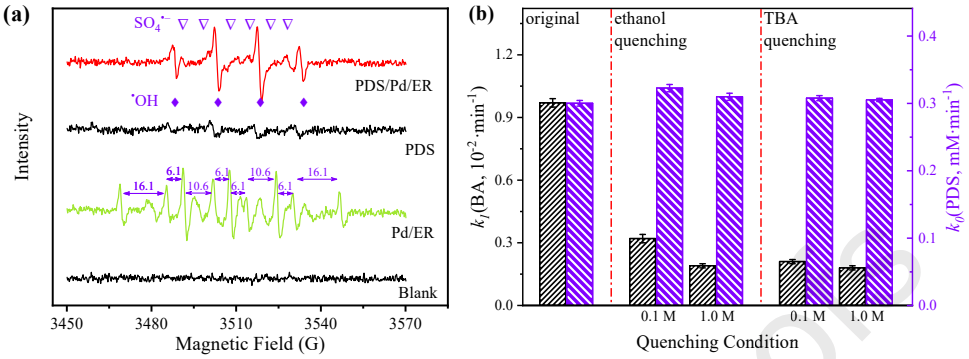

Fig. 3. (a) Identification of reactive species by ESR analysis; (b) *k*-value comparison of BA degradation (k_1) and PDS consumption (k_0) under different quenching conditions. (BA, 50 μM; PDS, 20 mM; Pd/Al_2O_3, 0.5 g/L; Applied current, 0.10 A; initial solution pH, 3.0; deoxygenated atmosphere)

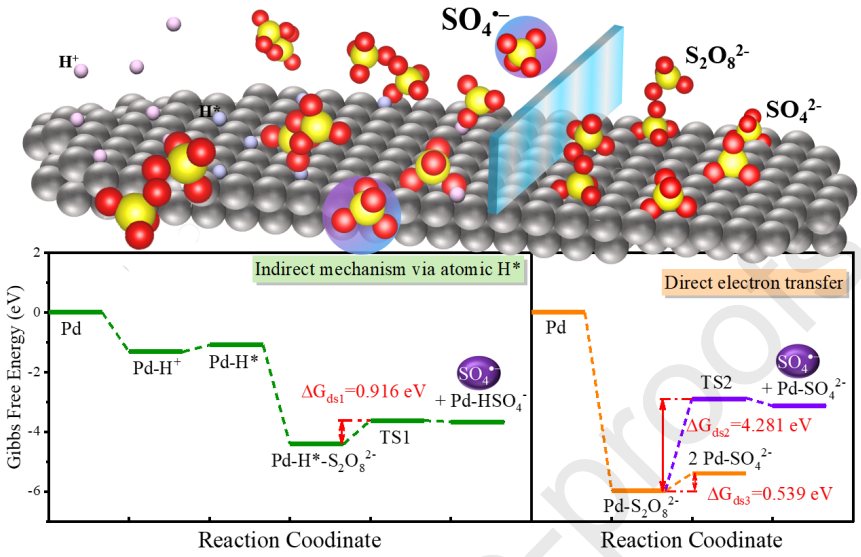

Fig. 4. Gibbs free energy variation for PDS decomposition on Pd(111) facet via different reduction approaches: indirect reduction via atomic H* and direct electron transfer.

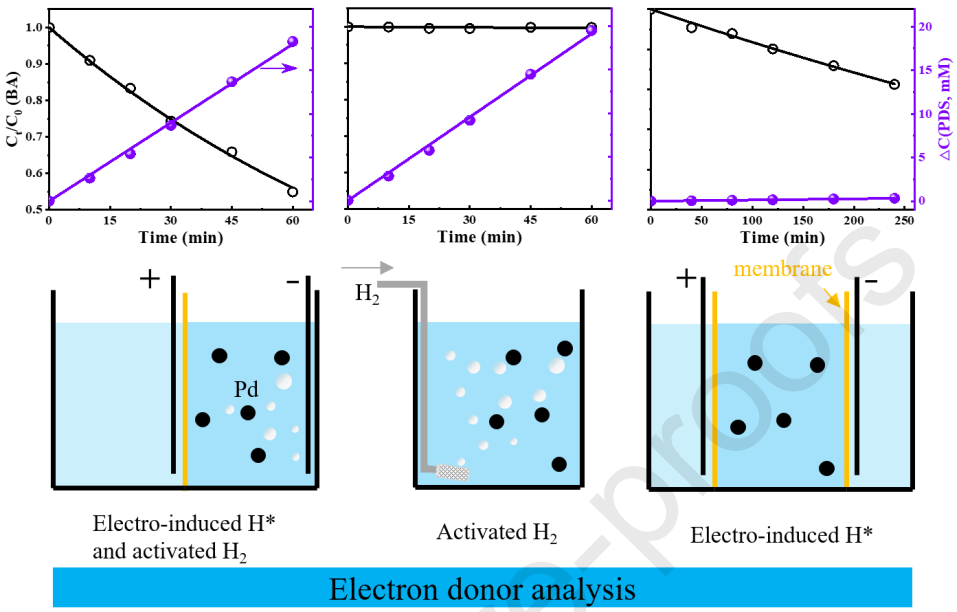

Fig. 5. The effect of different approaches for atomic H* generation on the BA degradation and PDS decomposition. (BA, 50 μM; PDS, 20 mM; Pd/Al_2O_3, 0.5 g/L; applied current, 0.10 A; initial solution pH, 3.0; deoxygenated atmosphere)

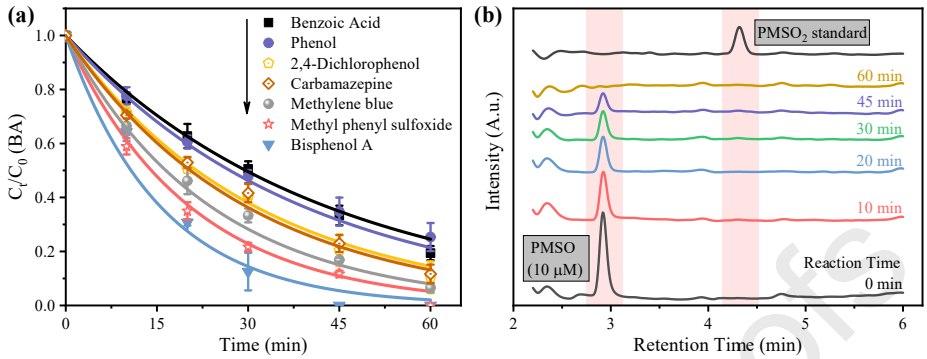

Fig. 6. (a) Degradation performance on various organics in the H*/PDS system; (b) the HPLC spectra of samples in the H*/PDS system. ([Organic compounds], 10 μM; [Pd/Al_2O_3], 0.5 g/L; [PDS], 20 mM; current, 0.1 A; solution pH 3.0; λ_{HPLC}, 230 nm)

Table. 1. Effect of the applied current, PDS concentration and Pd/Al_2O_3 dosage on the kinetics constants (*k*-value) of PDS consumption and BA degradation. (BA, 50 μM; initial solution pH, 3.0; deoxygenated atmosphere)

No.	Current (A)	C(PDS) (mM)	C(Pd/Al_2O_3) (g/L)	k_1 (BA) (min^{-1})	k_0 (PDS) (mM/min)
1.	0.1	20	0.5	0.0097	0.2982
2.	0.05	20	0.5	0.0051	0.1595
3.	0.02	20	0.5	0	0.0657
4.	0.1	20	1.0	0.0169	0.3026
5.	0.1	20	0.2	0.0031	0.3163
6.	0.1	20	0.1	0.0019	0.3121
7.	0.1	50	0.5	0.0087	0.3002
8.	0.1	10	0.5	0.0074	0.2802

Highlights:

1. Degradation of organic pollutant can be highly improved in H*/PDS system.
2. PDS can electrochemically form $SO_4^{\bullet-}$ using electro-induced atomic H* as activator.
3. Via direct electron transfer mechanism, PDS is decomposed into inert SO_4^{2-} by H_2.

ACTA UNIVERSITATIS LAPPEENRANTAENSIS

911. NJOCK BAYOCK, FRANCOIS MITERAND. Thermal analysis of dissimilar weld joints of high-strength and ultra-high-strength steels. 2020. Diss.

912. KINNUNEN, SINI-KAISU. Modelling the value of fleet data in the ecosystems of asset management. 2020. Diss.

913. MUSIKKA, TATU. Usability and limitations of behavioural component models in IGBT short-circuit modelling. 2020. Diss.

914. SHNAI, IULIIA. The technology of flipped classroom: assessments, resources and systematic design. 2020. Diss.

915. SAFAEI, ZAHRA. Application of differential ion mobility spectrometry for detection of water pollutants. 2020. Diss.

916. FILIMONOV, ROMAN. Computational fluid dynamics as a tool for process engineering. 2020. Diss.

917. VIRTANEN, TIINA. Real-time monitoring of membrane fouling caused by phenolic compounds. 2020. Diss.

918. AZZUNI, ABDELRAHMAN. Energy security evaluation for the present and the future on a global level. 2020. Diss.

919. NOKELAINEN, JOHANNES. Interplay of local moments and itinerant electrons. 2020. Diss.

920. HONKANEN, JARI. Control design issues in grid-connected single-phase converters, with the focus on power factor correction. 2020. Diss.

921. KEMPPINEN, JUHA. The development and implementation of the clinical decision support system for integrated mental and addiction care. 2020. Diss.

922. KORHONEN, SATU. The journeys of becoming ang being an international entrepreneur: A narrative inquiry of the "I" in international entrepreneurship. 2020. Diss.

923. SIRKIÄ, JUKKA. Leveraging digitalization opportunities to improve the business model. 2020. Diss.

924. SHEMYAKIN, VLADIMIR. Parameter estimation of large-scale chaotic systems. 2020. Diss.

925. AALTONEN, PÄIVI. Exploring novelty in the internationalization process - understanding disruptive events. 2020. Diss.

926. VADANA, IUSTIN. Internationalization of born-digital companies. 2020. Diss.

927. FARFAN OROZCO, FRANCISCO JAVIER. In-depth analysis of the global power infrastructure - Opportunities for sustainable evolution of the power sector. 2020. Diss.

928. KRAINOV, IGOR. Properties of exchange interactions in magnetic semiconductors. 2020. Diss.

929. KARPPANEN, JANNE. Assessing the applicability of low voltage direct current in electricity distribution - Key factors and design aspects. 2020. Diss.

930. NIEMINEN, HARRI. Power-to-methanol via membrane contactor-based CO2 capture and low-temperature chemical synthesis. 2020. Diss.

931. CALDERA, UPEKSHA. The role of renewable energy based seawater reverse osmosis (SWRO) in meeting the global water challenges in the decades to come. 2020. Diss.

932. KIVISTÖ, TIMO. Processes and tools to promote community benefits in public procurement. 2020. Diss.

933. NAQVI, BILAL. Towards aligning security and usability during the system development lifecycle. 2020. Diss.

934. XIN, YAN. Knowledge sharing and reuse in product-service systems with a product lifecycle perspective. 2020. Diss.

935. PALACIN SILVA, VICTORIA. Participation in digital citizen science. 2020. Diss.

936. PUOLAKKA, TIINA. Managing operations in professional organisations – interplay between professionals and managers in court workflow control. 2020. Diss.

937. AHOLA, ANTTI. Stress components and local effects in the fatigue strength assessment of fillet weld joints made of ultra-high-strength steels. 2020. Diss.

938. METSOLA, JAAKKO. Good for wealth or bad for health? Socioemotional wealth in the internationalisation process of family SMEs from a network perspective. 2020. Diss.

939. VELT, HANNES. Entrepreneurial ecosystems and born global start-ups. 2020. Diss.

940. JI, HAIBIAO. Study of key techniques in the vacuum vessel assembly for the future fusion reactor. 2020. Diss.

941. KAZARNIKOV, ALEXEY. Statistical parameter identification of reaction-diffusion systems by Turing patterns. 2020. Diss.

942. SORMUNEN, PETRI. Ecodesign of construction and demolition waste-derived thermoplastic composites. 2020. Diss.

943. MANKONEN, ALEKSI. Fluidized bed combustion and humidified gas turbines as thermal energy conversion processes of the future. 2020. Diss.

944. KIANI OSHTORJANI, MEHRAN. Real-time efficient computational approaches for hydraulic components and particulate energy systems. 2020. Diss.

945. PEKKANEN, TIIA-LOTTA. What constrains the sustainability of our day-to-day consumption? A multi-epistemological inquiry into culture and institutions. 2021. Diss.

946. NASIRI, MINA. Performance management in digital transformation: a sustainability performance approach. 2021. Diss.

947. BRESOLIN, BIANCA MARIA. Synthesis and performance of metal halide perovskites as new visible light photocatalysts. 2021. Diss.

948. PÖYHÖNEN, SANTERI. Variable-speed-drive-based monitoring and diagnostic methods for pump, compressor, and fan systems. 2021. Diss.

LUT University

ISBN 978-952-335-625-2
ISBN 978-952-335-626-9 (PDF)
ISSN-L 1456-4491
ISSN 1456-4491
Lappeenranta 2021